



MONASH University

**MODELLING THE MULTIPHASE FLOW IN
HYDROCYCLONES**

By

Li Ji

A THESIS SUBMITTED FOR THE DEGREE

OF

DOCTOR OF PHILOSOPHY

**IN THE LABORATORY FOR SIMULATION AND MODELLING
OF PARTICULATE SYSTEMS, DEPARTMENT OF CHEMICAL
ENGINEERING, MONASH UNIVERSITY, CLAYTON, VIC 3800,
AUSTRALIA**

JULY 2017

**To my family,
Love and Thanks.**

COPYRIGHT NOTICE

I certify that I have made all reasonable efforts to secure copyright permissions for third-party content included in this thesis and have not knowingly added copyright content to my work without the owner's permission.

TABLE OF CONTENTS

TABLE OF CONTENTS.....	I
LIST OF FIGURES	IV
LIST OF TABLES.....	XIX
ABSTRACT.....	XXI
PUBLICATIONS DURING ENROLMENT	XXIII
DECLARATION FOR THESIS INCLUDING PUBLISHED WORKS	XXI
ACKNOWLEDGMENTS	XXV
CHAPTER 1 INTRODUCTION	1
CHAPTER 2 LITERATURE REVIEW	6
2.1 Introduction	7
2.2 Working principles	8
2.3 Previous studies on hydrocyclones and unsolved issues.....	10
2.3.1 Performance parameters	10
2.3.2 Geometrical parameters	14
2.3.3 Operational parameters.....	21
2.3.4 Material parameters	25
2.4 Methods to study the multiphase flow in hydrocyclones.....	33
2.4.1 Experimental method.....	33
2.4.2 CFD-LPT approach	34
2.4.3 TFM approach	36
2.4.4 CFD-DEM/TFM-DEM approach.....	39
2.4.5 Empirical model	42
2.5 Proposed research.....	46
CHAPTER 3 NUMERICAL METHOD AND VALIDATION	48
3.1 Introduction	49

3.2 Simulation method and conditions	51
3.2.1 Simulation method.....	51
3.2.2 Simulation conditions	54
3.3 Model validation	60
3.3.1 CG CFD-DEM validation.....	60
3.3.2 CG TFM-DEM validation	63
3.4 Effect of feed solid concentration	64
3.5 Conclusions	70
CHAPTER 4 COMPUTATIONAL ANALYSIS AND OPTIMIZATION OF HYDROCYCLONE SIZE TO MITIGATE ADVERSE EFFECT OF PARTICLE DENSITY	72
4.1 Introduction	73
4.2 Simulation method	76
4.2.1 Model description	76
4.2.1 Model applicability.....	77
4.3 Simulation conditions.....	78
4.4 Results and discussion.....	81
4.4.1 Separation performance	81
4.4.2 Flow and force characteristics	86
4.5 Conclusions	96
CHAPTER 5 NUMERICAL STUDY OF THE EFFECT OF INLET FEED TYPE ON THE MULTIPHASE FLOW AND PERFORMANCE OF HYDROCYCLONES	98
5.1 Introduction	99
5.2 Simulation method and conditions.....	101
5.2.1 Model Description	101
5.2.1 Model Applicability.....	102
5.2.3 Simulation conditions	102
5.3 Results and discussion.....	105

5.4 Conclusions	113
CHAPTER 6 COMPUTATIONAL STUDY OF THE EFFECT OF FEED SIZE DISTRIBUTION ON THE SEPARATION PERFORMANCE OF HYDROCYCLONES	115
6.1 Introduction	116
6.2 Simulation method and conditions	118
6.2.1 Model description	118
6.2.1 Model applicability	118
6.2.3 Simulation conditions	119
6.3 Results and discussion	122
6.4 Conclusions	130
CHAPTER 7 PREDICTION OF SEPARATION PERFORMANCES OF HYDROCYCLONES BY A NEWLY DEVELOPED MODEL	131
7.1 Introduction	132
7.2 Model development	135
7.2.1 Strategy and database	135
7.2.2 Model fitting	138
7.2.3 Fitting accuracy	139
7.3 Model validation	141
7.4 Conclusions	147
CHAPTER 8 CONCLUSIONS AND FURTHER WORKS	149
8.1 Conclusions	150
8.2 Future work	152
LIST OF REFERENCES	154

LIST OF FIGURES

Fig. 2- 1 Hydrocyclone configuration.....	9
Fig. 2-2 Working principles of hydrocyclone.....	10
Fig. 2-3 Uncorrected and corrected partition curves	11
Fig. 2- 4 Partition curve representations	13
Fig. 2- 5 Representations of misplaced particles (Plitt, 1979).....	13
Fig. 2- 6 Representations of the hydrocyclone geometry	14
Fig. 2- 7 Representations of cyclones with different body sizes (Azadi et al., 2010) .	16
Fig. 2- 8 Corrected efficiency curves for hydrocyclones with different diameters	16
Fig. 2- 9 Partition curves of hydrocyclones with two different body diameters in the industry report (Atkinson and Swanson, 2008)	17
Fig. 2- 10 Effects of cyclone size on the partition curve (Wang and Yu, 2006)	18
Fig. 2- 11 Hydrocyclones with (a) the tangential inlet and (b) involute inlet: (I) 3-D view and (II) top view.....	19
Fig. 2- 12 Classification curves of hydrocyclones with the tangential inlet and involute inlet (Yoshida et al., 2004).....	20
Fig. 2- 13 Hydrocyclones with ‘spiral and slope’ inlet (Cavex hydrocyclones, Weir Minerals).....	21
Fig. 2- 14 Classification curves at different flowrates (Slechta and Firth, 1984).....	22
Fig. 2- 15 Classification curves at different feed pressures in the work of Frachon and Cilliers (Frachon and Cilliers, 1999).....	23
Fig. 2- 16 Experimental partition curves under different feed solid concentrations (Davailles et al., 2012)	24
Fig. 2- 17 Simulated partition curves at different feed solid concentrations (Kuang et al., 2012)	24
Fig. 2- 18 Experimental partition curves of coal with different densities (O'Brien et al., 2001)	26
Fig. 2- 19 Reduced partition curves of different materials (Slechta and Firth, 1984) .	27
Fig. 2- 20 Feed size distributions used in the work of Slechta and Firth (Slechta and Firth, 1984)	29
Fig. 2- 21 Four regions of similar size distributions within an operating hydrocyclone (Renner and Cohen, 1978)	31

Fig. 2- 22 Trajectories of particles with different diameters in the work of Wang et al. (Wang et al., 2007).....	31
Fig. 2- 23 considered size distributions with (a) different mean sizes and (b) different spread constants in a previous study (Chen et al., 2016)	32
Fig. 2- 24 Modelling strategy for CFD-LPT model.....	35
Fig. 3- 1 CG CFD-DEM modelling strategy used in this work.....	51
Fig. 3- 2 Schematic representation of the general idea of the CG CFD-DEM model in a computational cell (there are two different sized particles in each system): (a) the original system; (b) Coarse-grained system; (c) an example of inappropriate coarse-grain scheme (only particles with the same size can be contained in a CG particle) ..	53
Fig. 3- 3 Modified modelling strategy	54
Fig. 3- 4 (a) Geometry and (b) mesh representation of simulated 75 mm diameter hydrocyclones	55
Fig. 3- 5 (a) Geometry and (b) mesh representation of simulated 100 mm diameter hydrocyclones	56
Fig. 3- 6 Size distributions of materials for (a) 75mm and (b) 100mm hydrocyclones	58
Fig. 3- 7 Experimental and simulated partition curves of for 75mm diameter hydrocyclone at a feed solid concentration of 4%	60
Fig. 3- 8 Particle flow patterns in 75mm hydrocyclone at feed solid concentration of 4% at (a) $t=1.9s$, (b) $t=2.0s$ and (c) $t=2.1s$	61
Fig. 3- 9 Partition curves simulated by CG CFD-DEM and TFM models at different feed solid concentration of 1%, 4%, and 8%	62
Fig. 3- 10 Comparisons of the experimental and simulated partition curves at a feed solid concentration of 8%	62
Fig. 3- 11 Partition curves simulated by the CG CFD-DEM and TFM models in 100mm hydrocyclone at feed solid concentrations of (a) 6%, and (b) 10%	63
Fig. 3- 12 Partition curves simulated by the CG CFD-DEM and CG TFM-DEM models in hydrocyclones with diameters of (a) 75mm and (b) 100mm, at feed solids concentrations of 8% and 10%, respectively.	64
Fig. 3- 13 Solid volume distributions in 75mm diameter hydrocyclone at different feed solid concentrations of: (a) 1%, (b) 4%, (c) 8% by the CG CFD-DEM model and (d) 8% by the CG TFM-DEM model.....	65

Fig. 3- 14 Particle flow properties in 75mm diameter hydrocyclone at different feed solid concentrations of (a) 1%, (b) 4%, (c) 8% by the CG CFD-DEM model and (d) 8% by the CG TFM-DEM model.....	66
Fig. 3- 15 Total force distributions in 75mm-hydrocyclone at different feed solid concentrations of (a) 1%, (b) 4%, (c) 8% by the CG CFD-DEM model and (d) 8% by CG TFM-DEM.....	67
Fig. 3- 16 Radial acceleration difference in 75mm diameter hydrocyclones at different feed solid concentrations of (a) 1%, (b) 4%, (c) 8% by the CG CFD-DEM model, and (d) 8% by the CG TFM-DEM.....	68
Fig. 3- 17 Solid volume distribution in 100 mm diameter hydrocyclone at feed solid concentrations of (a) 6% and (b) 10% by the CG CFD-DEM model and (c) 10% by the CG TFM-DEM model.....	69
Fig. 3- 18 Radial acceleration difference in 100 mm diameter hydrocyclone at feed solid concentrations of (a) 6% and (b) 10% by the CG CFD-DEM model and (c) 10% by the CG TFM-DEM model.....	70
Fig. 4- 1 Steps used in the present modelling.	76
Fig. 4- 2 Geometric profile (a) and mesh (b) of the hydrocyclones simulated.....	79
Fig. 4- 3 Effect of cyclone size on the partition curves for the coal density of: (a) 1275 kg/m ³ , (b) 1500 kg/m ³ , and (c) 2200 kg/m ³	81
Fig. 4- 4 Effects of cyclone size on performance parameters at different particle densities: (a) cut size, (b) Ecart probable, (c) inlet pressure drop, and (d) water split.....	83
Fig. 4- 5 Profiles of (a) volume fraction and (b) axial velocity at the spigot.....	85
Fig. 4- 6 Partition number of ultrafine and coarse particles as a function of cyclone size at different particle densities.....	86
Fig. 4- 7 Spatial distribution of coal volume fraction at the cyclone size of (a) 1000 mm and (b) 300 mm.....	87
Fig. 4- 8 Distributions of water tangential velocities: (a) representative contour, (b) effect of particle density at the cyclone size of 300 mm, and (c) effect of cyclone size at the particle density of 1275 kg/m ³	89
Fig. 4- 9 Distributions of pressure gradient corresponding to Fig. 4-8.....	90
Fig. 4- 10 Distributions of radial accelerations (a) due to centrifugal forces and (b) due to pressure gradient forces and drag forces for 1.41 mm particles, as well as (c) comparison of the total radial accelerations for 1.41 mm and 0.045 mm particles. The	

particle density and cyclone size considered here are 2200 kg/m ³ and 300 mm, respectively.	92
Fig. 4- 11 Distributions of volume fraction for the particles of: (a) 1.41 mm and (b) 0.045 mm, corresponding to Fig. 4-10.....	93
Fig. 4- 12 Comparison of the total accelerations of particles of different densities for (a) 300-mm and (b) 1000-mm hydrocyclones. The particle size is 1.41 mm.....	94
Fig. 4- 13 Flow fields within the lower part of 1000-mm hydrocyclone for (a) 1.41 mm and (b) 0.045 mm particles	95
Fig. 4- 14 Flow fields within the lower part of 300-mm hydrocyclone for (a) 1.41 mm and (b) 0.045 mm particles.	96
Fig. 5- 1 Modelling Steps used in the present work	101
Fig. 5- 2 (a) Geometry and (b) mesh representation of simulated hydrocyclones.....	104
Fig. 5- 3 Effects of inlet type on the partition curves for the coal density of: (a) 1275 kg/m ³ , (b) 1500 kg/m ³ , and (c) 2200 kg/m ³	106
Fig. 5- 4 Spatial distributions of coal volume fraction with densities of (a) 1275 kg/m ³ , (b) 1500 kg/m ³ and (c) 2200 kg/m ³ (where SC is the feed solid concentration).....	108
Fig. 5- 5 Distributions of water axial velocity at particle density of 1500 kg/m ³ under 7.4% feed solid concentration in (a) vertical central slice and (b) horizontal slice at 100 mm above the bottom of overflow outlet.....	109
Fig. 5- 6 Distributions of total radial acceleration of 1.41mm diameter particles (a) representative contours, and radial acceleration with different inlet types at different feed solid concentrations of particles of density: (a) 1275 kg/m ³ , (b) 1500 kg/m ³ and (c) 2200 kg/m ³	110
Fig. 5- 7 Flow field within lower part for 0.45 mm diameter particles in hydrocyclones with different inlet types at feed solid concentrations of (a) 7.4% and (b) 15.2%	113
Fig. 6- 1 (a) Geometry and (b) mesh representation of simulated hydrocyclones.....	119
Fig. 6- 2 Distributions of (a) the probability density function, and (b) mass fraction with different values of σ_j	120
Fig. 6- 3 Partition curves for materials with different size distributions	122
Fig. 6- 4 Spatial distributions of relative volume fraction for the (a) total solids, (b) 0.35 mm diameter particles and (c) 0.46 mm diameter particles with the parameter $\sigma_j=0.5, 1, \text{ and } 2$	124

Fig. 6- 5 Distributions of radial velocity for particles having diameters of (a) 0.045 mm, (b) 0.25mm, (c) 0.35, (d) 0.46 mm, and (e) 1.1 mm when the parameter $\sigma_j=0.5$	125
Fig. 6- 6 Distributions of drag force for materials with: (a) $\sigma_j=0.5$, (b) $\sigma_j=1$, and (c) $\sigma_j=2$	126
Fig. 6- 7 Distributions of total radial acceleration for materials with : (a) $\sigma_j=0.5$, (b) $\sigma_j=1$, and (c) $\sigma_j=2$	127
Fig. 6- 8 Distributions of total radial acceleration: (a) representative contours in the longitudinal section; and those along lines z1 to z5 for the material with (b) $\sigma_j=0.5$, (c) $\sigma_j=1$, and (d) $\sigma_j=2$	129
Fig. 7- 2 Hydrocyclone geometrical representations	137
Fig. 7- 3 Comparisons between the calculated and simulated separation performance: (a) cut size, (b) sharpness, (c) pressure drop, (d) water split	139
Fig. 7- 4 Comparisons between the calculated and simulated separation performance as a function of material density: (a) cut size, (b) sharpness, (c) pressure drop, (d) water split.....	140
Fig. 7- 5 Comparisons between the predicted and simulated separation performances obtained from literature (Wang, 2009, Wang and Yu, 2006, Wang et al., 2016): (a) cut size, (b) sharpness, (c) pressure drop, (d) water split.....	141
Fig. 7- 6 Comparisons between the predicted and experimental separation performances obtained from literature: (a) cut size, (b) sharpness, (c) pressure drop, and (d) water split	142
Fig. 7- 7 Comparisons between the predicted and experimental results of cut sizes versus material density for: (a) 1000 mm diameter hydrocyclone at a feed solid concentration of 15.2% cited in the industry report C6047 (O'Brien et al., 2001) and (b) 250 mm diameter hydrocyclone at a feed solid concentration of 5.5% cited in the industry report C3084 (Firth et al., 1999)	143
Fig. 7- 8 Comparisons between the predicted and experimental results of cut sizes versus solid concentration for the hydrocyclones in the works of: (a) Rajamani (Rajamani and Milin, 1992), and (b) Muzanenhamo (Muzanenhamo, 2014)	143
Fig. 7- 9 Comparisons between the predicted and experimental results of separation sharpness versus material density for: (a) 1000 mm diameter hydrocyclone at a feed solid concentration of 15.2% cited in the industry report C6047 (O'Brien et al., 2001)	

and (b) 250 mm diameter hydrocyclone at a feed solid concentration of 5.5% cited in the industry report C3084 (Firth et al., 1999) 144

Fig. 7- 10 Comparisons between the predicted and experimental results of sharpness versus solid concentration for hydrocyclones in the works of (a) Rajamani’s paper (Rajamani and Milin, 1992), and (b) Muzanenhamo’s thesis (Muzanenhamo, 2014) 144

Fig. 7- 11 Partition curves for 1000 mm diameter hydrocyclone at the feed solid concentration of 15.2% cited in the industry report C6047 (O'Brien et al., 2001) based on (a) the present predictive model and Plitt model, and (b) the present predictive model and Narasimha model 145

Fig. 7- 12 Comparisons of partition curves for different models with the experimental ones at a feed solid concentration of 5% reported in the industry report C3087 (Firth et al., 1999) 146

Fig. 7- 13 Partition curves predicted by different models for the conditions in Rajamani’s experiments (Rajamani and Milin, 1992) 147

LIST OF TABLES

Table 2- 1 Performance parameters of hydrocyclone	10
Table 2- 2 Geometrical, operational and material parameters of hydrocyclones	14
Table 2- 3 One of the density distributions in the experiment of O'Brien et al. (O'Brien et al., 2001)	25
Table 2- 4 Summary of the work on hydrocyclones by experiments	33
Table 3- 1 Geometrical and operational conditions of 75 mm diameter hydrocyclone	56
Table 3- 2 Geometrical and operational conditions of 100 mm diameter hydrocyclone	57
Table 3- 3 Boundary and initial conditions for CG CFD-DEM simulations of 75 mm diameter hydrocyclone	57
Table 4- 1 Geometric and operational parameters in the present simulation	78
Table 4- 2 Size and density distributions in the simulations.	80
Table 5- 1 Geometrical and operational conditions of 1000 mm diameter hydrocyclone.....	103
Table 5- 2 Size and density distributions in the simulations	105
Table 6- 1 Geometrical and operational conditions of the hydrocyclone.....	121
Table 7- 1 Independent variables in the database	136
Table 7- 2 Dependent variables in the database.....	137

ABSTRACT

Hydrocyclones have been widely used to separate fine particles by size in industries. Much empirical and numerical effort has been spent on studying hydrocyclones. The empirical models provide convenience to industrial uses as they simply correlate cyclone performances with variables under specific experimental conditions. The numerical approach mainly performs well in explaining the underlying fundamentals of hydrocyclone operations, though it can also predict the unit performance at the cost of longer computation time. To develop a mathematical description of the underlying fundamentals of hydrocyclone operations more effectively, a predictive model based on the acquired extensive numerical results is developed in this thesis. This new model is not limited to the conditions used in the modelling. Further, it can also overcome the deficiency of previous models by considering some important pertinent variables, e.g. the material density and feed solid concentration. To generate the numerical database for developing the model, an appropriate numerical approach is identified. In particular, the effects of material density and its interaction with the cyclone designs are investigated to clarify the challenging problem of particle density.

This thesis represents an effort on solving a long-standing unsolved issue encountered in the practical applications of hydrocyclones and developing a new PC-based predictive model. It consists of five major components.

The first component is to identify an appropriate approach to generate the numerical database. Three numerical approaches, namely, the Two-fluid Model (TFM), the combined approach of Computational Fluid Dynamics and Discrete Element Method based on the coarse-grain concept (CG CFD-DEM), and the CG TFM-DEM approach, are assessed. The results show that the TFM model can model the multiphase flow in hydrocyclones under a wide range of feed solid concentrations. However, it is challenging for the TFM model to handle particles with a broad range of size/density distributions. This deficiency can be overcome by the CG CFD/TFM-DEM approach. The CG CFD-DEM model is only applicable to dilute flows. The first built CG TFM-DEM approach is applicable to the dense flows, however, needs further research. The TFM model is adapted to generate the numerical database because the size/density distributions considered in this thesis are within its handling ability.

The effect of material density is investigated by the TFM approach. The study on the effect of material density is further extended to its interactions with the geometry designs, i.e. the optimum cyclone body size and inlet feed type in Component 2 and 3, respectively. The results show that a mid-range cyclone size and a ‘spiral and slope’ inlet are recommended for industrial uses. The effect of feed size distribution, which was simply described by material-specific constants, is studied in Component 4. The results show that an increase in the amount of median particles leads to a deteriorated separation of intermediate-sized particles and an increase in the cut size.

Finally, a PC-based model based on the numerical data acquired is developed to predict the separation performance of hydrocyclones in Component 5. Reasonably good agreements between the predicted and experimental results indicate that this model is valid. The comparisons with the previous models show that the model can give more accurate predictions and overcome some deficiencies of some previous models.

PUBLICATIONS DURING ENROLMENT

Published journal papers:

- **Li Ji**, Shibo Kuang , Zheng Qi, Yuan Wang, Jiang Chen and Aibing Yu (2017): Computational analysis and optimization of hydrocyclone size to mitigate adverse effect of particle density, International Journal of Separation and Purification, 174:251-263.
- Maryam Ghodrat, Zheng Qi, Shibo Kuang, **Li Ji**, Aibing Yu (2016): Computational investigation of the effect of particle density on the multiphase flows and performance of hydrocyclone, Minerals Engineering, 90 (2016) 55-69.

Published conference papers:

- **Li Ji**, Kaiwei Chu, Shibo Kuang, and Aibing Yu (2017). Coarse-Grained CFD-DEM Modelling of the Multiphase Flow in a Hydrocyclone. The 19th International Conference on Separation and Purification Technology, Barcelona, Spain, February 27-28 .
- Kaiwei Chu, **Li Ji**, Jiang Chen and Aibing Yu (2014), Coarse-grained CFD-DEM modelling of the multiphase flow in a dense medium cyclone: Model validation. The 7th World Congress on Particle Technology. Beijing, China, May 19-22.

DECLARATION FOR THESIS INCLUDING PUBLISHED WORKS

I hereby declare that this thesis contains no material which has been accepted for the award of any other degree or diploma at any university or equivalent institution and that, to the best of my knowledge and belief, this thesis contains no material previously published or written by another person, except where due reference is made in the text of the thesis.

This thesis includes 1 original paper published in peer reviewed journals. The core theme of the thesis is modelling the multiphase flow in hydrocyclones. The ideas, development and writing up of all the papers in the thesis were the principal responsibility of myself, the candidate, working within the Department of Chemical Engineering under the supervision of Prof. Aibing Yu, Dr. Shibo Kuang, and Dr. Kaiwei Chu.

The inclusion of co-authors reflects the fact that the work came from active collaboration between researchers and acknowledges input into team-based research.

In the case of (Chapters 4) my contribution to the work involved the following:

Thesis Chapter	Publication Title	Status (published, in press, accepted or returned for revision, submitted)
Chapter 4	Computational analysis and optimization of hydrocyclone size to mitigate adverse effect of particle density	Published

I have renumbered sections of published papers in order to generate a consistent presentation within the thesis.

Student signature:



Date: 14/07/2017

The undersigned hereby certify that the above declaration correctly reflects the nature and extent of the student's and co-authors' contributions to this work. In instances where I am not the responsible author I have consulted with the responsible author to agree on the respective contributions of the authors.

Main Supervisor signature:



14/07/2017 Date 14/07/2017

ACKNOWLEDGMENTS

I would like to express my sincere gratitude to my primary supervisor, Prof. Aibing Yu, for giving me the opportunity to work on this project and all the help and guidance. I also wish to thank my associate supervisors, Dr. Shibo Kuang and Dr. Kaiwei Chu, for teaching me the basics of the project and for their helpful advice and guidance. This work would not be possible without their wise guidance and extraordinary inspiration.

I wish to thank Monash University and the University of New South Wales (UNSW), for providing me with the tuition fee scholarship, and financial support for this work. I also wish to thank China Scholarship Council (CSC) for providing me with the living stipend.

Thanks are also given to colleagues and fellow students in SIMPAS (Lab for Computer Simulation and Modelling of Particulate Systems) for providing me with a great deal of help in my studies and fantastic life in Melbourne and Sydney. I am also grateful to the staff in the Department of Chemical Engineering at Monash University and the School of Materials Science and Engineering at UNSW for their various help during the course of my study.

Special thanks to my parents and my younger brother for their love, encouragement and support, which have always been a source of inspiration to my work.

CHAPTER 1 INTRODUCTION

A hydrocyclone is a separation or classification equipment which is widely used in chemical engineering and mineral processing industries. The reason for its popularity is attributed to its simplicity in the design and operation, high throughput in the capacity, and low cost in the maintenance and operation. Generally, a hydrocyclone comprises a cylinder, a central pipe called a vortex finder, a cone, a discharge pipe called spigot or apex, and an inlet attached to the top section of the cylindrical section. The working principles of the hydrocyclone are known to depend on the difference of terminal settling velocity of particles with different sizes and densities. The flow in a hydrocyclone is very complex, because of the existence of swirling turbulence, air-core and segregation involving gas, liquid, and solid phases. In the past years, much effort has been spent on studying hydrocyclones with regards to geometrical, operational and material parameters.

Previous researchers utilized experimental, empirical, and numerical methods to study the multiphase flows in hydrocyclones. The advantages and deficiencies of these methods are as follows. The experimental method contributes to the insight into the multiphase flow in hydrocyclones, but those experiments are expensive. Thus, researchers have focused on collecting the experimental data to develop empirical models to predict the hydrocyclone performance. The empirical approach is fast, portable and easy to apply in the industry. However, previously developed empirical models are weak in their applicability because they are generally limited to the experimental conditions used in the modelling. Therefore, it is desirable and more reliable to develop a mathematical description of the fundamentals which govern the multiphase flow of hydrocyclones. Furthermore, the previous empirical models have failed to consider variables comprehensively; for example the effects of material density were ignored. Actually, the presence of particles of different densities further complicates the separation within hydrocyclones. However, the effects brought about by the density difference have not been well addressed. The third approach, i.e. the numerical method, provides a lower-cost and more flexible way to study the multiphase flows in hydrocyclones compared with the experimental method. Further, it can be also used to understand the underlying fundamentals of hydrocyclones compared to the empirical approach. However, the numerical model has its own disadvantages. For example, it is not suitable to be used as an industrial on-line tool because of the time-demanding computation.

In this work, a PC-based model based on the numerical results is developed to predict the hydrocyclone performance, aiming to develop a mathematical description of the underlying fundamentals of hydrocyclone operations. That is to say that this model is expected to meet the industrial needs and contributes to explaining the underlying fundamentals of hydrocyclone operations. Further, the effects of material density and the particle-fluid flows under a wide range of feed solid concentrations are considered in this new model, to overcome the deficiency of the previously developed models. To develop this model, an appropriate method that can generate a considerably large database of numerical data should be first selected. Then, the effect of material density, which represents a long-standing unsolved issue, is investigated by the numerical method. The study on the effect of particle density is further extended to its interactions with the geometry design i.e. the optimum cyclone body size and inlet feed type. The effect of feed size distribution which had been ignored is also investigated. Finally, the newly obtained numerical results are included in the database and a simple but comprehensive predictive model is developed.

This thesis is organized as follows.

Chapter 2 reviews previous studies on the geometrical, operational, and material parameters of hydrocyclones. Moreover, the methods that can be utilized to study hydrocyclones are explored in some details.

Chapter 3 assesses the widely-used TFM (Two-fluid Model) approach and the newly developed CG CFD-DEM/TFM-DEM (The combined approach of computational fluid dynamics/TFM and Discrete Element Method based on the coarse-grain concept) approach, with regards to modelling the multiphase flow under a wide range of feed solid concentrations. It is noted that the TFM approach is one branch of the CFD method. The results show that the TFM model is able to model the multiphase flow in hydrocyclones under a wide range of feed solid concentrations. However, it is quite challenging for the TFM model to handle particles with a broad range of size distributions and density distributions. This deficiency can be overcome by the CFD/TFM-DEM approach, which is for the first time applied to the hydrocyclone studies. However, it is found that the CG CFD-DEM approach underestimates the separation performance when the feed solid concentration is high. This is caused by the extremely large size ratio of CG particle to real particle, causing significant

differences in properties between the two types of particles. On the other hand, the CG TFM-DEM model is applicable, but it needs further research on determining the critical particle size below which particles can be considered as a continuum medium. As both dense and dilute flows are targeted in this thesis, the TFM model is adapted to generate the numerical database because the size/density distributions considered in this thesis are within its handling ability.

Chapter 4 presents an effort to address the uncertainty in the cyclone size selection in the presence of particles with different densities. The numerical results show that more ultrafine particles are misplaced to the underflow in smaller cyclones, which is pronounced for heavier particles. On the other hand, coarse light particles are more likely to unexpectedly report to the overflow in larger cyclones. Moreover, the handling of lighter particles gives rise to a decreased separation precision and an increased cut size. Another factor is the extent of particle accumulation near the spigot. Such accumulation reduces the separation space of hydrocyclone and blocks the paths of particles for separation, although it mitigates to some extent the water entrainment effect on ultrafine particles. Based on the results from this chapter, a mid-range cyclone size is recommended for mitigating the adverse effect of particle density and obtaining a relatively precise particle separation on the condition that the expected cut size can be achieved.

Chapter 5 discusses the effect of inlet feed type on the hydrocyclone performance. Hydrocyclones with the ‘spiral and slope’ inlet are studied and compared to those with an involute inlet in terms of the separation precision and particle misplacement. The results show that the partition curves of hydrocyclones with the ‘spiral and slope’ inlet are generally sharper than those with the involute inlet, and the amount of misplaced particles to the underflow can be reduced by the use of the ‘spiral and slope’ inlet. The differences between these two inlet types are pronounced for dense flows. In order to obtain a sharp separation and mitigate the particle misplacement, hydrocyclones with the ‘spiral and slope’ inlet are recommended for use in the industry, especially for dense flows.

Chapter 6 studies the effect of feed size distribution on the multiphase flow and performance of hydrocyclones. The feed size distributions with different values of σ_j parameter, i.e. different amounts of particles of median size, are considered in this

chapter. It is found that an increase in the amount of such median particles leads to a deteriorated separation of the intermediate-sized particles, an increase in the cut size, and a smaller difference in partitions between two intermediate-sized particles. However, the effect of the fraction of median particles on the separations of fine and coarse particles is minor.

Chapter 7 describes the development of a PC-based predictive model based on the numerical results. This newly developed model combines the advantages of the empirical and numerical models. That is, this model can meet the industrial requirements and contribute to explaining the underlying fundamentals in relation to the effect of each variable. The effects of material density and the particle-fluid flows under a wide range of feed solid concentrations are considered in this new model, to overcome the deficiency of the previously developed models. Reasonably good agreements between the predicted and experimental results indicate that this model is valid. The comparisons with some other models show that this new model is able to give more accurate predictions. Further, it has wider model applicability because it is developed based on the numerical results and considers comprehensive variables such as the material density.

Chapter 8 concludes this thesis work and discusses some future work.

CHAPTER 2 LITERATURE REVIEW

2.1 Introduction

A hydrocyclone is a separation or classification equipment which is widely used in chemical engineering and mineral processing industries. The reason for its popularity is that the hydrocyclone is simple in the design and operation. Further, it has a high capacity with low maintenance and operation costs. The flow in a hydrocyclone is very complex, because of the existence of swirling turbulence, air-core and segregation involving gas, liquid, and solid phases. Normally, a mixture of particles and fluid is fed into the hydrocyclone, then the centrifugal force within the hydrocyclone separate the particles from the suspended liquid based on the size or density differences. In recent years, much effort has been spent on studying hydrocyclones with regards to geometrical, operational and material conditions. In this chapter, a comprehensive review of these conditions is carried out. Further, important but unsolved issues in the hydrocyclone studies such as the effect of cyclone diameter, particle density, feed size distribution, and inlet feed type are also identified in this chapter.

General methods used to study hydrocyclones are also reviewed in this chapter. The experimental method contributes to gaining the insight into the multiphase flows in hydrocyclones, but those experiments are expensive. This empirical model developed based on the experimental data is fast, portable and easy to apply in the industry. However, these previously developed empirical models are weak in the applicability because they are generally limited to the experimental conditions used in the modelling. Therefore, it is desirable and more reliable to develop a mathematical description of the fundamentals which govern the multiphase flow of hydrocyclones. Further, the previous empirical models have failed to consider variables comprehensively. The third approach, i.e. the numerical method, provides a lower-cost and more flexible way to study the multiphase flows in hydrocyclones. Further, it can be used to understand the underlying fundamentals of hydrocyclone. However, it is not suitable to be used as an industrial tool because of the time-consuming computations.

2.2 Working principles

Fig. 2-1 shows the typical hydrocyclone configuration and Fig. 2-2 demonstrates its working principles (Svarovsky, 1984). It is to be noted that this configuration has been used in more than the last 80 years (Svarovsky, 1984, Bradley, 1965). Generally, a hydrocyclone comprises a cylinder, a central pipe called a vortex finder, a cone, a discharge pipe called a spigot or apex, and an inlet attached to the top section of the cylindrical section. Hydrocyclones are known to work on the principle of difference in the terminal settling velocity of particles with different sizes and densities. The operation procedure is also clearly shown in Fig. 2-2. Specifically, a mixture of particles and fluid is fed into the cylindrical chamber through the inlet. An air-core is created on the axis, extending from the bottom spigot to the top overflow through the vortex finder. The fluid flows along the central axis moves upwards to the overflow before being discharged. As for particles, the coarser or heavier particles tend to move outwards to the wall and then downwards to the spigot. The finer or lighter particles, on the other hand, are more easily dragged inwards closer to the axis and then discharged from the overflow. To ensure an efficient separation, the centrifugal force in the flow field must be a few times larger than the gravitational force.

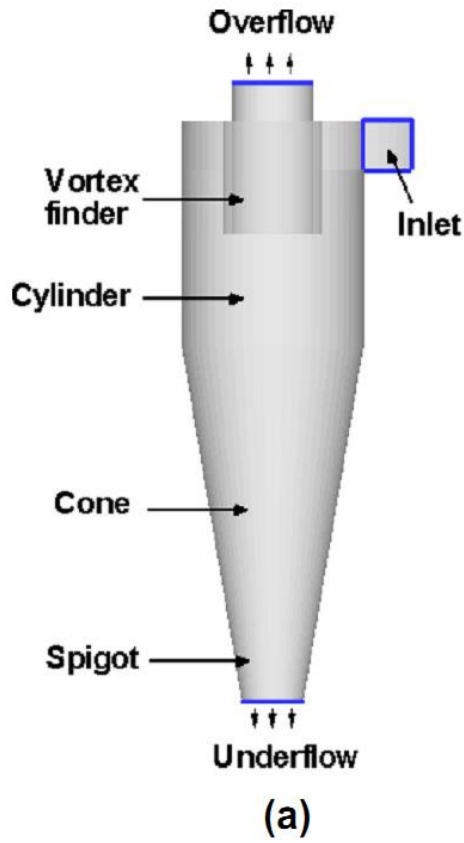
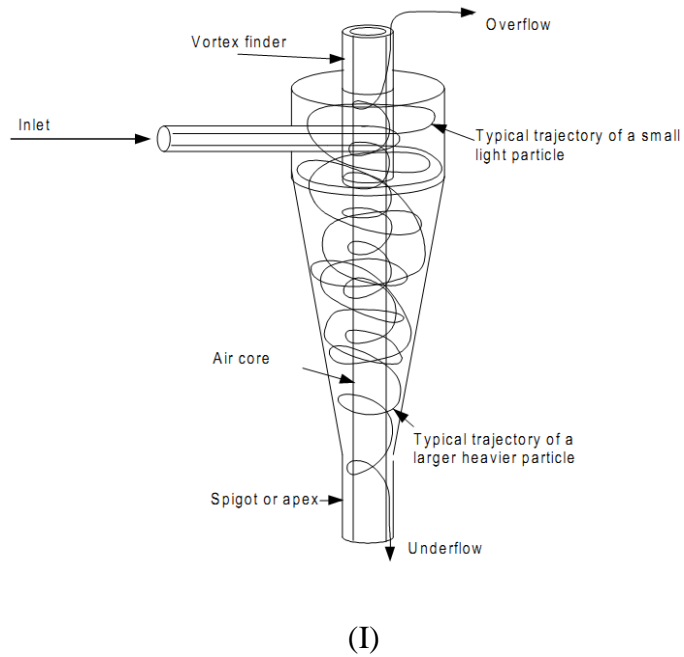


Fig. 2- 1 Hydrocyclone configuration



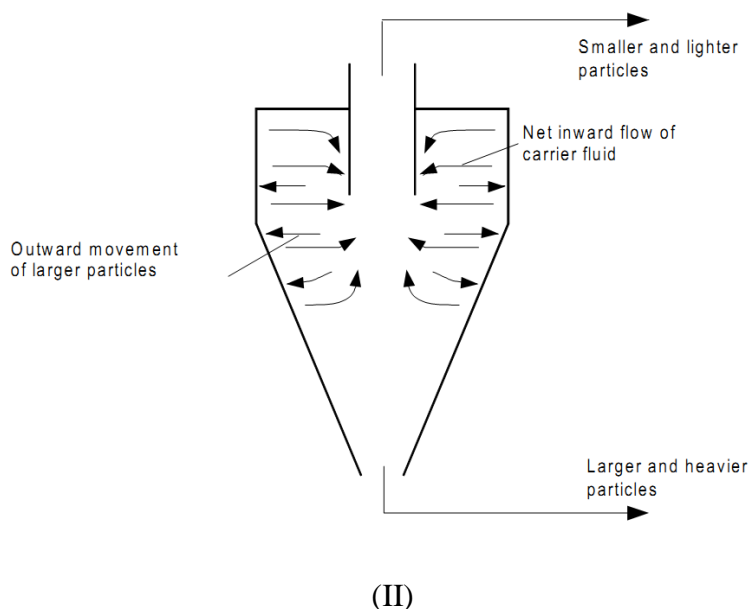


Fig. 2-2 Working principles of hydrocyclone

2.3 Previous studies on hydrocyclones and unsolved issues

2.3.1 Performance parameters

To be quantitative in the analysis, the hydrocyclone performance is generally examined with respect to the separation sharpness, cut size, inlet pressure drop, water split, and sometimes split ratio. Table 2-1 gives the general performance parameters of hydrocyclones in the current studies.

Table 2- 1 Performance parameters of hydrocyclone

Factors	Symbol
Cut size	d_{50}
Separation sharpness	$\alpha/m/E_p$
Pressure drop	P
Water split	R_f
Split ratio	S

The definitions of the terms used in Table 2-1 are as follows:

Cut size d_{50} : the size at which the partition number to underflow is 50%;

Sharpness: represented by the Ecart probable E_p ($= (d_{75} - d_{25})/2$), a smaller E_p corresponds to a larger value of sharpness and thus a more precise separation;

Inlet pressure drop P : the difference between the inlet pressure and outlet pressure, a parameter reflecting energy consumption;

Water split R_f : the water fraction reported to underflow, associated with the bypass effect; and

Split ratio: the ratio of the underflow volumetric flow rate to overflow volumetric flow rate.

The curve showing the partition number for each particle size is called the partition curve or classification curve, as shown in Fig. 2-3.

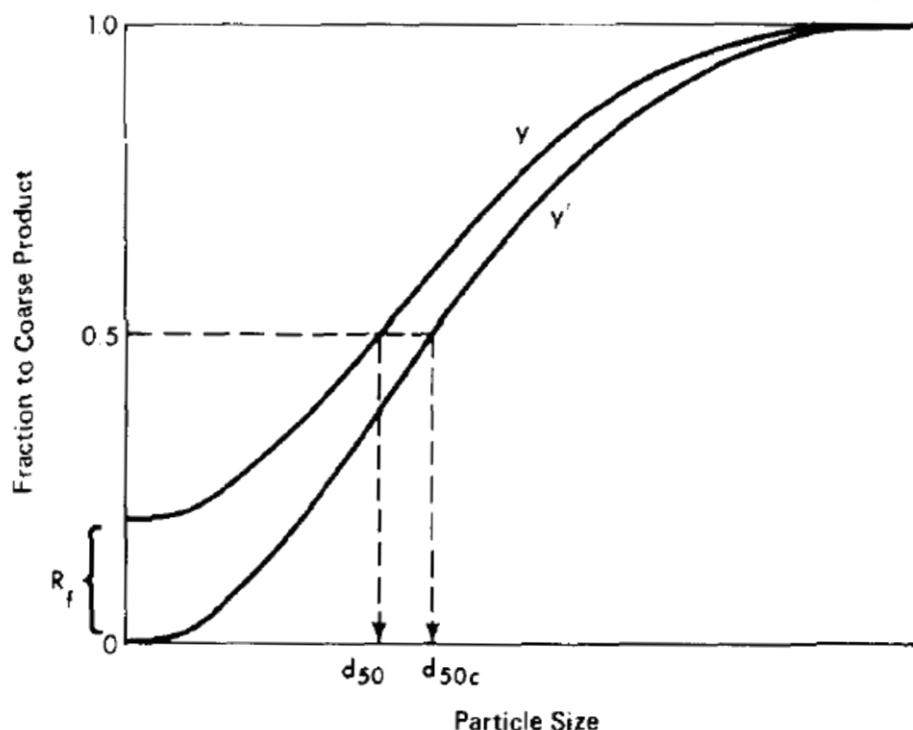


Fig. 2-3 Uncorrected and corrected partition curves

As a fraction of fine particles is entrained with water to the underflow, the directly observed classification curve is suggested to be transferred to the corrected

classification curve with real partition numbers of particles. The relationship between the observed partition number to the underflow and the corrected one is expressed as below:

$$y' = \frac{y - R_f}{1 - R_f} \quad (2-1)$$

where y and y' are the observed and corrected partitions, respectively. Corresponding to the corrected partition curve, there is a corrected cut size d_{50c} which has the equal possibility (50%) to the underflow and overflow.

Note that there are three common methods to describe the sharpness of separation. Plitt proposed a parameter m for the corrected classification curve to describe the sharpness (Plitt, 1971). Normally, a larger value of parameter m represents a sharper separation. As in the Plitt's work, a parameter m over 3 stands for a sharper classification, while a parameter m below 2 represents a poorer separation. The corrected partition curve includes the parameter m , which is shown as below (Plitt, 1979):

$$y' = 1 - \exp[-0.693(d/d_{50c})^m] \quad (2-2)$$

The second approach to describe the separation sharpness is to use a parameter α which was suggested by Lynch (Lynch and Rao, 1968). The equation is given as follows:

$$y' = \frac{\exp(\alpha d/d_{50c}) - 1}{\exp(\alpha d/d_{50c}) + \exp(\alpha) - 2} \quad (2-3)$$

Similar to the parameter m , a larger α represents a higher separation precision. Actually, the parameter m can be converted to the parameter α by the following equation (Plitt, 1979):

$$\alpha = 1.54m - 0.47 \quad (2-4)$$

Apart from the parameters m and α , an alternative way to represent the separation precision is the use of the Ecart probable (E_p), which is widely used in the studies of dense medium cyclones (DMCs). It is found that E_p is more robust to identify the difference in the sharpness between two partition curves when the data points around the cut size are not dense enough (Ghodrat et al., 2013). E_p can be calculated as follows:

$$E_p = \frac{d_{75} - d_{25}}{2} \quad (2-5)$$

Where d_{75} and d_{25} are the particle sizes at which partition numbers are 25% (δ_{25}) and 75% (δ_{75}) as shown in Fig. 2-4. A smaller E_p corresponds to a larger value of sharpness and thus a more precise separation.

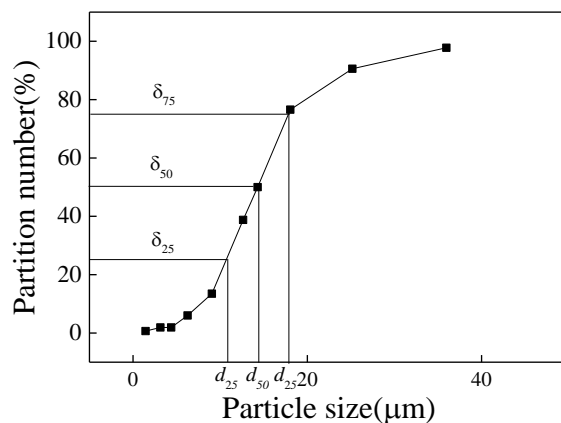


Fig. 2- 4 Partition curve representations

Apart from the cut size, separation sharpness, pressure drop, water split and split ratio, the amount of misplaced particles are usually used to evaluate the separation performance of hydrocyclones. The misplaced particles include the fine particles discharged from the spigot and coarse particles ejected from the overflow. A small amount of misplaced particles stands for a sharper classification if the cut size is the same. The hatched parts in Fig. 2-5 represent the misplaced particles.

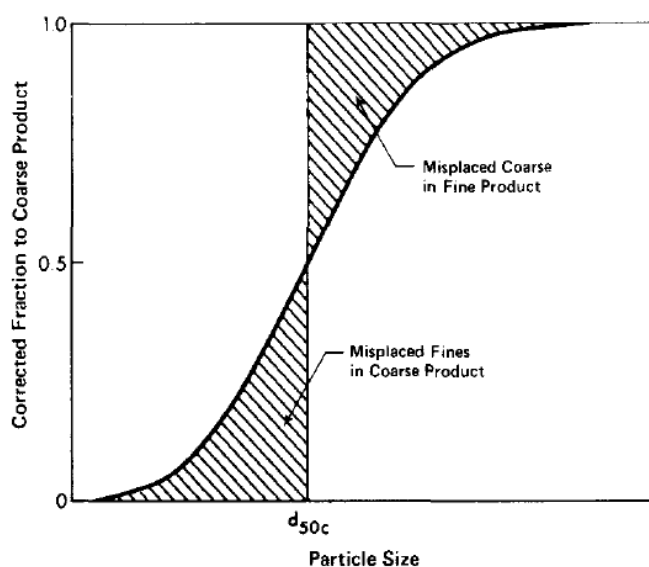


Fig. 2- 5 Representations of misplaced particles (Plitt, 1979)

It is evident that the particle misplacement leads to the loss of the product and the deterioration of the subsequent dewatering process, due to the high surface area of the entrained ultrafine particles. On the other hand, some light coarse particles are unexpectedly reported to the overflow or the upper outlet. Such particles often have a negative impact on the downstream operations like the flotation, where the solid recovery drops when the particle size is too large.

2.3.2 Geometrical parameters

Fig. 2-6 shows the classic hydrocyclone geometry, and Table 2-2 lists the corresponding geometry variables as well as the involved operational and material parameters in hydrocyclone studies.

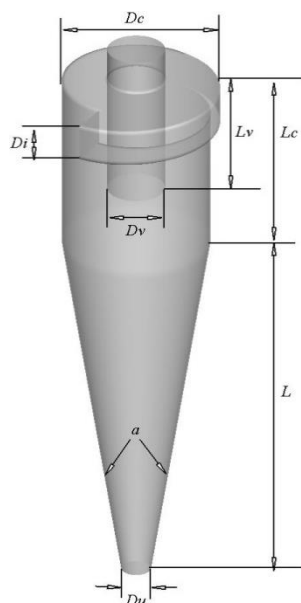


Fig. 2- 6 Representations of the hydrocyclone geometry

Table 2- 2 Geometrical, operational and material parameters of hydrocyclones

Parameter	Symbol
<i>Geometrical parameters</i>	
Diameter of the body	D_c
Diameter of inlet	D_i

Diameter of vortex finder	D_v
Diameter of spigot	D_u
Length of cylindrical part	L_c
Length of vortex finder	L_v
Inlet feed type	Involute, tangential, and 'spiral and slope'
Included angle	a
<i>Operational parameters</i>	
Inlet velocity	u
Feed solids concentration	ρ_{feed}
<i>Material parameters</i>	
Particle density	ρ_p
Particle size	d
Particle material	Limestone, coal, and iron etc.

Much effort has been dedicated to studying the parameters related to the inlet, vortex finder, spigot, cylinder and cone (Rao et al., 1976, Jiang et al., 2007, Kfuall, 1953, Huang et al., 2014, Mousavian and Najafi, 2009, Wang and Yu, 2009, Gao et al., 2011, Ghodrat et al., 2013, Ghodrat, 2014). However, the effects of cyclone body size (diameter) and inlet feed type have not been fully understood. Previous studies on these two geometrical parameters are concluded in this chapter in details.

2.3.2.1 Effect of hydrocyclone body diameter

Representations of cyclones with different body sizes are shown in Fig. 2-7 (Azadi et al., 2010). In recent years, much effort had been made to study the effect of the cyclone size.

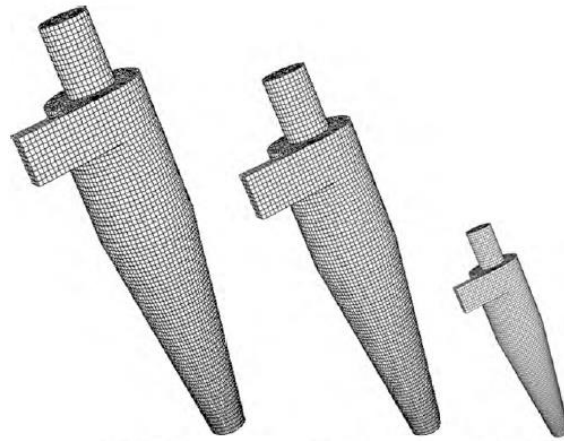


Fig. 2- 7 Representations of cyclones with different body sizes (Azadi et al., 2010)

The results from different investigators are not consistent with each other. For example, Lynch (1974, 1975) experimentally revealed that for geometrically similar hydrocyclones with sizes ranging from 102 mm to 381 mm, the reduced efficiency curve and resulting cut size do not vary much with the cyclone size for limestone particles of nearly a uniform density, as shown in Fig. 2-8.

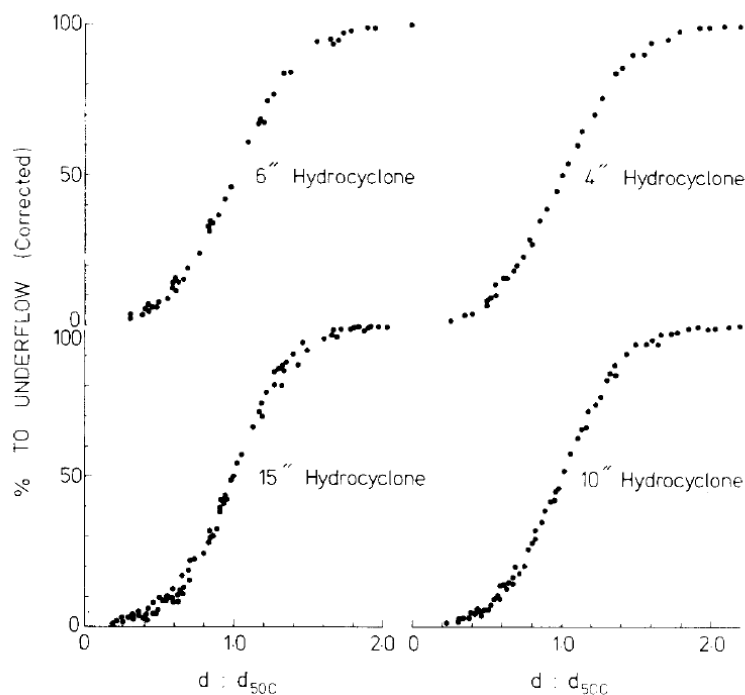


Fig. 2- 8 Corrected efficiency curves for hydrocyclones with different diameters

However, other investigators (Arterburn, 1982, Heiskanen, 1993) suggested that cut size is proportional to the cyclone size and is one of the main variables necessary for

preliminary sizing and selection of a cyclone. This has been found to be valid to the mini-hydrocyclones (5-30 mm) which were used to handle particles less than 10 μm by different investigators through various experimental measurements (Mognon et al., 2015, Neesse et al., 2015, Lv et al., 2015). Also, based on physical experiments, some investigators (Young et al., 1994, Lv et al., 2015) suggested that the separation precision of mini-hydrocyclones become worse as the cyclone size increases.

Conversely, O'Brien et al. experimentally reported that the sharpness of the partition curve of larger hydrocyclones is equivalent to that of smaller ones based on his experimental results (O'Brien et al., 2001). Atkinson and Swanson (Atkinson and Swanson, 2008) compared the classification curve of hydrocyclones with diameters of 1000 mm and 480 mm, the comparison results are shown in Fig. 2-9.

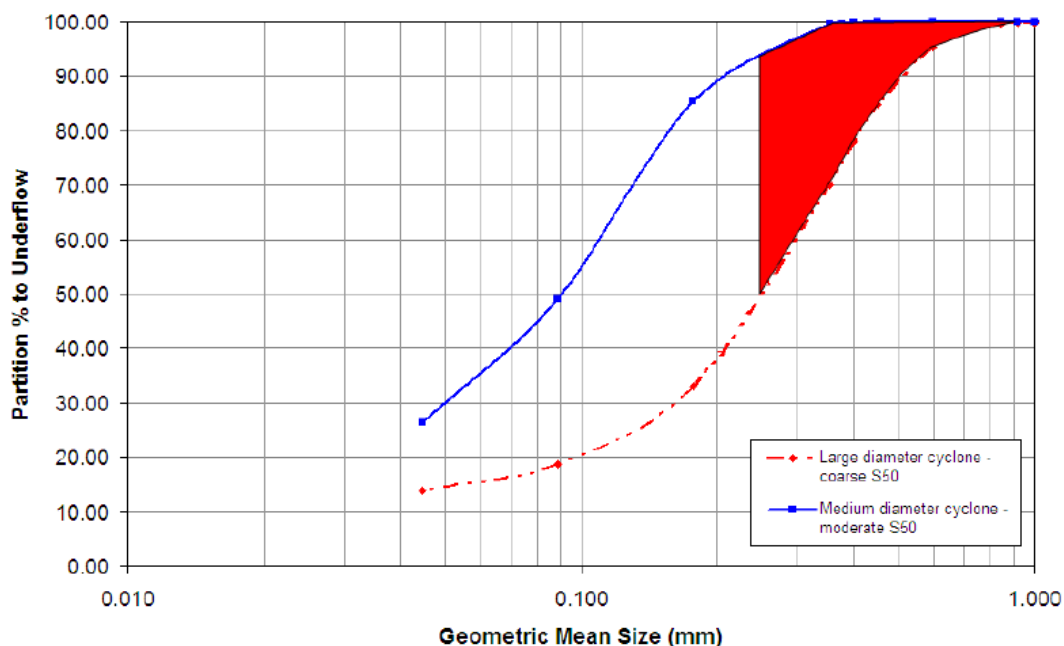


Fig. 2- 9 Partition curves of hydrocyclones with two different body diameters in the industry report (Atkinson and Swanson, 2008)

Atkinson and Swanson concluded that the curve sharpness of 1000 mm diameter hydrocyclone is similar to that of 480 mm diameter hydrocyclone. However, a larger number of particles with the size range of 0.25-0.8 mm are misplaced to the overflow in 1000 mm diameter hydrocyclones, which deteriorates the subsequent flotation efficiency and results in poorer ash levels of tailings. Therefore, a mid-range

hydrocyclone is suggested to be used with regards to eliminating the particle misplacement.

In recent years, some numerical studies have also been carried out to reveal how the cyclone size affects the performance and flows. In particular, the numerical and analytical work of Cilliers (2000) suggested that the diameter of the cylindrical section is the major variable affecting the particle size that can be separated. Delgadillo and Rajamani (2009) found that the air-core diameter increases with the hydrocyclone diameter in their simulations of the water-air mixture. Wang and Yu (2006) numerically showed that when operated in a dilute regime, smaller cyclones are helpful to achieve a higher efficiency and a lower pressure drop, the same as the predictions given by the empirical model of Plitt (1976). The simulated partition curves in the work of Wang and Yu (Wang and Yu, 2006) are shown in Fig. 2-10. Similar numerical results have been obtained by Ghodrati et al. (Ghodrati et al., 2013) who further revealed that the effect of cyclone size significantly varies with the feed solid concentration.

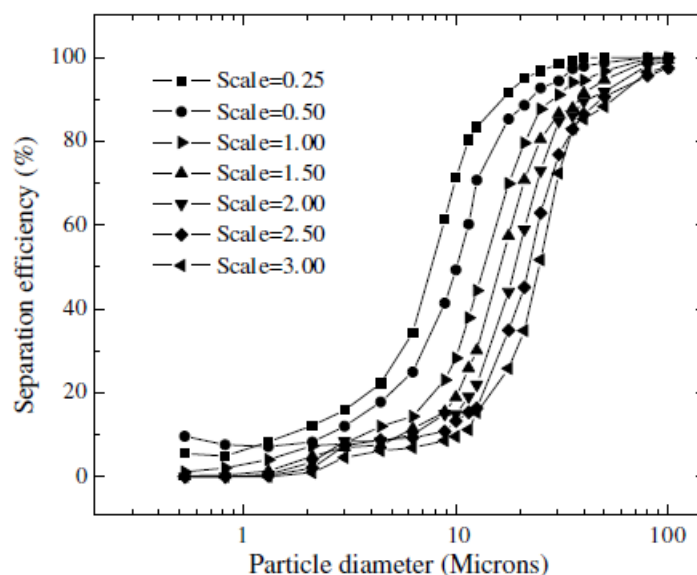


Fig. 2- 10 Effects of cyclone size on the partition curve (Wang and Yu, 2006)

2.3.2.2 Effect of hydrocyclone inlet feed type

Fig 2-11 shows two typical types of feed inlet, namely, the tangential one and involute (spiral) one.

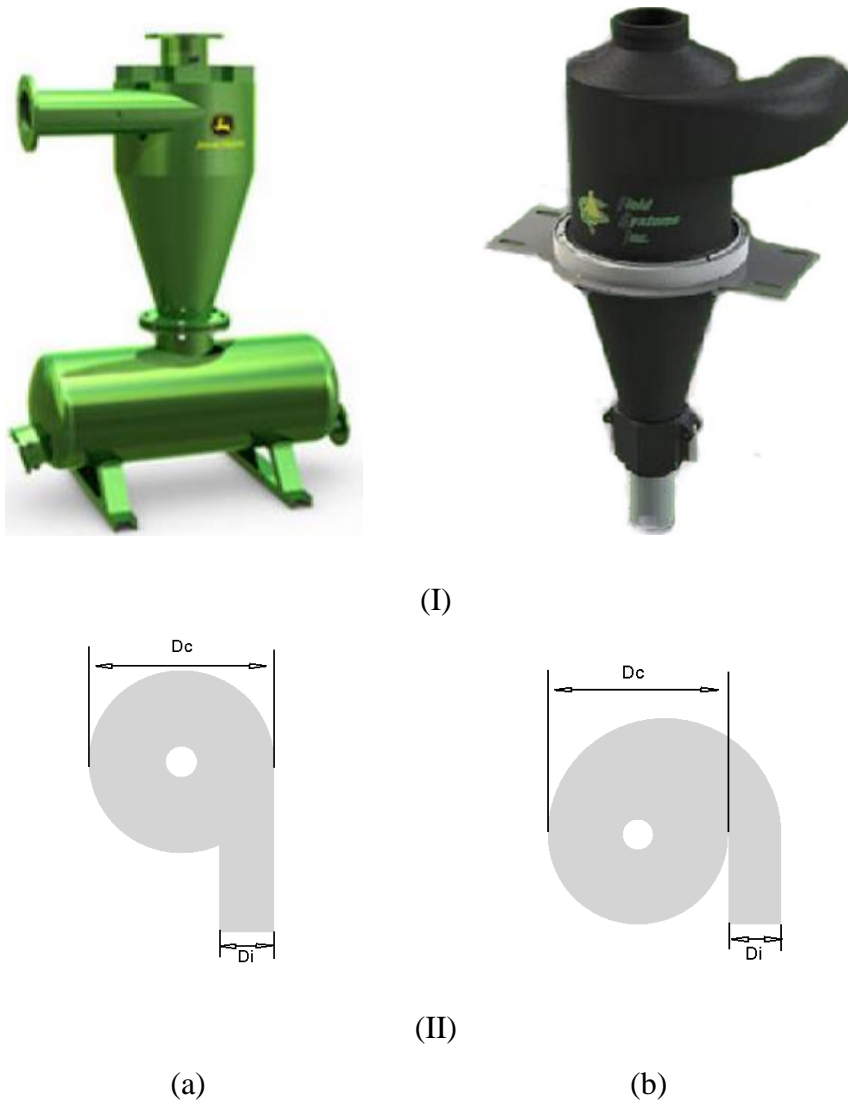


Fig. 2- 11 Hydrocyclones with (a) the tangential inlet and (b) involute inlet: (I) 3-D view and (II) top view

A few studies can be found on the effects of these two inlet feed types on the separation performance of hydrocyclones as well as of gas cyclones and dense medium cyclones (DMCs) (Zhao et al., 2006, Yoshida et al., 2004, Noroozi and Hashemabadi, 2009, Zhang et al., 2013, Zhang et al., 2017, Wang, 2009). For instance, the experimental partition curve of hydrocyclones with the tangential inlet and involute one were compared (Yoshida et al., 2004) as shown in Fig 2-12.

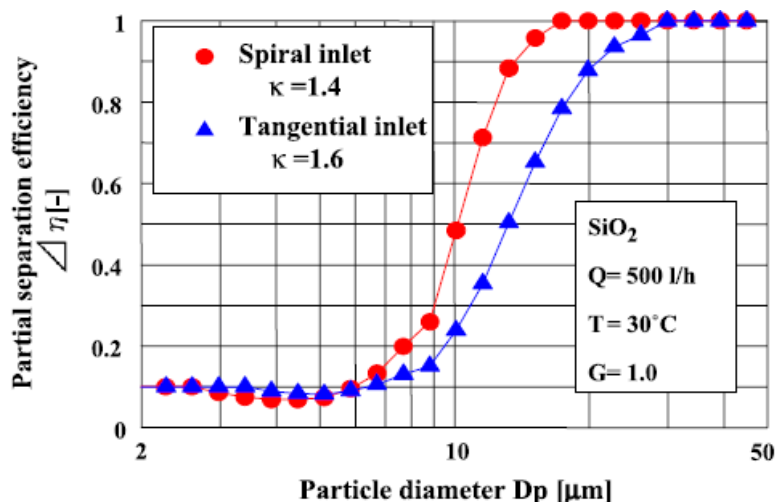


Fig. 2- 12 Classification curves of hydrocyclones with the tangential inlet and involute inlet (Yoshida et al., 2004)

The parameter κ is defined as the accuracy of classification and obtained by the following equation:

$$\kappa = \frac{d_{75}}{d_{25}} \quad (2-6)$$

It was concluded from this study that the hydrocyclone with the involute inlet has a smaller cut size, compared to that of the tangential inlet. Further, the partition curve for the involute inlet is sharper than that with the tangential inlet. This conclusion is the same as that concluded by Zhang et al. (Zhang et al., 2013).

Not only the cut size and separation sharpness are affected by the inlet feed type, but also the pressure drop and wear rate are affected as well (Xu et al., 2009). It is found that pressure drop for the tangential inlet is lower than that for the involute one. However, the erosion rate for the tangential inlet is higher compared with the involute one. It has been observed that there is an evident wear hot spot at the bottom of the cone section of the tangential-inlet hydrocyclones (Xu et al., 2009). While for the involute-inlet hydrocyclones in which pressure energy is smoothly transferred to the rotational momentum, the erosion rate is lower with a relatively uniform distribution.



Fig. 2- 13 Hydrocyclones with ‘spiral and slope’ inlet (Cavex hydrocyclones, Weir Minerals)

In recent years, a new inlet feed type named as ‘spiral and slope’ inlet here has been increasingly used in the industry (O'Brien et al., 2001). The configuration of hydrocyclones with ‘spiral and slope’ inlet is shown in Fig. 2-13. According to the brochure on Cavex hydrocyclones provided by Weir Minerals, this ‘spiral and slope’ inlet is superior to the previous inlet types with regards to the classification efficiency and wear rate. However, only a few deep and fundamental studies on this new inlet have been reported in literature.

2.3.3 Operational parameters

2.3.3.1 Feed flowrate and feed pressure

The operational parameters in hydrocyclone studies generally includes the feed flowrate, feed pressure, feed velocity and feed solid concentration. Actually, the variation of the inlet feed velocity can be reflected in the variation of feed flowrate if the inlet diameter is fixed. Therefore, the inlet feed flowrate is considered as an independent variable that affects the separation performance here.

Fig 2-14 shows the effect of flowrate on the classification curve as reported in a previous work (Slechta and Firth, 1984). It can be clearly seen that the classification

efficiency first increases with the increase of feed flowrate. If the feed flowrate continues to increase, the classification efficiency, however, begins to decrease, and finally have a roping phenomenon which represents a severely deteriorated classification. Similar findings were reported in a more recent research work (Mousavian and Najafi, 2009).

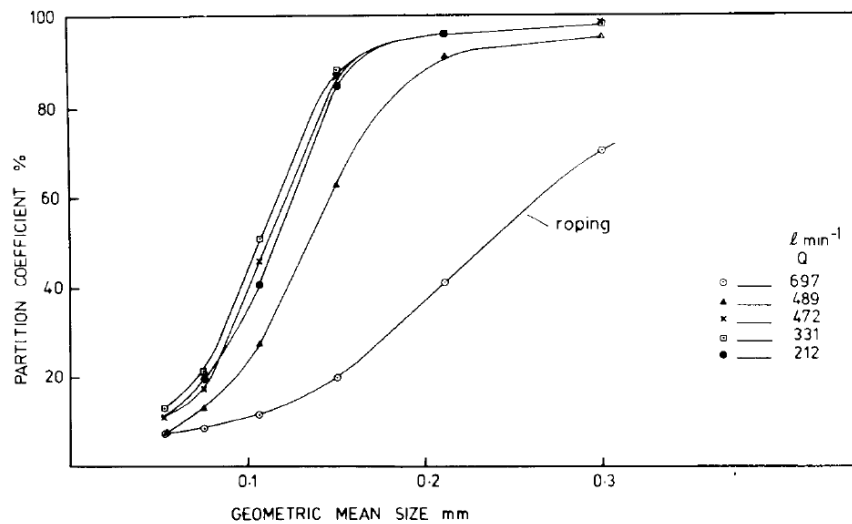


Fig. 2- 14 Classification curves at different flowrates (Slechta and Firth, 1984)

Some efforts have been made on investigating the effect of feed pressure on the separation performance of hydrocyclones in the past. Fig. 2-15 shows the results from a previous study on the feed pressure (Frachon and Cilliers, 1999). It is found that an increase in the feed pressure leads to a decrease in the cut size and an increase in the partition to the underflow. However, the classification sharpness was not affected by the variation of feed pressure. There are also some studies on the effect of feed pressure on the air-core instability (Cullivan et al., 2004), air-core diameter (Neesse and Dueck, 2007), and distributions of tangential velocity and axial velocity (Chiné and Concha, 2000).

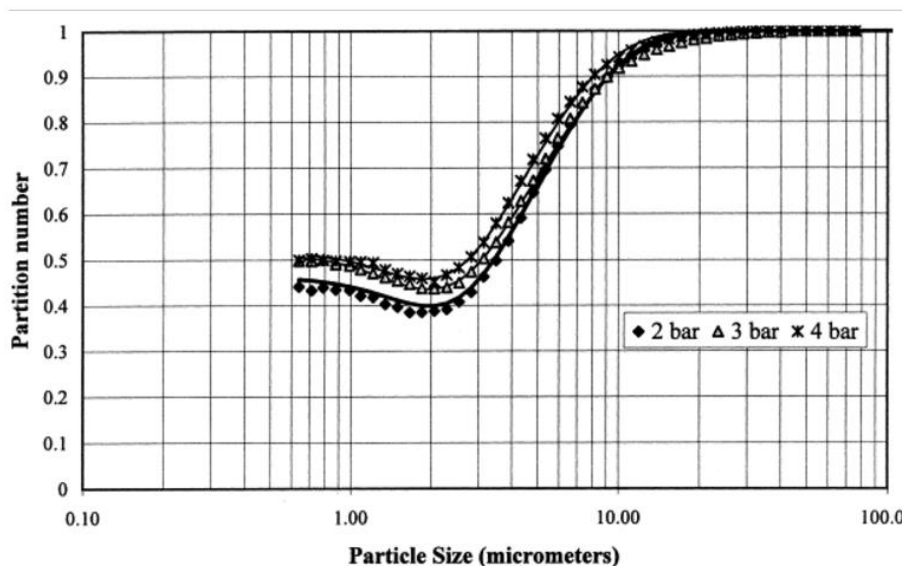


Fig. 2- 15 Classification curves at different feed pressures in the work of Frachon and Cilliers (Frachon and Cilliers, 1999)

2.3.3.2 Feed solid concentration

Hydrocyclones are usually confronted with dealing with materials under a wide range of solid concentrations in the industry, which contributes to the importance of understanding the effect of feed solid concentration. Some effort has been dedicated to studying the effect of feed solid concentration on the separation performance. For instance, Davailles et al. investigated the separation performance of hydrocyclones under a wide range of feed solid concentrations (Davailles et al., 2012) as shown in Fig. 2-16. It was concluded in this work that an increase in the feed solid concentration leads to an increase in the cut size and a decrease in the separation precision. Similar findings were also reported in other studies (Cilliers, 2000, Braun and Bohnet, 1990).

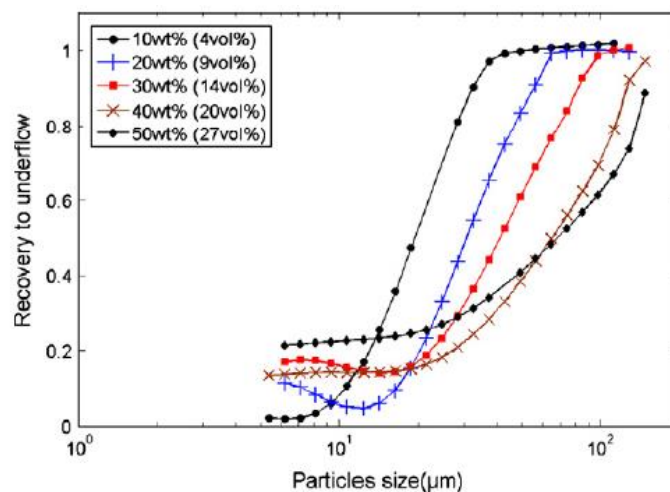


Fig. 2- 16 Experimental partition curves under different feed solid concentrations (Davailles et al., 2012)

Fig. 2-17 shows the simulated effect of feed solid concentration on the hydrocyclone classification curve as reported by a recent study (Kuang et al., 2012). The simulated variation trend of the cut size and separation sharpness with the feed solid concentration is consistent with the experimental work conducted by Davailles et al. (Davailles et al., 2012). More studies on the feed solid concentration coupled with geometrical parameters have also been conducted by Ghodrat et al. (Ghodrat et al., 2014a, Ghodrat et al., 2013).

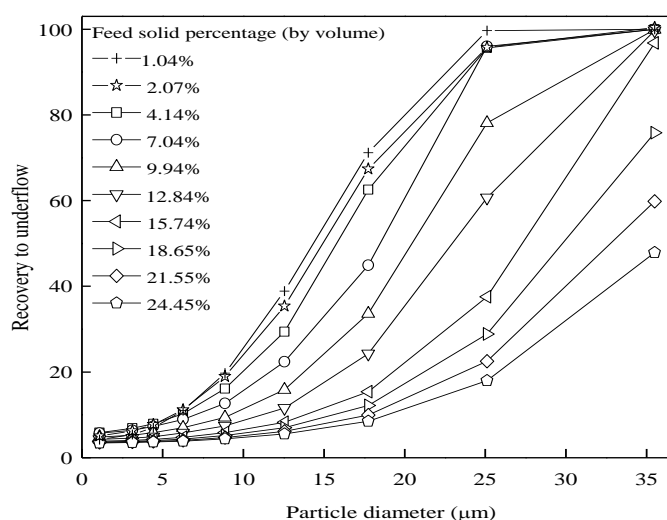


Fig. 2- 17 Simulated partition curves at different feed solid concentrations (Kuang et al., 2012)

2.3.4 Material parameters

2.3.4.1 Density effect

Generally, materials with the uniform density were considered in most of the previous studies on hydrocyclones. However, a broad particle density distribution can be present in the hydrocyclones, especially for dealing with coal particles, which can cause adverse effects on the performance of hydrocyclones and their downstream processes (Firth et al., 1999, Atkinson and Swanson, 2008). In this case, some ultrafine coal particles, either heavy or light, are entrained in the underflow stream or bypass the separation process. This situation leads to the loss of product (light particles) and the deterioration of the subsequent dewatering process, due to the high surface area of the entrained ultrafine particles. On the other hand, some light coarse particles are unexpectedly reported to the overflow or the upper outlet. Such particles often have a negative impact on the downstream operations such as the flotation, where the solid recovery drops when the particle size is too large.

One of the density distributions in the experiment of O'Brien et al. (O'Brien et al., 2001) is listed in Table 2-3.

Table 2- 3 One of the density distributions in the experiment of O'Brien et al. (O'Brien et al., 2001)

Size	Density					In size
	1.275	1.35	1.5	1.89	2.2	
1.41	8	3	1.5	0.5	1	14
0.71	9	3	0.5	0.5	1	14
0.42	3	1	0.5	0.5	1	6
0.30	3	1	0.5	0.5	1	6
0.21	3	0.5	0.5	0.5	1	5.5
0.15	3	0.5	0.5	0.5	1	5.5
0.115	3	0.5	0.5	0.5	1	5.5
0.08	2	0.5	0.5	0.5	1	4.5
0.045	6	9	4	3	17	39

However, only a few studies are found to focus on the effect of particle density. O'Brien et al. investigated the effect of particle density on the classification curve as shown in Fig. 2-18 (O'Brien et al., 2001). It can be concluded that an increase in the particle density contributes to a rise in the separation efficiency and a decrease in the cut size. The same variation trend of separation sharpness and cut size with the particle density can also be found in the work of Firth et al. (Firth et al., 1999).

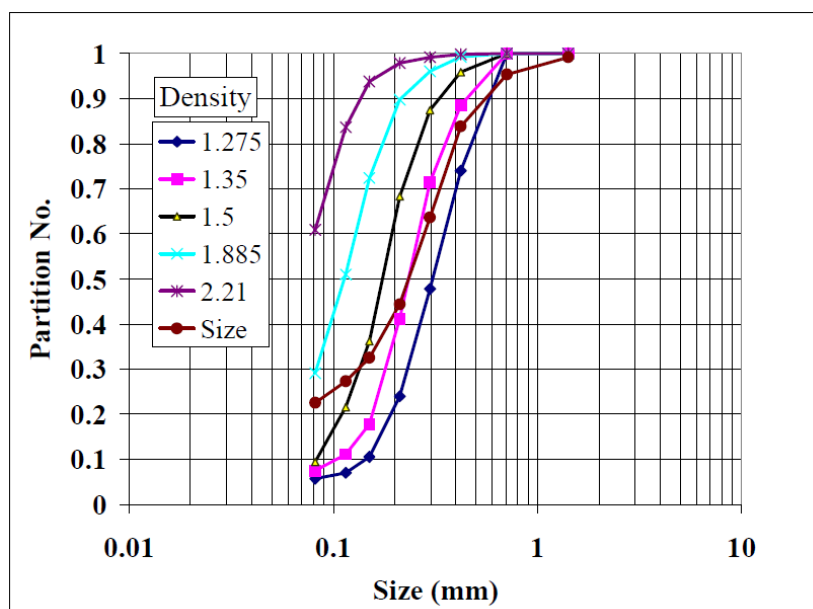


Fig. 2- 18 Experimental partition curves of coal with different densities (O'Brien et al., 2001)

Ghadirian et al. (Ghadirian et al., 2015) numerically and experimentally studied the separation behaviours of both light and heavy particles in a 51-mm hydrocyclone operated in a dilute regime, and found that increasing the vortex finder length results in an increased recovery of light particles to the overflow. Recently, Ghodrati et al. demonstrated that the misplacement problem associated with particle density can be mitigated using a long or convex-shaped conical section for a 1000 mm diameter hydrocyclone (Ghodrat et al., 2016).

Slechta et al. once investigated the effect of material relative density (ratio of the material density to water density) on the reduced partition curve as shown in Fig. 2-19 (Slechta and Firth, 1984). It can be concluded from this work that the reduced partition curve for coal is nearly as sharp as that for limestone and silica. This indicates that the effect of relative density on the reduced partition curve is not that

significant (Slechta and Firth, 1984), which is not consistent with findings on the effect of particle density reported by O'Brien et al. (O'Brien et al., 2001) and Firth et al. (Firth et al., 1999). That is to say that there are still uncertainties about the effect of particle density.

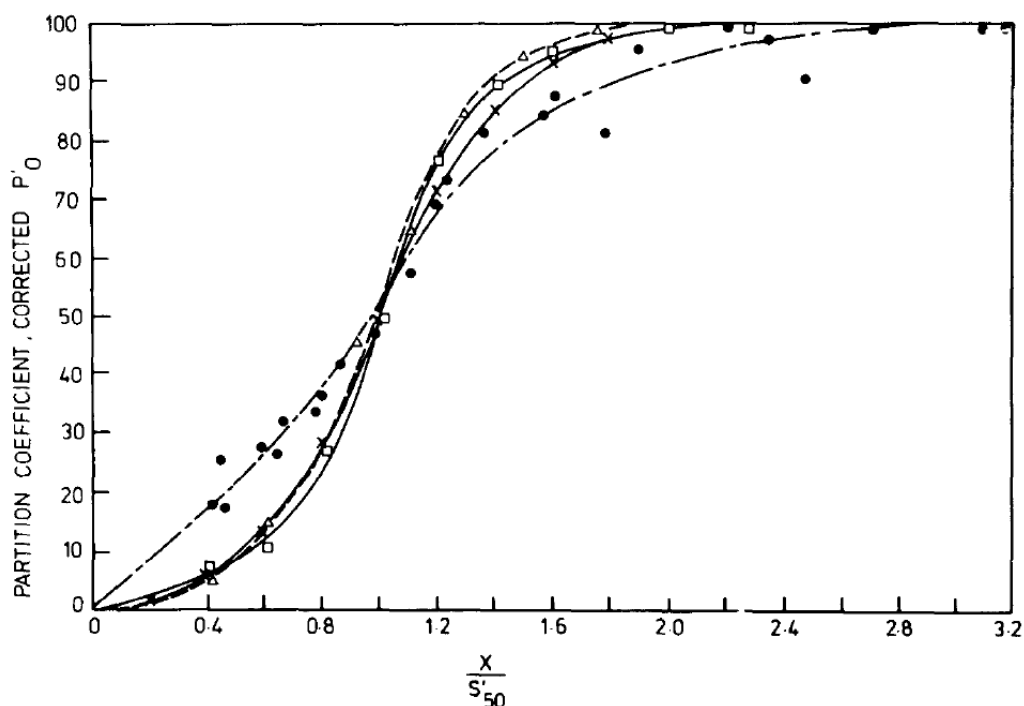


Fig. 2- 19 Reduced partition curves of different materials (Slechta and Firth, 1984)

Despite the limited studies on the separation behaviours of particles with different densities, particle density has been widely treated as a variable in empirical models predicting performances of hydrocyclones (Silva1 et al., 2012 , Narasimha et al., 2014, Schubert, 2007, Kraipech et al., 2006, Nageswararao et al., 2004, Kawatra et al., 1996, Cilliers and Hindet, 1991). Note that particle density in those empirical models was not considered as an independent variable; instead, it was first introduced in the equation of particle forces and then included in the performance equations of hydrocyclones For instance, the particle density was included in the equation of centrifugal force in Plitt's work (Plitt, 1976):

$$F_c = \pi \frac{d^3}{6} (\rho_s - \rho) \frac{V^2}{r} \quad (2-7)$$

There are also some empirical models which used the material-specific parameters to describe the effect of particle density. This simplified method of describing the effects of particle density can be found in the Nageswararao model (Nageswararao et al.,

2004, Nageswararao, 1978), Flintoff model (Flintoff and Plitt, 1987), and Narasimha model (Narasimha et al., 2014). However, the determination of these material-specific constants relies on previous surveys or test data of desired materials, which significantly affects the applicability of the approach. Further, this approach would not contribute to gaining the fundamental understanding of the effects of particle density.

Unlike the very limited studies on the density effect for hydrocyclones, extensive studies on the particle density effect have been made in recent years for DMCs which are also widely used to separate coal particles (see, e.g. Refs (Qi et al., 2015, Wang et al., 2014, Kuang et al., 2014, Narasimha et al., 2007b, Barbee et al., 2005, Chu et al., 2014, Chu et al., 2012a, Chu et al., 2009)). However, the functioning of DMC depends on the difference of particle density rather than particle size for hydrocyclones, and in addition, DMCs mainly deal with coarse coal particles from 0.5 mm to 50 mm. Thus, the DMC-related findings cannot be applied to hydrocyclones. To date, the effects of particle density on the flows and performance of hydrocyclones have not been well addressed.

2.3.4.2 Effect of feed size distribution

Similarly to the effect of particle density, the effect of feed size distribution was rarely reported as well. Slechta et al. once investigated two different feed size distributions which are shown in Fig. 2-20 (Slechta and Firth, 1984). Compared to the normalized size distribution, the modified size distribution in Fig. 2-19 has a much larger amount of near-size material (size range of 0.09-0.15 mm).

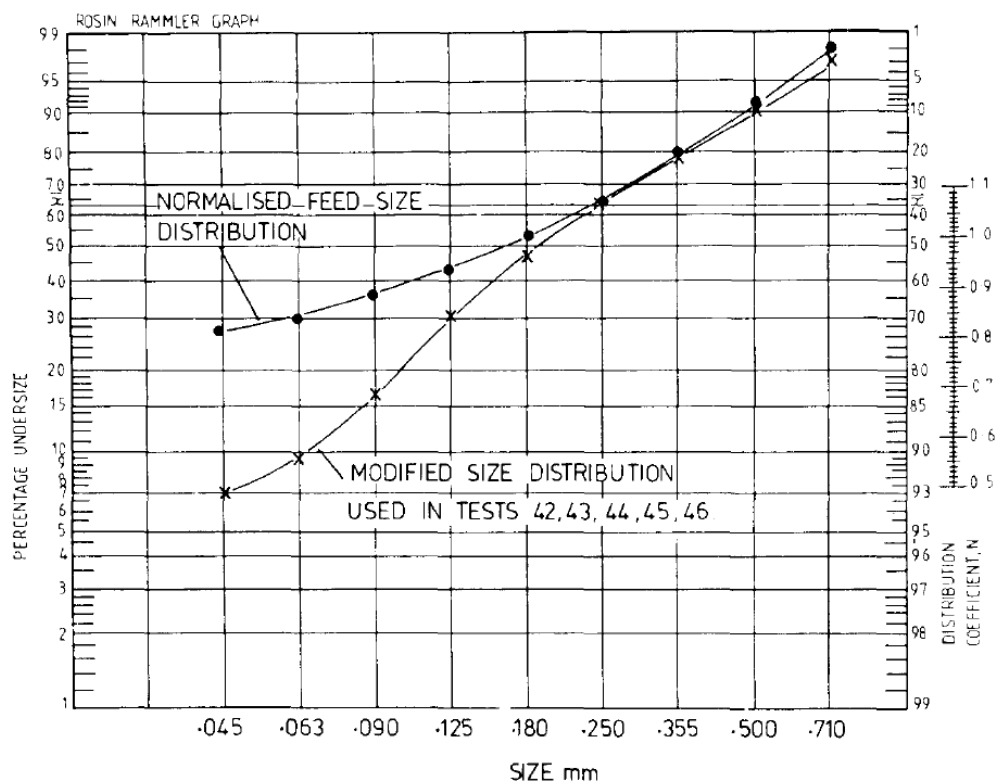


Fig. 2- 20 Feed size distributions used in the work of Slechta and Firth (Slechta and Firth, 1984)

It is found from this work that these two feed size distributions have a similar amount of water split. Further, the obtained reduced partition curve indicates that the classification capability of the hydrocyclone is not affected by the increased amount of near-size material which, however, leads to an increase in the amount of misplaced material.

Plitt once proposed that the effect of feed size distribution is not evident and can be neglected for normal situations (Nageswararao et al., 2004). However, he then reported that the trend that the cut size increases with the decrease of particle size can be obtained from his empirical equations (Plitt, 1976).

Nageswararao believed that it is logical to get different cut sizes if the size distribution of the feed is different even though all other parameters are kept the same (Nageswararao, 1978). It was explained as follows in his work. Generally, fine particles in the feed tend to flow with water; therefore they affect the particle classification with regards to increasing the apparent density and apparent viscosity of the fluid. Unlike the fine particles, the coarser particles are separated as a result of the

centrifugal action. The critical size at which particles are subjected to centrifugal action is related to the inlet feed velocity which determines the force field within the cyclone. For the feed which predominantly consists of coarse particles, particle-particle interactions and interferences contribute to the differences in classification behaviours. On the other hand, for the feed which predominantly consists of fine particles, the critical parameter affecting the cut size is thought to be the fraction of fine particles in the feed. These differences between the coarse particles and fine particle account for the obtained different cut sizes. To isolate the effect of size distribution on the cut size, he adopted a quantitative way by combining different equations. In his later published work (Nageswararao et al., 2004), he concluded that it is too complex to properly describe the feed material. To solve this issue, he adopted a method by including the feed material characteristics in the material-specific constants. Similar approaches were also used in other work (Narasimha et al., 2014, Flintoff and Plitt, 1987). However, as mentioned in Section 2.3.4.1, the determination of these material-specific constants relies on previous surveys or test data of desired materials, which significantly affects the applicability of this approach. Further, this approach would not contribute to gaining a fundamental understanding of effects of feed size distribution.

Even though there have been very limited studies on the effect of feed size distribution on the hydrocyclone performance, there are some studies on the trajectory or distribution of a single particle or a group of particles within hydrocyclones, which could be helpful for analyzing the effect of size distribution on the separation performance of hydrocyclones.

Fig. 2-21 shows how different-sized particles are distributed within a hydrocyclone in the work of Renner and Cohen (Renner and Cohen, 1978). They divided the whole hydrocyclone into four zones, each of which consisting of a specific size distribution. Region A is made up of material which has the identical size distribution to the feed; region B contains materials close to the size distribution of coarse particles; region C consists of materials with the same size with the fine product; and region D contains a larger number of intermediate-sized fractions than the feed. A similar study on the size distribution of a dispersed phase within a hydrocyclone has been conducted by using Phase Doppler Particle Analyser (PDPA) (Yang et al., 2011).

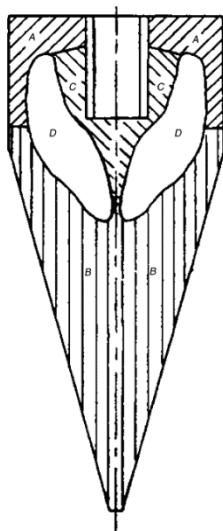


Fig. 2- 21 Four regions of similar size distributions within an operating hydrocyclone (Renner and Cohen, 1978)

Wang et al. (2007) investigated trajectories of different-sized particles in hydrocyclones, as shown in Fig. 2-22. He found that coarse particles are mainly trapped while fine particles escape from the cyclone. Because the centrifugal force acting on the finest particle is smaller than the fluid drag force, such particles find it difficult to move outwards to the wall of the cyclone. Conversely, coarse particles tend to stay near the conical cyclone wall when their sizes are over a critical value. For particles of the cut size in some areas of the conical section, they have the same possibility to escape from the vortex finder or to be discharged through the underflow. That is to say, such particles are found to be very unstable, and they have a longer residence time than particles with other sizes.

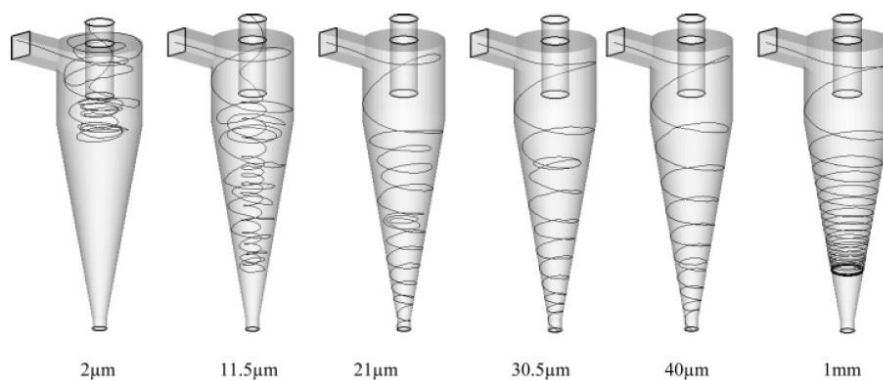


Fig. 2- 22 Trajectories of particles with different diameters in the work of Wang et al. (Wang et al., 2007)

Unlike in the case of hydrocyclones for which there are only very limited studies on the effect of size distribution on the separation performance, a systematic study on the feed size distribution has been reported for DMCs (Chen et al., 2016). In this work, Johnson's SB function was used as the general function to represent the particle size distribution of materials as suggested in the earlier studies (Yu and Standish, 1990, Yu, 1994). The probability density distribution function (PDF) of the size distribution is given by:

$$f_{SB}(d) = \frac{d_{max} - d_{min}}{(d - d_{min})(d_{max} - d)} \times \exp \left\{ -\frac{\sigma_j^2}{2} \left[\ln \left(\frac{d - d_{min}}{d_{max} - d} \right) - \ln \left(\frac{d_{0.5} - d_{min}}{d_{max} - d_{0.5}} \right) \right]^2 \right\} \quad (2-8)$$

where $d_{min} \leq d \leq d_{max}$, $d_{0.5}$ represents the median size, and σ_j describes the spread of the particle size distribution. Johnson's SB function can be reduced to a two-parameter function because d_{min} and d_{max} may be determined from measurements or other physical considerations. A series of size distributions was considered in the work of Chen et al. as shown in Fig. 2-23, in which Fig. 2-23 (a) demonstrates these size distributions with a varied mean size while σ_j is being kept constant, and Fig. 2-23 (b) shows the size distributions with different values of σ_j while the mean size is being kept constant. It is found that the size distribution parameters, i.e. $d_{0.5}$ and σ_j , affect the separation performance of DMCs significantly (Chen et al., 2016).

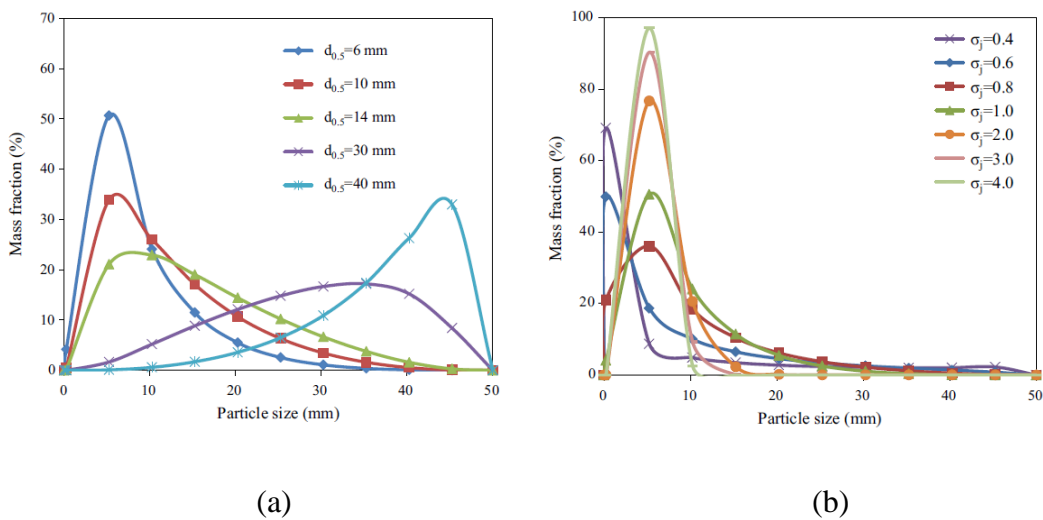


Fig. 2- 23 considered size distributions with (a) different mean sizes and (b) different spread constants in a previous study (Chen et al., 2016)

2.4 Methods to study the multiphase flow in hydrocyclones

2.4.1 Experimental method

In the past years, much effort has been spent on experimentally studying the multiphase flow in hydrocyclones. Various techniques have been adopted to better understand the flow field and particle motion in hydrocyclones. Some typical experimental measurements are listed in Table 2-3. Even though carrying out experiments is a basic and reliable way to study hydrocyclones, it is expensive and not so flexible.

Table 2- 4 Summary of the work on hydrocyclones by experiments

Researchers	Technique	Main contributions
Kelsall (Kelsall, 1952)	Photography	Measurement of the tangential and axial velocity
Knowles et.al. (Knowles et al., 1973)	Photography	Measurement of the tangential and axial velocity with the absence of air-core
Dabir (Dabir, 1983)	Laser Doppler Velocimetry (LDV)	Measurement of the tangential and axial velocity and reverse flows
Williams et.al. (Williams et al., 1995)	Electric Resistance Tomography (ERT)	Measurement of the movement of air-core
Dai et.al.(Dai et al., 1999)	particle dynamics analyser (PDA)	LZVV line
Inaki Schlaberg (Inaki Schlaberg et al., 2000)	Ultrasonic Tomography (UT)	Measurement of the size and position of air-core
Chu et.al. (Chu	PDA	Measurement of the radial and axial

et al., 2002)		velocity under different parameters
Fisher et.al. (Fisher and Flack, 2002)	LDA	Measurement of the velocity field under different flowrates and reject rates
Bai et.al. (Bai et al., 2009)	PDA	Measurement of the air bubble diameter
Marins et.al. (Marins et al., 2010)	LDA/PDA	Measurement of the velocity field which can be used to validate numerical models
Yang et.al. (Yang et al., 2011)	PDA	Measurement of the zero axial velocity wave zone and size distribution of particles
Zhang et.al. (Y.H. Zhang, 2011)	PDA	Measurement of the velocity field, circular flow, and zero velocity value
Hang. et.al. (Hang et al., 2011)	Positron Emission Particle Tracking (PEPT)	High-speed flows with the sufficient spatial and temporal resolution to reveal flow details
Wang et.al. (Wang et al., 2016)	Volumetric 3-component velocimetry (V3V)	Visualization of the vertical velocity (LZVV), short-circuit flows and secondary vortexes

2.4.2 CFD-LPT (Lagrangian Particle Tracking) approach

Generally speaking, the modelling method of hydrocyclones can be discrete- or continuum-based with respect to the treatment of solid phase, which is respectively represented by the LPT, TFM, or DEM approach. The general modelling strategy for CFD-LPT is shown in Fig. 2-24. To be specific, water and air are considered as fluids in the step 1. Reynolds stress model (RSM) is used to model the turbulence, and volume of fluid (VOF) model used is for the determination of interface between the

liquid and air-core. A stable velocity and pressure field are first obtained by this step. After that, the Lagrangian approach is used to directly track the trajectory of each individual particle based on the velocity and pressure predicted by the CFD simulation in the step 1 (Wang and Yu, 2006).

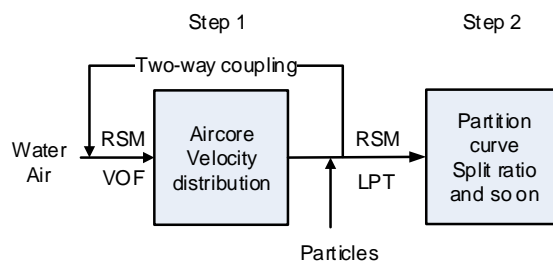


Fig. 2- 24 Modelling strategy for CFD-LPT model

Because this approach ignores the effect of inter-particle interactions as well as the reactions of particles on the fluid, it is suitable for dilute flows and systems where the particles-wall interaction does not significantly change fluid transport properties. In particular, this approach works well for those systems in which the particle size is large and the particle number is small. A particle can be tracked along its path by balancing the force acting on it in the carrier fluid. Further, corrections of the particle trajectory because of the interaction effects with its surrounding environment can be included as well. The effect of particles on the fluid can be considered by including a source term in the governing equations of fluids.

The Lagrangian approach has been used to numerically study hydrocyclones. For instance, Hsieh et.al (Hsieh, 1988, Hsieh and Rajamani, 1991) used this method to predict classification curves of hydrocyclones. The results show that the predicted ones agree well with the experimental ones. Wang et al. utilized the CFD-LPT approach to study the multiphase flow in hydrocyclones under a wide range of geometrical conditions (Wang, 2009, Wang and Yu, 2006). Similarly, Delgadillo et al. explored a series of new designs of hydrocyclones by this method (Delgadillo and Rajamani, 2007). Murthy et al. also adopted this approach to investigate the velocity and pressure field in hydrocyclones (Murthy and Bhaskar, 2012).

The researchers also dedicated some efforts on applying the Lagrangian approach to model dense flows by coupling it with some techniques. The earliest attempt is

attributed to Rajamani et.al. who predicted slurry concentrations and modified the fluid viscosity for dense flows (Rajamani and Milan, 1992). The method turned out to be applicable even when the feed solid concentration is as high as 35% by weight. Wang et al. also modified the fluid viscosity to simulate the dense flow in hydrocyclones based on an equation of viscosity in his later work (Cai and Wang, 2013). Further, the dense discrete phase model (DDPM) which combines the LPT with the kinetic theory was used over a wide range of feed solids concentrations in a recent study (Zhou et al., 2016).

2.4.3 TFM approach

The TFM approach considers both the fluid (liquid and air) and solid phases as the interpenetrating continua. Particles of different sizes or densities represent different phases. TFM methods include the full Eulerian multiphase approach and simplified Eulerian approach such as the Mixture and VOF models.

2.4.3.1 VOF model

In the VOF model, two fluids i.e. gas and liquid share a single set of momentum equation, and the volume fraction of each fluid is computed in the whole computational domain (ANSYS, 2012, Wang and Yu, 2009). The determination of the interface between the air-core and liquid is a transient process. The VOF model has been used to study the air-core in hydrocyclones (Narasimha et al., 2006, Evans et al., 2008, Delgadillo and Rajamani, 2009)

2.4.3.2 Mixture model

The mixture model is a simplified TFM method to compute the flow of dispersed phases in an efficient way. Unlike the VOF approach, all the phases involved are interpenetrating and can move either at the same velocity or different velocities (ANSYS, 2012). For simulations in which particles are moving at different velocities, certain slip velocities between different phases are introduced. Particles with the same size or density are considered as one phase. Only one set of governing equation is solved for the mixture of liquid, air, and particles. More details about the mixture model can be found elsewhere (Kuang et al., 2012, Ghodrat, 2014, ANSYS, 2012). Apart from being used to model the multi-phases, the mixture model can also be used to determine the interface between the air and solid as VOF model does (Kuang et al.,

2012, Wang and Yu, 2009, Brennan et al., 2007). Different from the VOF model which excludes the slip velocity to evaluate volume fractions, the mixture model needs a bubble size to calculate the slip velocity (Kuang et al., 2012).

The mixture model has been widely used to study the multiphase flow in hydrocyclones. For instance, Brennan et al. reported that the mixture model can predict the velocity field, air-core location, and classification curves (Brennan et al., 2007). Further, both Kuang et al. (Kuang et al., 2012) and Davailles et al. (Davailles et al., 2012) utilized the mixture model to study the effect of feed solid concentration on the separation performance of hydrocyclones. The reasonable agreement between the experimental data and numerical data provides support for the applicability of the mixture model in hydrocyclones studies. Ghodrat et al. also applied the mixture model to investigate hydrocyclones with different geometrical conditions at a wide range of feed solid concentrations (Ghodrat et al., 2014b, Ghodrat et al., 2014a). In a later work of Ghodrat et al., the mixture model was reported to be not accurate enough to model different-sized particles with a wide range of densities in hydrocyclones (Ghodrat, 2014).

2.4.3.3 Eulerian-Eulerian model

The full TFM model is known as the Eulerian-Eulerian model. Compared with the VOF and mixture models, the Eulerian-Eulerian model is much more complicated and computationally intensive because it solves the full set of the conservative equations with regard to momentum and mass of each phase involved. Consequently, it was reported that the Eulerian-Eulerian model is expected to produce a more accurate solution than the mixture model. The averaged continuity and momentum equations for the phase k are given by (Ghodrat et al., 2016):

$$\frac{\partial}{\partial t}(\alpha_k \rho_k) + \nabla \cdot (\alpha_k \rho_k \vec{u}_k) = 0 \quad (2-9)$$

and

$$\frac{\partial}{\partial t}(\alpha_k \rho_k \vec{v}_k) + \nabla \cdot (\alpha_k \rho_k \vec{u}_k \vec{u}_k) = -\alpha_k \nabla p - \nabla p_{s,k} + \nabla \cdot \bar{\tau}_k + \alpha_k \rho_k \vec{g} + F_D \quad (2-10)$$

where k denotes different phases: $k = 1$ is for water, 2 for air, and 3 - N for the k th type of particles; α_k , ρ_k and \vec{u}_k are the volume fraction, density and velocity of phase

k respectively; $p_{s,k}$ ($k \geq 3$) is the k th solid pressure and described by the correlation of Lun et al. (1984), and $\bar{\tau}_k$ is the k th phase stress-strain tensor and expressed as:

$$\bar{\tau}_k = \alpha_k \mu_k (\nabla \vec{u}_k + \nabla \vec{u}_k^T) + \alpha_k \left(\lambda_k - \frac{2}{3} \mu_k \right) \nabla \cdot \vec{v}_k \bar{I} \quad (2-11)$$

where μ_k and λ_k are the shear and bulk viscosity of phase k , which are respectively given by correlations of Gidaspow et al. (1991) and Lun et al. (1984) for solid phases.

The kinetic theory based on the algebraic model of temperature model (Syamlal et al., 1993) is used to determine the solid granular temperature needed to describe solid properties such as solid pressure drop, solid shear viscosity, and bulk viscosity:

$$0 = -(p_k \bar{I} + \bar{\tau}_k) : \nabla \vec{u}_k - \gamma_\theta + \phi_{l,k} \quad (2-12)$$

where $-(p_k \bar{I} + \bar{\tau}_k) : \nabla \vec{u}_k$ is the generation of energy by the solid tensor, γ_θ is the collisional dissipation of energy, and $\phi_{l,k}$ is the energy exchange between the l th fluid or solid phase and the k th solid phase.

The drag force F_D in Eq. (2-10) is determined by the well-known Wen and Yu (1966) & Ergun (1952) correlations for particles:

$$F_D = \begin{cases} \frac{3}{4} C_D \frac{\alpha_k \alpha_1 \rho_1 |\vec{u}_k - \vec{u}_1|}{d_k} \alpha_1^{-2.65} (\vec{u}_1 - \vec{u}_k) & \alpha_1 \leq 0.8 \\ \left(150 \frac{\alpha_k (1 - \alpha_1) \mu_1}{\alpha_1 d_k^2} + 1.75 \frac{\alpha_k \rho_1 |\vec{u}_k - \vec{u}_1|}{d_k} \right) (\vec{u}_1 - \vec{u}_k) & \alpha_1 > 0.8 \end{cases} \quad (2-13)$$

and by the Schiller and Naumann (1933) correlations for air bubbles.

$$F_D = \begin{cases} 18 \mu_1 \frac{\alpha_k}{d_k^2} (1 + 0.15 Re^{0.687}) (\vec{u}_1 - \vec{u}_k) & Re \leq 1000 \\ 0.33 \mu_1 \frac{\alpha_k}{d_k^2} (Re) (\vec{u}_1 - \vec{u}_k) & Re > 1000 \end{cases} \quad (2-14)$$

To model the anisotropic turbulence problems as encountered in hydrocyclones, either Reynolds stress model (RSM) or large eddy simulation (LES) should be used. The two models generally give comparable results (Delgadillo et al., 2012, Mousavian and Najafi, 2009, Brennan et al., 2007, Delgadillo and Rajamani, 2005, Narasimha et al., 2006). However, the LES model is computationally very demanding for large hydrocyclones as considered here, because its meshes need to be strictly scaled to the 9/4 power of the Reynolds number (Wilcox, 1994) to produce valid results. More importantly, for Eulerian-Eulerian multiphase models, a reliable and general LES

model has not been developed. Consequently, when the TFM model is adopted, LES turbulence models cannot be accessed in the commercial software — ANSYS Fluent. As such, RSM is adopted and combined with a standard wall function (Launder et al., 1975).

$$\frac{\partial}{\partial t}(\rho \overline{u'_i u'_j}) + \frac{\partial}{\partial x_k}(\rho u_k \overline{u'_i u'_j}) = D_{T,ij} + P_{ij} + \phi_{ij} + \varepsilon_{ij} \quad (2-15)$$

where $D_{T,ij}$, P_{ij} , ϕ_{ij} and ε_{ij} represent the turbulent diffusion, stress production, pressure strain, and dissipation, respectively.

The full Eulerian model has been used to study hydrocyclones. For instance, Nowakowski et al. proposed the concept and principle of utilizing this model to predict the hydrocyclone performance (Nowakowski et al., 2000). The Eulerian–Eulerian model was also used to study the flow behaviour and effects of flow rate on the separation efficiency (Swain and Mohanty, 2013). Similarly, effects of feed solid concentration, inlet feed velocity, rod inserted in the middle of the hydrocyclone and spigot diameter on the separation performance of hydrocyclones were also studied by this model (Safa and Goharrizi, 2014). Recently, Ghodrat et al. (Ghodrat et al., 2016) applied the full Eulerian model for investigating the effect of particle density.

Even though the TFM models, including the full Eulerian approach and simplified Eulerian approaches such as the Mixture and VOF models, have been widely applied to investigate the flow in hydrocyclones, it is quite challenging for TFM models to handle particles with a broad range of size distributions and density distributions which are common in hydrocyclones.

2.4.4 CFD-DEM/TFM-DEM approach

The combined approach of CFD or TFM with DEM offers the convenience to model the particle size/density distribution which is challenging for the TFM models. It can also consider particle-particle and particle-fluid interactions which are ignored by the CFD-LPT model. However, one deficiency of the CFD-DEM or TFM-DEM approach is its high computational cost because each individual particle is tracked by Newton's second law.

Normally, for the CFD-DEM or TFM-DEM approach, the motion of particles is considered as discrete entities, with Newton's laws of motion being applied to

individual particles, while the fluid (solid particles are included for TFM-DEM) is treated as a continuous phase, by applying the local averaged Navier-Stokes equations in each computational cell. The detailed descriptions about CFD-DEM or TFM-DEM approached can be found elsewhere in literature (Chu et al., 2011).

The CFD-DEM or TFM-DEM (Hernández-Jiménez et al., 2015, Wang et al., 2015) approach has been adopted to model different fluid-particle flow systems like in DMCs (Chu et al., 2012a, Chu et al., 2012b, Chu and Yu, 2008), gas cyclones (Chu et al., 2011), and fluidized bed (Alobaid and Epple, 2013, Alobaid et al., 2013, Cello et al., 2009, Fries et al., 2013). However, very few CFD-DEM or TFM-DEM studies on hydrocyclones are found except in a preliminary work by Zhou et al. (2010). In this work, mono-sized particles with a diameter of 2 mm are considered in a 75 mm diameter hydrocyclone. This is not consistent with the industry applications of 75 mm diameter hydrocyclones, which generally deal with multi-sized particles of much smaller sizes than 2 mm.

Actually, it is extremely computational demanding for the standard CFD-DEM or TFM-DEM model to model industry-scale particle systems. For instance, in a hydrocodone with a diameter of 75 mm, there would be hundreds of billions of particles at the feed solid concentration of 4%, which is extremely challenging for the stand CFD-DEM or TFM-DEM models. This situation is even worse for dense flows which are also common in the hydrocyclone industry. To overcome this deficiency, the CFD-DEM or TFM-DEM model with different treatments such as parcel-particle concept, coarse-grain (CG) model, similar particle assembly model or scaling laws have been developed for various particulate systems (Chu et al., 2009, Sakai and Koshizuka, 2009, Thakur et al., 2016, Mokhtar et al., 2012, Chu et al., 2016). Actually, the CG concept has been extensively used to dramatically reduce the computational cost in molecular dynamics simulation which has a very similar algorithm to DEM (Tozzini, 2005, Klein and Shinoda, 2008, Noid, 2013).

Chu et al. introduced the CG concept in details and applied it to studying DMCs (Chu et al., 2016). A brief introduction of the CG concept is described here for brevity. The total energy (including potential and kinetic energy) of a CG particle system is the same as that in a real system:

$$E^{cg} = \sum_{i=1}^{i=N_p} E^o \quad (2-16)$$

where E is the total energy. Superscripts cg and o represent variables corresponding to CG particles and original particles respectively. N_p is the number of real particles included in a coarse grain, and $N_p = \alpha^3$ (α is the size ratio of CG particles to real particles). The density of CG particles and real particles is the same ($\rho^{cg} = \rho^o$). This setting is to make sure that the similar packing porosity and density of the CG and original systems can be reached. Consequently, $m_i^{cg} = \alpha^3 m_i^o$ and $V_i^{cg} = \alpha^3 V_i^o$, m and V are the mass and volume of CG real particles, respectively.

Both the potential and kinetic energy are included for the energy E in Eq. (2-16). The potential energy considered here is due to the gravity, which is conserved on the condition that mass is conserved. To make sure of the conservation of kinetic energy, the velocity of coarse grains should be the same as that of the original particles if their mass is equal. Therefore, Eq. (2-16) is transferred to:

$$\mathbf{V}^{cg} = \mathbf{V}^o \quad (2-17)$$

where \mathbf{V} is the velocity of CG or original particles. Eq. (2-17) can be rewritten as below according to Momentum and Impulse:

$$\mathbf{f}^{cg} t^{cg} = \alpha^3 \mathbf{f}^o t^o \quad (2-18)$$

where t^{cg} and t^o are the acting time of forces acting on the CG and original particles, respectively. Now the main aim is to solve Eq. (2-18) and to obtain the value of \mathbf{f}^{cg} , after which the motion of the coarse particle can be determined.

For particle-fluid forces, the acting time of the CG system is equal to that of the real system. Consequently, Eq. (2-18) is rewritten as:

$$\mathbf{f}_{pfi}^{cg} = \alpha^3 \mathbf{f}_{pfi}^o \quad (2-19)$$

However, the acting time of particle-particle interaction forces exerted on CG and original particles may be different. Here, only the normal contact force (represented by the subscript “cn”) is scaled when interaction forces are modelled. To solve Eq. (2-18) in terms of modelling normal contact force between CG particles, the moving velocity of CG particles is equal to and that of real particles, the relationship that $t_{cn}^{cg} \approx \alpha t_{cn}^o$ can be assumed if $d^{cg} = \alpha d^o$. Therefore, Eq. (2-18) is rewritten as below:

$$\mathbf{f}_{cn,ij}^{cg} = \alpha^2 \mathbf{f}_{cn,ij}^o \quad (2-20)$$

Note that there are no general agreements on the particle-particle interaction forces and the scaling may be varied with the specific situations (Thakur et al., 2016).

2.4.5 Empirical model

In the past, researchers (T.C.Rao et al., 1976, Dietz, 1981, Cilliers and Hindet, 1991, Schubert, 2007, Narasimha et al., 2012, Narasimha et al., 2014) have focused on collecting the experiment data to develop empirical models to predict the hydrocyclone performance. This empirical approach is fast, portable and easily applied in the industry. Three previously developed empirical models which are widely used to predict the hydrocyclone performance are reviewed in the following sections.

2.4.5.1 Plitt model

Plitt et al. (Plitt, 1971, Plitt, 1979) proposed the Plitt model which has been widely used to predict the hydrocyclones performance without relying on additional experimental data. In the Plitt model, the cyclone performance is described by four fundamental parameters, i.e. pressure drop, cut size, split ratio, and separation sharpness.

Pressure drop ΔP :

$$\Delta P = \frac{1.316 \cdot 10^5 \cdot Q^{1.78} \exp(0.55\varphi)}{D_c^{0.37} \cdot D_i^{0.94} \cdot (L - l)^{0.28} \cdot (D_u^2 + D_o^2)^{0.87}} \quad (2-21)$$

Cut size d_{50c} :

$$d_{50c} = \frac{0.00269 \cdot D_c^{0.46} \cdot D_i^{0.6} \cdot D_o^{1.21} \exp(6.3\phi)^{0.36}}{D_u^{0.71} \cdot (L-l)^{0.38} \cdot Q^{0.45} \cdot (\rho_s - \rho_l)^{0.5}} \quad (2-22)$$

Split ratio S (ratio of the volumetric flow rate in the underflow to that in the overflow):

$$S = \frac{34.4 \left[\frac{D_u}{D_o} \right]^{3.31} \cdot (L-l)^{0.54} \cdot (D_u^2 + D_o^2)^{0.36} \exp(0.54\phi)}{(\Delta P)^{0.24} \cdot D_c^{1.11}} \quad (2-23)$$

Separation sharpness m :

$$m = 1.272 \exp(-1.58R_V) \left(\frac{D_c^2 h}{Q} \right)^{0.15} \quad (2-24)$$

R_V is the volume recovery to the underflow, defined by:

$$R_V = \frac{S}{S+1} \quad (2-25)$$

where D_u is the spigot diameter; D_i is the inlet diameter (or equivalent diameter by area); D_o is the vortex finder diameter; D_c is the cyclone diameter; ϕ is the volume fraction of solid in the feed; L is the total length of cyclone; l is the length of vortex finder; ρ_s is the solid density; ρ_l is the fluid density; h is the distance from the bottom of vortex finder to the spigot ($h = L - l$); Q is the volumetric feed flow rate. Note all the parameters in the Plitt model described in this chapter are in SI units.

The original Plitt model provides default model parameters which are independent of the feed size characteristics (Plitt, 1971). In his later work, an optional model with F_{50} (median feed size, that is 50% passing size) was provided as a variable, which was considered as a simple approximation to the feed size effect. However, this approximation was commented as questionable by Nageswararao et al. (Nageswararao et al., 2004). Flintoff revised the Plitt model and provided F factors for calibrations due to the differences in feed material characteristics (Flintoff and Plitt, 1987).

2.4.5.2 Nageswararao model

Nageswararao developed a set of equations to describe the relationship between the geometrical, operational, and material variables and hydrocyclone performance characteristics (Nageswararao, 1978, Nageswararao et al., 2004).

The resulting equations are:

$$\frac{Q}{D_o^2 \sqrt{P/\rho_P}} = K_{Q_o} D_c^{-0.10} \left(\frac{D_o}{D_c}\right)^{0.68} \left(\frac{D_i}{D_c}\right)^{0.45} \left(\frac{L_c}{D_c}\right)^{0.20} \theta^{-0.10} \quad (2-26)$$

$$\frac{d_{50c}}{D_c} = K_{D_o} D_c^{-0.65} \left(\frac{D_o}{D_c}\right)^{0.52} \left(\frac{D_u}{D_c}\right)^{-0.50} \left(\frac{D_i}{D_c}\right)^{0.20} \left(\frac{L_c}{D_c}\right)^{0.20} \theta^{0.15} \left(\frac{P}{\rho_P g D_c}\right)^{-0.22} \lambda^{0.93} \quad (2-27)$$

$$R_f = K_{W_o} D_c^{0.00} \left(\frac{D_o}{D_c}\right)^{-1.19} \left(\frac{D_u}{D_c}\right)^{2.40} \left(\frac{D_i}{D_c}\right)^{0.50} \left(\frac{L_c}{D_c}\right)^{0.22} \theta^{-0.24} \left(\frac{P}{\rho_P g D_c}\right)^{-0.53} \lambda^{0.27} \quad (2-28)$$

$$R_V = K_{V_o} D_c^{0.00} \left(\frac{D_o}{D_c}\right)^{-0.94} \left(\frac{D_u}{D_c}\right)^{1.83} \left(\frac{D_i}{D_c}\right)^{0.25} \left(\frac{L_c}{D_c}\right)^{0.22} \theta^{-0.24} \left(\frac{P}{\rho_P g D_c}\right)^{-0.31} \quad (2-29)$$

where λ is the hindered settling factor, defined as below:

$$\lambda = \frac{C_V}{(1 - C_V)^2} \quad (2-30)$$

θ is the cone angle; C_V is the feed volume fraction of solids; P is the inlet pressure; K_{Q_o} , K_{D_o} , K_{W_o} , and K_{V_o} are constants related to material properties.

Unlike the Plitt model which provides default model parameters, Nageswararao model is used to predict performance characteristics based on the specific material constants which can be obtained from test data of the desired material. Alternatively, the appropriate K values can be obtained from previous surveys or a parameter database. Even though a source of the material-specific constants was developed to enable users to select their values, it is suggested that caution should be exercised to use the simulation results based on these selected values. As suggested in the published work (Nageswararao et al., 2004), the ideal way to determine the material specific constants for this model is from a test using a geometrically similar (or same) cyclone. Further, the same materials should be classified in cyclones with the same inlet feed type. Certainly, this may be difficult to obtain in practice and the experience using this model is necessary. Therefore, the determination of these specific material constants significantly limits the applicability of this model. Further, the Nageswararao model was developed only based on the higher feed solid concentration i.e. 38-73% (by weight), which further affects its applicability.

2.4.5.3 Narasimha model

Narasimha et al. developed a semi-empirical hydrocyclone model by collecting historical data (Narasimha et al., 2014). CFD simulations were used to elucidate the inputs on the particle classification mechanism and to identify the key parameters that affect the cyclone performance. The relationship between the key variables and hydrocyclone performance parameters (which include cut size, water split, capacity, and separation sharpness) are found.

The water split R_f is expressed as

$$R_f = K_w \left(\frac{D_o}{D_c}\right)^{-1.06787} \left(\frac{D_u}{D_c}\right)^{2.2062} \left(\frac{V_t^2}{R_{max}g}\right)^{-0.20472} \left(\frac{1}{\tan\left(\frac{\theta}{2}\right)}\right)^{0.829} \\ \times \left(\frac{\mu_m}{\mu_w}\right)^{-0.7118} \left(\frac{L_c}{D_c}\right)^{2.424} \left(\frac{V_h}{V_t}\right)^{-0.8843} \left(\frac{\rho_s - \rho_f}{\rho_f}\right)^{0.523} \times (\cos(i/2))^{1.793} \quad (2-31)$$

The cut size d_{50c} :

$$\frac{d_{50c}}{D_c} = K_d \left(\frac{D_o}{D_c}\right)^{1.093} \left(\frac{D_u}{D_c}\right)^{-1.00} \left(\frac{(1-f_v)^2}{10^{(1.82 \times f_v)}}\right)^{-0.703} R_e^{-0.436} \left(\frac{D_i}{D_c}\right)^{-0.936} \\ \times \left(\frac{L_c}{D_c}\right)^{0.187} \left(\frac{1}{\tan(\theta)}\right)^{-0.1988} (\cos(i/2))^{-1.034} \left(\frac{\rho_s - \rho_f}{\rho_f}\right)^{-0.217} \quad (2-32)$$

The capacity Q :

$$Q = K_{Qo} \left(\frac{D_i}{D_c}\right)^{0.45} D_c^2 \sqrt{P/\rho_p} \left(\frac{D_o}{D_c}\right)^{1.099} \left(\frac{D_u}{D_c}\right)^{0.037} \left(\frac{1}{\tan\left(\frac{\theta}{2}\right)}\right)^{0.405} \\ \times \left(\frac{L_c}{D_c}\right)^{0.30} \left(\frac{V_h}{V_t}\right)^{-0.048} \times (\cos(i/2))^{-0.092} \quad (2-33)$$

The separation sharpness α :

$$\alpha = K_\alpha \frac{\left(\frac{D_o}{D_c}\right)^{0.27} \left(\frac{V_t^2}{R_{max}g}\right)^{0.016} (\cos(i/180))^{0.868} \left(\frac{(1-f_v)^2}{10^{(1.82 \times f_v)}}\right)^{0.72}}{\left(\frac{D_u}{D_c}\right)^{0.567} \left(\frac{\rho_s - \rho_p}{\rho_s}\right)^{1.837} \times \left(\frac{\mu_m}{\mu_w}\right)^{0.127} \left(\frac{1}{\tan\left(\frac{\theta}{2}\right)}\right)^{0.182} \left(\frac{L_c}{D_c}\right)^{0.20}} \quad (2-34)$$

where i is the inclination angle; V_t is the particle terminal velocity; V_C is the cyclone periphery tangential velocity; V_h is the particle hindered settling velocity; R is the radius of cyclone; μ is the fluid viscosity (subscripts: p=pulp or m= slurry, l= liquid, w= water); ρ is the fluid density (subscripts: p = pulp or m = slurry or suspension, l = liquid, and s = solid); f_V is the feed volume fraction of solid; R_e is Reynolds number; K_w , K_d , K_{Q_o} , and K_α are the application-dependent system constants which need to be refitted to each set of data, which limits the applicability of the Narasimha model. Even though this model considers a wide range of feed solid concentrations, the fact that the Narasimha model depends on the application-dependent system constants significantly limits its applicability.

2.5 Proposed research

The particle-fluid flow in hydrocyclones has been an important topic in the fundamental research and industry targeted applications. In the past years, much effort has been spent on studying hydrocyclones by experimental, empirical, and numerical methods. The advantages and deficiencies can be summarized as follows. Experimental method contributes to gaining the insight into the multiphase flow in hydrocyclones, but those experiments are expensive. The empirical model developed based on the experimental data is fast, portable and easily applied in the industry. However, previously developed empirical models are weak in the applicability because they are generally limited to the experimental conditions used in the modelling. Therefore, it is desirable and more reliable to develop a mathematical description of the fundamentals which govern the multiphase flow of hydrocyclones. Furthermore, the previous empirical models have failed to consider variables comprehensively: for example, the effects of the material properties (particle density and feed size distributions), cyclone size and inlet feed type which are important in hydrocyclone studies were ignored. The third approach, i.e. the numerical method, provides a lower-cost and more flexible way to study the multiphase flow in hydrocyclones compared to the experimental method. Further, it can be also used to explain the underlying fundamentals related to the effect of each variable compared to the empirical approach. Unavoidably, the numerical model has its own disadvantages as well. For example, it is not suitable for use as an industrial tool because of the time-demanding computation.

In this thesis, the final aim is to develop a PC-based predictive model based on the acquired numerical results. This model is a mathematical description of the underlying fundamentals of hydrocyclone operations, combining the advantages of both the empirical and numerical models. To develop this model, the following studies which constitute the major components of the thesis are carried out:

1) A considerably large numerical database is first required to be developed for developing the predictive model. TFM approach and CG CFD-DEM /TFM-DEM approach which can generate numerical data are assessed, with regards to modelling the multiphase flow under a wide range of feed solid concentrations. The model assessment and the determination of the appropriate one compose the first step to develop the predictive model (Chapter3).

2) Important variables that were ignored or not comprehensively understood in previous studies are investigated by the full Eulerian model. The effects of material density and its interactions with the cyclone size and inlet feed type are studied in Chapter 4 and 5 respectively. The effect of feed size distribution is investigated in Chapter 6.

3) A PC-based model based on the numerical results is developed in Chapter 7 to predict the hydrocyclone performance. This model is a mathematical description of the underlying fundamentals of hydrocyclone operations. Further, the effects of material density and the particle-fluid flows under a wide range of feed solid concentrations are considered in this new model, which overcome the deficiency of the previously developed models.

CHAPTER 3 NUMERICAL METHOD AND VALIDATION

3.1 Introduction

Hydrocyclones have been widely used in the mineral and chemical processing industries. The flow in a hydrocyclone is very complex, because there exist in it swirling turbulence, an air-core and segregation of gas, liquid and solid phases. The research on hydrocyclones has been conducted in two to three methods, namely, experimentally, empirically or mathematically, and numerically. Experimental method (Neesse and Dueck, 2007, Scheid et al., 2012, Chu et al., 2000, Chu et al., 2002, Dai et al., 1999, Narasimha et al., 2012) contributes to providing insights into multiphase flow in hydrocyclones, but those experiments are expensive. The empirical or mathematical method (Cilliers and Hindet, 1991, Schubert, 2007, Narasimha et al., 2014, Plitt, 1976) is more convenient but has many limitations. More importantly, this approach would not lead to a deep understanding of the working mechanisms. Numerical method provides a lower-cost and more flexible way to study the multiphase flow in hydrocyclones. Generally, the numerical methods can be classified into three types, namely, the Two-fluid Model (TFM) which considers both fluids and particles as continua, the combined approach of computational fluid dynamics and Lagrangian particle tracking method (CFD-LPT), and the coupled CFD and discrete element method (CFD-DEM).

The TFM model, including the full Eulerian multiphase approach and simplified Eulerian approaches such as the mixture and VOF models, have been widely adopted to study hydrocyclones (Davailles et al., 2012, Brennan, 2006, Kuang et al., 2012, Nowakowski and Dyakowski, 2003, Nowakowski et al., 2000, Ji et al., 2017, Ghodrat et al., 2016, Hsieh and Rajamani, 1991). However, it is quite challenging for the TFM model to handle particles with a broad range of size distributions and density distributions in modelling a hydrocyclone. The combined approach of CFD or TFM with DEM offers the convenience to model particle size/density distribution. CFD-LPT provides a more accurate and direct way to describe particle flows in hydrocyclones by tracking the motion of individual particles (Murthy and Bhaskar, 2012, Wang et al., 2007, Wang and Yu, 2006, Xu et al., 2012). However, this method is only applicable to dilute flows because of the omission of particle-particle forces and particle-fluid interactions. The CFD-DEM or TFM-DEM (Hernández-Jiménez et al., 2015, Wang et al., 2015) accounting for the collisions between particles and

reactions of particles on fluids, has been adopted for modelling the fluid-particle flow in DMCs (Chu et al., 2012a, Chu et al., 2012b, Chu and Yu, 2008, Chu et al., 2009), gas cyclones (Chu et al., 2011), fluidized beds (Alobaid and Epple, 2013, Alobaid et al., 2013, Cello et al., 2009, Fries et al., 2013) and so on, but only a few CFD-DEM and TFM-DEM studies on hydrocyclones can be found. Thus it leads to a knowledge gap about the applicability of CFD-DEM or TFM-DEM model on hydrocyclones studies. It should be noted that there are studies on hydrocyclones focusing on the particle flow pattern, pressure drop spatial distribution and so on by taking the CFD-DEM approach (Zhou et al., 2010), but these studies have considered only mono-sized particles, which is far from representing industry conditions. That is to say that the CFD-DEM or TFM-DEM studies on hydrocyclones under industrial particle properties are nonexistent to the best of knowledge.

However, it is computationally demanding for the standard CFD-DEM or TFM-DEM model to process an industry-scale particle system since each individual particle is tracked by Newton's second law in the DEM approach (Cundall and Strack, 1979). This situation is worse for a hydrocyclone, in which particle sizes are fine and solids concentration may be high. To overcome this problem, the CFD-DEM or TFM-DEM model with different treatments such as the parcel-particle concept, coarse-grain (CG) model, similar particle assembly model or scaling laws have been developed for various particulate systems (Chu et al., 2009, Sakai and Koshizuka, 2009, Thakur et al., 2016, Mokhtar et al., 2012, Chu et al., 2016). Actually, the CG concept has been extensively used to dramatically reduce computational costs in molecular dynamics simulations which use algorithms very similar to DEM (Tozzini, 2005, Klein and Shinoda, 2008, Noid, 2013). For instance, 3265 CG beads have been used to represent 10 million atoms in modelling bending of bio-membrane (Klein and Shinoda, 2008). In this chapter, CG CFD-DEM and CG-DEM models are developed to model the swirling multiphase flow at different feed solid concentrations in two different hydrocyclones, and the results are analyzed in terms of flow structures, interaction forces and radial acceleration difference. Furthermore, the calculated separation performance is compared with the measurements and those obtained by the TFM model. The results obtained from the present study indicate that this approach needs further research, but offers an alternative way to examine the flow and performance of hydrocyclones.

3.2 Simulation method and conditions

3.2.1 Simulation method

The CG CFD-DEM modelling for hydrocyclones can be divided into two steps, as shown in Fig. 3-1. The first step is to solve the fluid flow and the second step is to handle the particle flow.

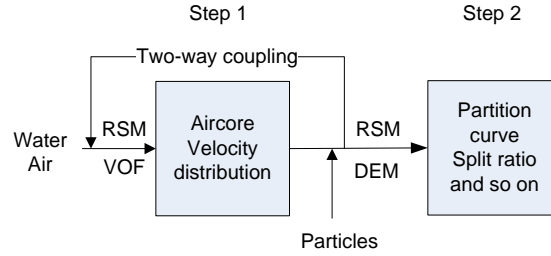


Fig. 3- 1 CG CFD-DEM modelling strategy used in this work

In step 1, only air and water are considered. The turbulence is modelled using the RSM, and the Volume of Fluid (VOF) model is used to determine the interface between the water and the air-core (Chu et al., 2009). In VOF, only a single set of momentum equations is solved for these two phases which are considered immiscible. At this stage, the location of the air-core and the initial velocity distribution is determined. Previous modellings of the multiphase flow in hydrocyclones adopted the similar method (Wang et al., 2007). The continuum fluid flow is calculated from the continuity condition and the Navier-Stokes equations based on the local mean variables defined over a computational cell. These are given by:

$$\frac{\partial(\rho_f \varepsilon)}{\partial t} + \nabla \cdot (\rho_f \varepsilon \mathbf{u}) = 0 \quad (3-1)$$

$$\frac{\partial(\rho_f \varepsilon \mathbf{u})}{\partial t} + \nabla \cdot (\rho_f \varepsilon \mathbf{u} \otimes \mathbf{u}) = -\nabla P - \mathbf{F}_{f-p} + \nabla \cdot (\varepsilon \boldsymbol{\tau}) + \rho_f \varepsilon \mathbf{g} + \nabla \cdot (-\rho_f \overline{\mathbf{u}' \otimes \mathbf{u}'}) \quad (3-2)$$

where ε , \mathbf{u} , \mathbf{u}' , t , ρ_f , P , \mathbf{F}_{f-p} , $\boldsymbol{\tau}$, and \mathbf{g} are, porosity, mean and fluctuating fluid velocities, time, fluid density, static pressure, volumetric fluid-particle interaction force, fluid viscous stress tensor, and gravity acceleration, respectively.

$\mathbf{F}_{f-p} = \frac{1}{V_{cell}} \sum_{i=1}^{k_c} \mathbf{f}_{p-f,i}$, where $\mathbf{f}_{p-f,i}$ is the total fluid force exerting on a particle i and k_c is

the number of particles in a cell of volume V_{cell} . $-\rho\overline{\mathbf{u}\mathbf{u}}$ is the Reynolds stress term due to turbulence and modelled by the Reynolds Stress Model (RSM) provided in ANSYS Fluent, while turbulence modification due to the presence of particles is not included in this work. The flow patterns obtained by solving Eqs. (3-1) and (3-2) represent the mixed flow of water and air.

In step 2, the flows of particles are obtained from the fluid flow patterns obtained above, using DEM method. A particle has two types of motion: translational and rotational, both being described by the Newton's second law of motion (Cundall and Strack, 1979). During the movement, the particles may have collisions with their neighboring particles or with the hydrocyclone wall and have interactions with the surrounding fluid, through which momentum is exchanged (Cundall and Strack, 1979). At any time t , the governing equations for translational and rotational motions of particle i in this system are:

$$m_i \frac{d\mathbf{v}_i}{dt} = \mathbf{f}_{p-f,i} + m_i \mathbf{g} + \sum_{j=1}^{k_i} (\mathbf{f}_{c,ij} + \mathbf{f}_{d,ij}) \quad (3-3)$$

and

$$I_i \frac{d\boldsymbol{\omega}_i}{dt} = \sum_{j=1}^{k_i} (\mathbf{T}_{c,ij} + \mathbf{T}_{r,ij}) \quad (3-4)$$

where $\mathbf{f}_{p-f,i}$ is the total particle-fluid interaction force, which includes the viscous drag force and pressure gradient force in the current case. As for other particle-fluid forces, such as the virtual mass force and the lift force, can be ignored. This can be indicated from trial simulations. The fluid properties used to calculate the particle-fluid interaction forces are related to the properties of water and air. For brevity, the lubrication effect on particle-particle interaction and particle dispersion due to turbulence are not considered. The equations used to calculate the forces can be found in literature (Xu and Yu, 1997, Zhou et al., 1999, Zhu et al., 2008, Rong et al., 2013).

The solids flow is modelled by DEM at the individual particle level, while the fluid flow by CFD is at the computational cell level. Their two-way coupling is that fluid forces act on particles and particles react on fluid. Specifically, at each time step, DEM provides information such as the locations and velocities of individual particles

for the calculation of porosity and volumetric particle-fluid interaction force in a computational cell. CFD then utilizes this information to determine the fluid flow field, from which the particle-fluid interaction forces exerting on individual particles are calculated. Incorporation of the resulting forces into DEM generates information about the motion of individual particles for the next time step (Xu and Yu, 1997).

Figure 3-2 shows the major concept and assumptions of the CG concept. The general idea is that one CG particle includes particles of the same properties such as the size and density, and all of the particles in the same parcel will move with the same translational and rotational momentum in the considered system. That is to say that a small number of parcel/CG particles will represent a large amount of real particles of the same properties. Note that a parcel/CG/ particle should not contain different sized particles shown in Figure 2(c), because the behaviors of particles vary with sizes especially within the fluid. Another important character that should be noted for the CG CFD-DEM model is that the number of CG particles must be enough to make the representation statistically reasonable. The CG CFD-DEM is similar to a standard CFD-DEM model with respect to the governing equations except that CG particles replace the real particles. Compared with the standard CFD-DEM model, the CG CFD-DEM model involves three major assumptions: (i) a big CG particle can contain particles of the same properties (this amount of parcels must be large enough); (ii) the collisions between CG particles represent those between real particles, which requires that the characteristics of the parcels are carefully determined to make sure the mass, momentum, and energy are conserved although there are no general agreements still on this issue (Chu et al., 2016). More details about CG CFD-DEM model can be found in the previous work (Chu et al., 2016).

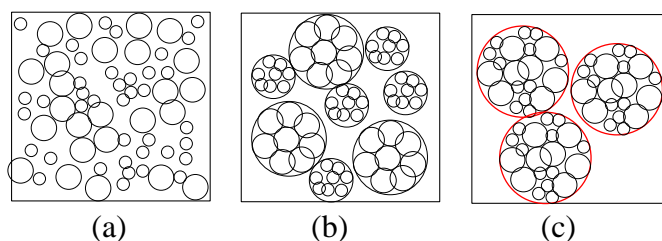


Fig. 3- 2 Schematic representation of the general idea of the CG CFD-DEM model in a computational cell (there are two different sized particles in each system): (a) the original system; (b) Coarse-grained system; (c) an example of inappropriate coarse-grain scheme (only particles with the same size can be contained in a CG particle)

Compared with the CG CFD-DEM modelling, the CG TFM-DEM modelling only tracks larger particles by DEM while considering finer particles as fluids as the mixture model does. In this way, the size ratio can be decreased drastically. The fine and coarse particles are defined according to the critical size which will be explained in the following part. The particles with diameters below and above the critical size are defined as fine and coarse particles respectively. Actually, this process is similar to the simulation work of DMC (Chu et al., 2009) for which magnetite particles are first calculated by the mixture model before injecting coal particles to the flow field. This simulation scheme for CG TFM-DEM model can be described as shown in Fig. 3-3.

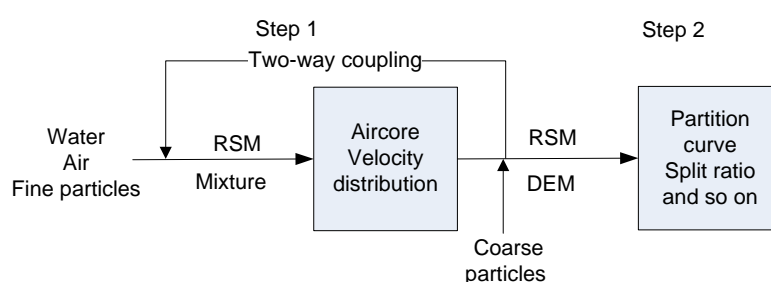


Fig. 3- 3 Modified modelling strategy

In the CG TFM-DEM model, the particle-particle interactions for the fine particles are modelled by kinetic theory, but by DEM for the coarse particles. Similar to the CG CFD-DEM models, each CG particle represents an assembly of particles with the same properties as the real particle. For CG CFD/TFM-DEM model, the CG ratios are determined by carrying out a series of trial cases. It is found that a smaller CG ratio contributes to more accurate simulation and a larger computational cost. Therefore, the ratio is determined by compromising the prediction accuracy and computational efficiency.

3.2.2 Simulation conditions

In order to better investigate the applicability of CG CFD-DEM and CG TFM-DEM models, numerical works are carried out in two hydrocyclones with different geometry conditions, operational conditions and material conditions. Fig. 3-4 shows (a) the geometry and (b) mesh representation of the hydrocyclones of body diameter 75 mm. Note that this hydrocyclone in Hsieh's experiments (Hsieh and Rajamani,

1991) has been widely employed to validate simulation results. Fig. 3-5 shows (a) the geometry and (b) mesh representation of hydrocyclone of 100 mm diameter which was studied in the Pharaoh Muzanenhamo' work (Muzanenhamo, 2014).

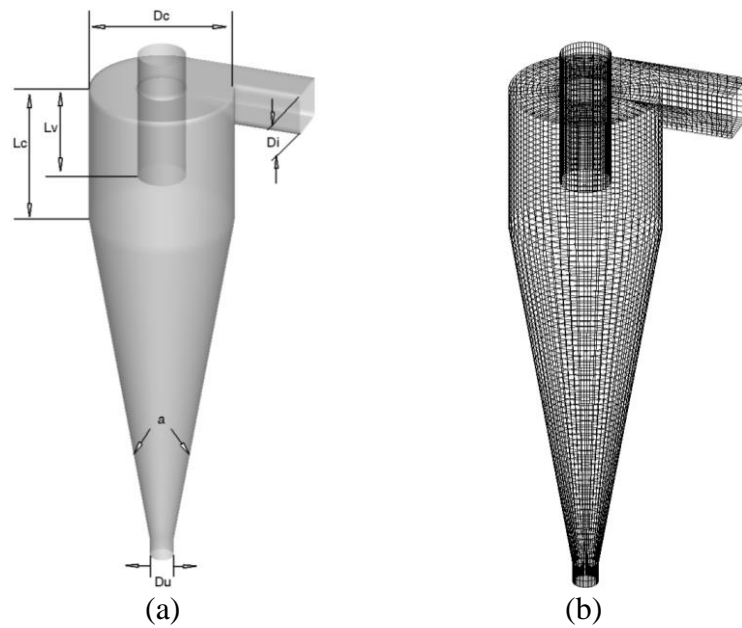


Fig. 3- 4 (a) Geometry and (b) mesh representation of simulated 75 mm diameter hydrocyclones

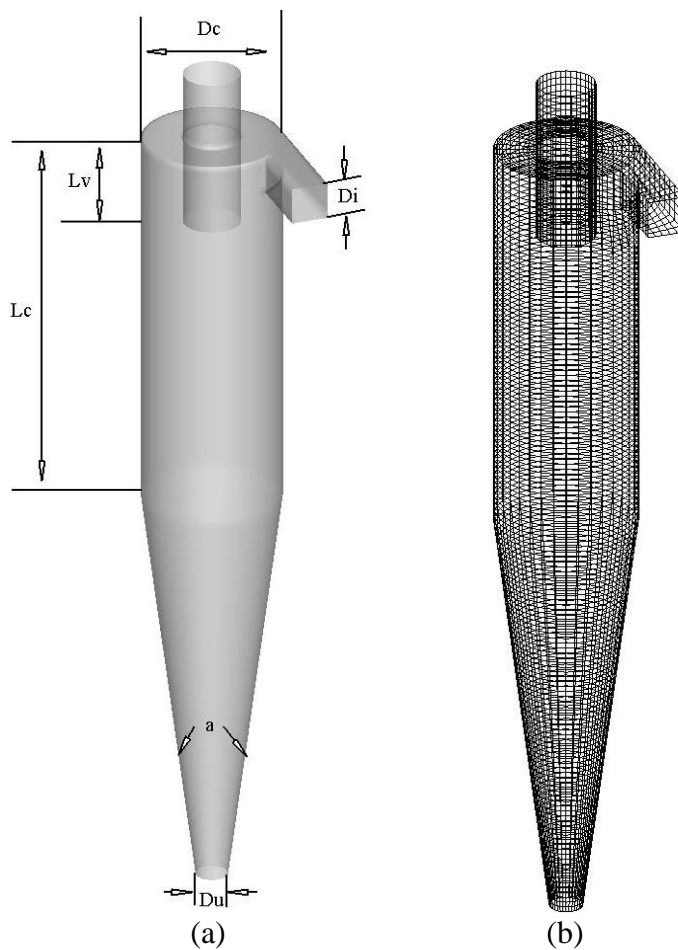


Fig. 3- 5 (a) Geometry and (b) mesh representation of simulated 100 mm diameter hydrocyclones

To obtain comparable results, the geometrical and operational conditions are the same as with those in the corresponding experiments as shown in Tables 3-1 and 3-2. For the simulation work of 75 mm diameter hydrocyclone, the inlet water velocity and particle velocity are both set to 2.49 m/s. Limestone particles are injected at three different feed solid concentrations of 1%, 4%, and 8%; note that the feed solid concentrations in this thesis are expressed by volume percentages. For the hydrocyclone with 100 mm diameter, the inlet water velocity and particle velocity are both set to 4.1 m/s. Iron particles are injected at two different feed solid concentrations of 6% and 10%.

Table 3- 1 Geometrical and operational conditions of 75 mm diameter hydrocyclone

Symbol	Parameter	Value
D_c	Diameter of the body	75 mm
D_i	Diameter of inlet	25 mm
D_v	Diameter of vortex finder	25 mm
D_u	Diameter of apex	12.5 mm
L_c	Length of cylindrical part	75 mm
L_v	Length of vortex finder	50 mm
a	Included angle	20°
u	Inlet velocity	2.5 m/s
ρ_p	Particle material	2700 kg/m ³
ρ_{feed}	Feed solids concentration	1, 4, 8 %

Table 3- 2 Geometrical and operational conditions of 100 mm diameter hydrocyclone

Symbol	Parameter	Value
D_c	Diameter of the body	100 mm
D_i	Diameter of inlet	30 mm
D_o	Diameter of vortex finder	41 mm
D_u	Diameter of apex	23 mm
L_c	Length of cylindrical part	28 mm
L_v	Length of vortex finder	65 mm
a	Included angle	15°
u	Inlet velocity	4.1 m/s
ρ_p	Particle material	3600 kg/m ³
ρ_{feed}	Feed solids concentration	6%,10 %

The simulated size distributions for these two hydrocyclones are also consistent with the experimental ones, as shown in Figs. 6 (a) and (b), respectively. The particle size range is 0.43-42 μm for the 75 mm diameter hydrocyclone and 1-841 μm for the 100 mm diameter hydrocyclone. Note that size ratio defined as the ratio of coarse grain size to real particle size is introduced in the previous work on the CG CFD-DEM model (Chu et al., 2016). When the CG CFD-DEM model is employed to simulate the flows in the 75 mm diameter hydrocyclone at a feed solid concentration of 8% and the 100 mm diameter hydrocyclone of 10%, the coarse-grained particle sizes are 1800 μm and 3000 μm , respectively. The corresponding maximum size ratios are 4186 and 3000. As aforementioned, the CG TFM-DEM model treats a fraction of fine particles as continuum phases. The critical particle sizes below which particle are treated as the continua by the mixture model is 5.27 μm for the 75 mm diameter hydrocyclone and 19 μm for the 100 mm diameter hydrocyclone, as shown in Fig. 6. The corresponding coarse-grained particle sizes are decreased to 1500 μm and 2800 μm , with the

maximum size ratio reduced to 285 and 147, respectively. In current work, the critical particle size is determined by trial simulations, which compromises the prediction accuracy and computational efficiency. Moreover, its value should vary with the conditions involved. Thus, how to develop a sound theoretical or empirical method to generally determine the value of critical size requires further efforts, which has listed in our future study in Chapter 8.

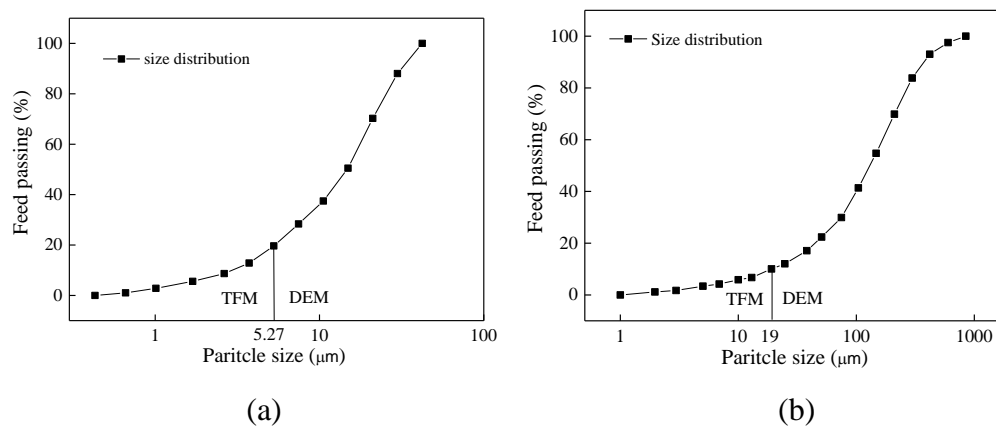


Fig. 3- 6 Size distributions of materials for (a) 75mm and (b) 100mm hydrocyclones

For each mesh, the grid is finer in the vicinity of the walls and vortex finder than in the remainder of the cyclone. It has been proved that with this grid scheme, the numerical solution is converged and grid-independent. In all of the simulations, a “velocity inlet” boundary condition is used at the cyclone inlet, and the “pressure-outlet” condition at the underflow and overflow. The pressure at the two outlets is 1 atm, i.e. the ambient atmospheric pressure. The boundary and initial conditions for CG CFD-DEM simulations are listed in Table 3-2 (the simulation of 75 mm hydrocyclone at a feed solid concentration of 4% is taken as an example). Note that for the CG TFM-DEM simulations, the solid viscosity for fine particle is given according to the kinetic theory.

Table3-3 Boundary and initial conditions for CG CFD-DEM simulations of 75 mm diameter hydrocyclone

Items	Value			
CFD Boundary and initial conditions:	Mixture	Water	Air	Solid
Inlet velocity, m/s	-	2.5	2.5	2.5
Inlet volume fraction	-	0.96	0	0.04
Density (kg/m ³)			1.225	2700

Viscosity(kg/m·s)		0.001003	1.79×10^{-5}	-
Overflow pressure, atm	1	-	-	-
Underflow pressure, atm	1	-	-	-
Backflow volume fraction at overflow	-	-	1	0
Backflow volume fraction at underflow	-	-	1	0
Wall specularity coefficient	-	Non-slip	Non-slip	Non-slip
Initial inner volume fraction	-	0	1	0
CG DEM setting				
Young's modulus(N/ m ²)			1×10^7	
Poisson's ratio			0.3	
Dapping coefficient			0.3	
Sliding friction coefficient			6×10^{-5}	
Rolling friction coefficient			0.3	
Number of CG particles			$<5 \times 10^4$	
Turbulence model				
Model formulation		Reynold stress model		
Reynold-stress model		Linear pressure-strain		
Reynold-stress options		Wall reflection effects		
Near-wall treatment		Standard wall functions		
RSM multiphase model		Mixture		
Solution methods				
Pressure-velocity coupling		Phase coupled SIMPLE		
Pressure		PRESTO		
Volume fraction		Quick		
Momentum		Second order upwind		
Spatial discretization	Turbulent kinetic energy	Second order upwind		
	Turbulent dissipation rate	Second order upwind		
	Reynolds stresses	Second order upwind		

The simulations are all unsteady, undertaken by the unsteady solver in ANSYS Fluent as a platform, achieved by incorporating a CG DEM code into Fluent through its User Defined Functions (UDF). This approach has been successfully used in our recent study of various complicated fluid–solid flow systems in dense medium cyclones (DMCs) (Chu et al., 2012a, Chu et al., 2012b) and gas cyclones (Chu et al., 2011). In order to get the partition performance of particles (partition number is defined as the

portion of particles of certain size reporting to the underflow), the information of particles exiting from the underflow is collected during the period of macroscopically steady flow state.

3.3 Model validation

3.3.1 CG CFD-DEM validation

The experimental data at a feed solid concentration of 4% in Hsieh's experiments are used to validate the applicability of CG CFD-DEM model. Fig. 3-7 demonstrates the simulated and experimental partition curves. It is seen that the simulated partition numbers reasonably agree well with the experimental ones.

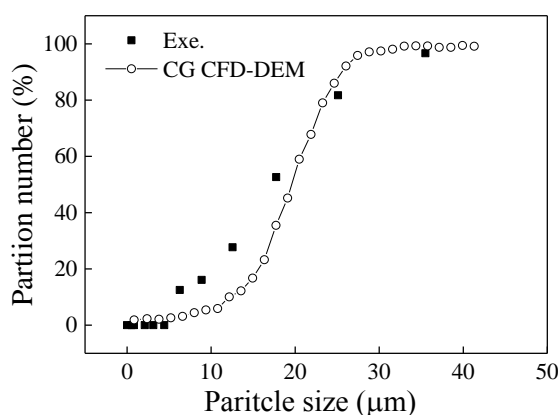


Fig. 3- 7 Experimental and simulated partition curves of for 75mm diameter hydrocyclone at a feed solid concentration of 4%

Fig. 3-8 shows the simulated flow pattern at three different time points when it reaches a macroscopically steady state. Even though the particle flow is dynamic, the phenomenon that coarse particles congregate at the wall and descend in strands can be clearly seen during the dynamic process. Note that there is a similar phenomenon in gas cyclones, and it was obviously observed both in the experimental and numerical work (Wang et al., 2006, Chu et al., 2011). Obtaining a comparable partition curve and observing the particle congregation phenomenon both demonstrate that CG CFD-DEM is applicable in simulating the flow properties in hydrocyclone at a feed solid concentration of 4%. It is noted that the agreement in Fig. 3-7 for the intermediate particles is not as good as that for the small and large particles. That is attributed to two main aspects. It is established that the particles with intermediate particle size tend to have a stochastic motion and a longer residence time within hydrocyclones

(Wang et al., 2007). This feature would bring out difficulties in simulating this fraction of particles. Furthermore, the CG CFD-DEM model involves assumptions as described aforementioned, which unavoidably bring some errors as well.

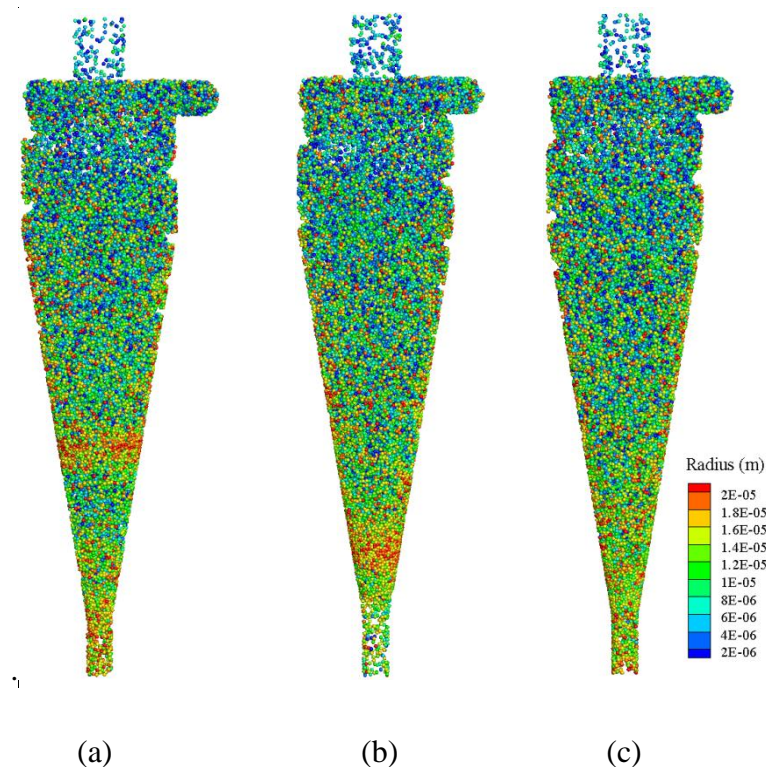


Fig. 3- 8 Particle flow patterns in 75mm hydrocyclone at feed solid concentration of 4% at (a) $t=1.9s$, (b) $t=2.0s$ and (c) $t=2.1s$

To further investigate the applicability of CG CFD-DEM, the separation performance at feed solid concentrations of 1% and 8% are also investigated. As aforementioned, TFM model has been used to study the effect of feed solid concentration on the hydrocyclone performance previously (Kuang et al., 2012, Davailles et al., 2012). Here, the simulated partition curves at feed solids concentrations of 1% and 8% by the CG CFD-DEM are compared with the results generated by the TFM model, as shown in Fig. 3-9. It can be seen that the simulated separation efficiency by the CG CFD-DEM reduces with the increase of feed solids concentration, while the cut-size has the opposite trend. This is qualitatively consistent with the findings concluded by previous experimental and TFM works (Davailles et al., 2012, Kuang et al., 2012, Rajamani and Milan, 1992, Muzanenko, 2014). However, quantitatively, the partition numbers predicted by CG CFD-DEM at a feed solid concentration of 8% are much lower than those simulated by the TFM model, especially for coarser particles.

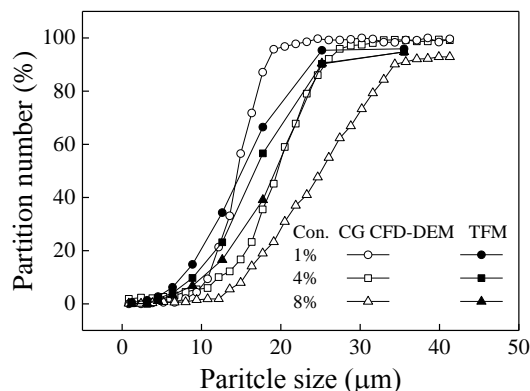


Fig. 3- 9 Partition curves simulated by CG CFD-DEM and TFM models at different feed solid concentration of 1%, 4%, and 8%

Experiments data are also introduced to further validate the CG CFD-DEM model. Partition numbers reported in literature (Rajamani and Milan, 1992) are utilized here to compare them. It is demonstrated that this experimental work conducted by Rajamani et.al (Rajamani and Milan, 1992) is a further study under a dense flow condition of the hydrocyclone used in Hsieh's work (Hsieh and Rajamani, 1991). The comparisons are shown in Fig. 3-10. It is found that the CG CFD-DEM model underestimates the separation performance when the feed solid concentration is higher.

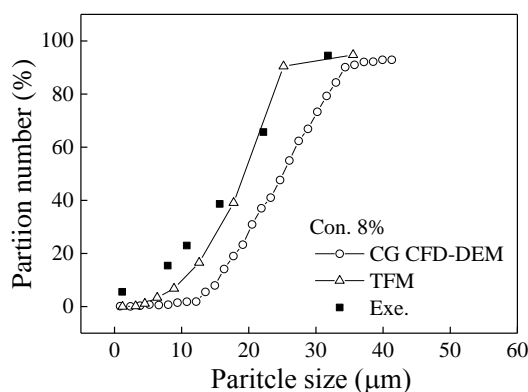


Fig. 3- 10 Comparisons of the experimental and simulated partition curves at a feed solid concentration of 8%

The similar issues are found in the simulation of 100mm diameter hydrocyclones, as shown in Fig. 3-11. Specifically, both CG CFD-DEM and TFM methods can give comparable results with experiments at a feed solid concentration of 6%. However, once the feed solid concentration is increased to 10%, the CG CFD-DEM method under predicts the partition numbers. Note that the partition numbers simulated by the TFM model still agree well with the experiment ones.

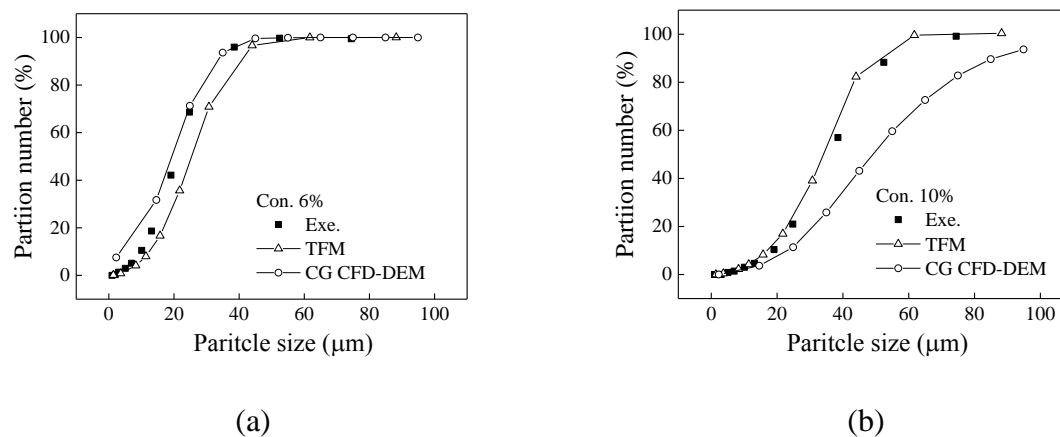


Fig. 3- 11 Partition curves simulated by the CG CFD-DEM and TFM models in 100mm hydrocyclone at feed solid concentrations of (a) 6%, and (b) 10%

The reasons for the underestimation of CG CFD-DEM model at higher feed solid concentrations should be attributed to the larger size ratio of the CG particles to real particles. Compared with the CG CFD-DEM model, the CG TFM-DEM model can reduce the size ratio dramatically by treating fine fractions of particles as continuum phases. As aforementioned, the maximum size ratio for the 75 mm diameter hydrocyclone at a feed solid concentration of 8% can be dramatically decreased from 4186 to 285 after employing the CG TFM-DEM model. Similarly, the maximum size ratio for the 100 mm diameter hydrocyclone at a feed solid concentration of 10% is reduced to 147 from 3000. Actually, the larger size ratio will affect the calculation of particle-particle interaction forces especially when the flow is dense. Therefore, for dense flows, the size ratio should be kept as smaller as possible or further theoretical/empirical approaches are needed to overcome this problem.

3.3.2 CG TFM-DEM validation

To overcome the discrepancies due to the large size ratio, the CG CFD-DEM model is now changed to the CG TFM-DEM model by considering finer particles as fluids, as shown in Fig. 3-3. The percentages of fine particles considered as fluids in TFM for Fig. 3-12 (a) and (b) are 10.14% and 19.65%, respectively. Fig. 3-12 compares the results obtained by CG TFM-DEM model and experiments. It can be clearly seen that the partition numbers predicted by the CG TFM-DEM model are much closer to the experimental ones compared to that by the CG CFD-DEM model, which means this CG TFM-DEM model is more applicable to the denser flows.

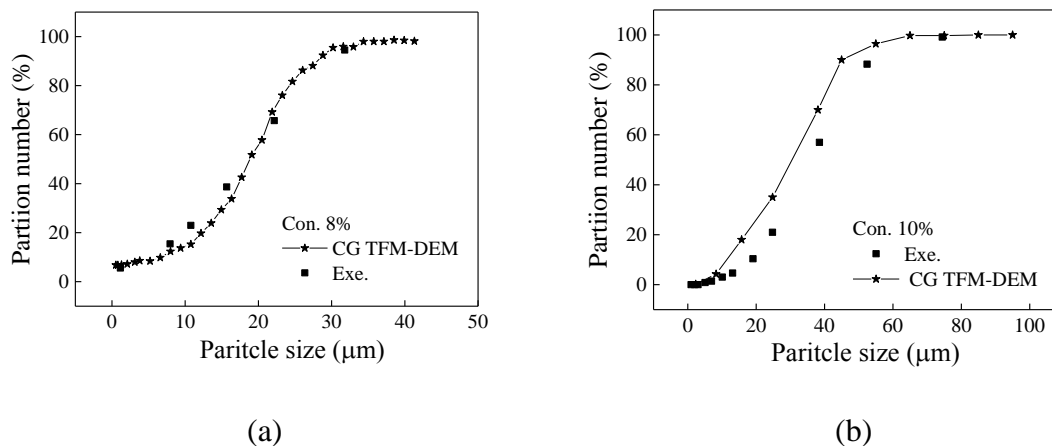


Fig. 3- 12 Partition curves simulated by the CG CFD-DEM and CG TFM-DEM models in hydrocyclones with diameters of (a) 75mm and (b) 100mm, at feed solids concentrations of 8% and 10%, respectively.

3.4 Effect of feed solid concentration

Fig. 3-13 compares the volume distribution in the simulation cases for the 75mm diameter hydrocyclone. It can be seen that the volume fraction in the spigot area increases when the feed solid concentration grows as shown in Figs. 3-13 (a)-(c), which is in line with the conclusion drawn in literature (Kuang et al., 2012). From Figs. 3-13 (c)-(d), it can be seen that the CG CFD-DEM over predicts the volume fraction at a feed solid concentration of 8%. A reduction of volume fraction is observed after employing the CG TFM-DEM model. Actually, the lower volume fraction distribution is supposed to benefit the separation performance as previously reported (Ghodrat et al., 2016, Ji et al., 2017). This may be one of the reasons for the separation efficiency improvement in the case of the CG TFM-DEM model.

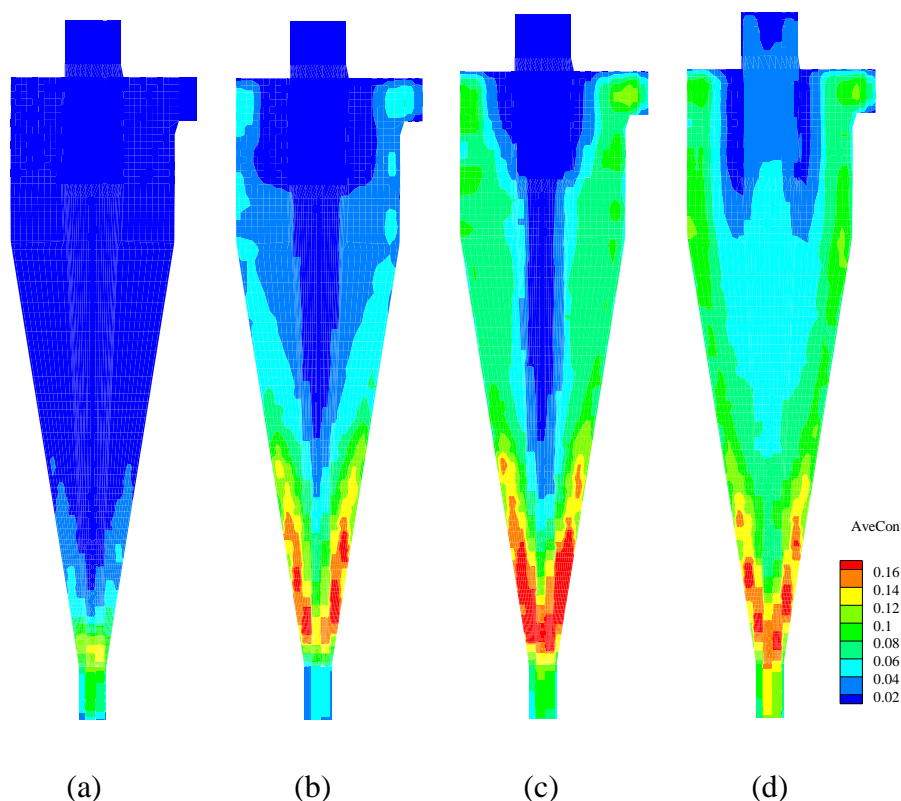


Fig. 3- 13 Solid volume distributions in 75mm diameter hydrocyclone at different feed solid concentrations of: (a) 1%, (b) 4%, (c) 8% by the CG CFD-DEM model and (d) 8% by the CG TFM-DEM model

As shown in Figs. 3-14 (a)-(c), with the increase of feed solid concentration, the upward velocity of coarse particles along the center and the radial velocity towards the air-core all increase, which leads to more coarse particles being misplaced to the overflow. This phenomenon is consistent with the variation trend of partition curve with the feed solid concentration as shown in Fig. 3-9. Fig. 3-14 (d) shows the particle velocity field when the CG TFM-DEM model is used for the case of 8% feed concentration. It can be clearly seen that the separation performance is improved. Specifically, the inward radial velocities of coarse particles are weakened which means that they tend to move closer to the wall. Besides, the upward motion along the center is decreased. That means even those particles have the possibility of being discharged to the overflow, it is likely for them to move towards to the wall again later.

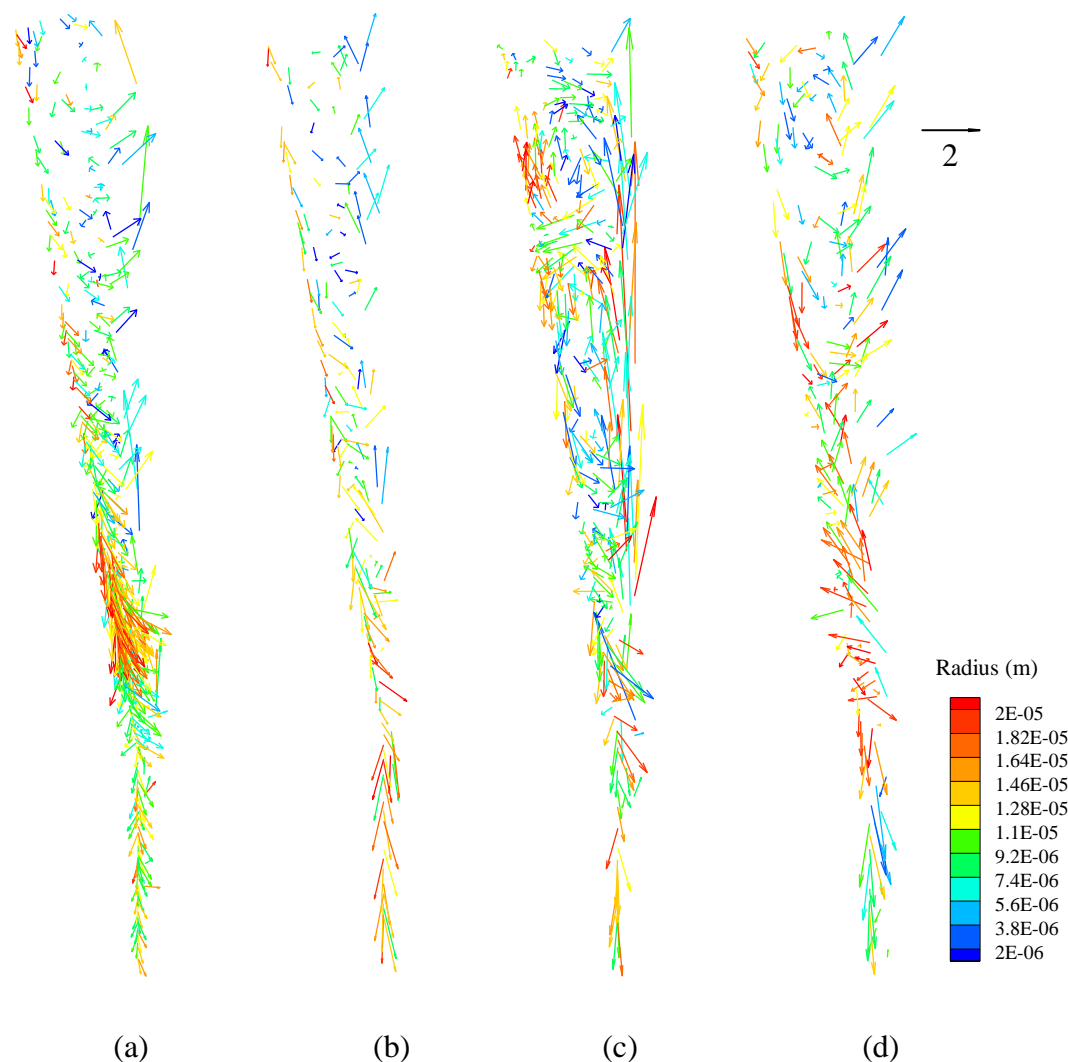


Fig. 3- 14 Particle flow properties in 75mm diameter hydrocyclone at different feed solid concentrations of (a) 1%, (b) 4%, (c) 8% by the CG CFD-DEM model and (d) 8% by the CG TFM-DEM model

To explain the particle flow properties, the total force (including pressure gradient force, drag force, particle-particle force and particle-wall force) acting on particles is investigated as shown in Fig. 3-15. It can be concluded that the total force is mainly pointing to the central axis in hydrocyclones. With the increase of the feed solid concentration, the total force tends to be more disordered. Further, the disordering phenomenon at the feed solid concentration of 8% is weakened when the CG TFM-DEM model is used, which means that the CG CFD-DEM model may estimate the total force in a more chaotic way at the feed solid concentration of 8%. However, only the total force distribution is not sufficient to explain the particle separation performance. Therefore, the total forces of different particles are compared next with their corresponding centrifugal forces (mv^2/r) in their specific locations. It is believed

that if the centrifugal force is larger than the total force at a specific location, the particles tend to move outwards to the wall; otherwise, the particles are likely to flow to the center.

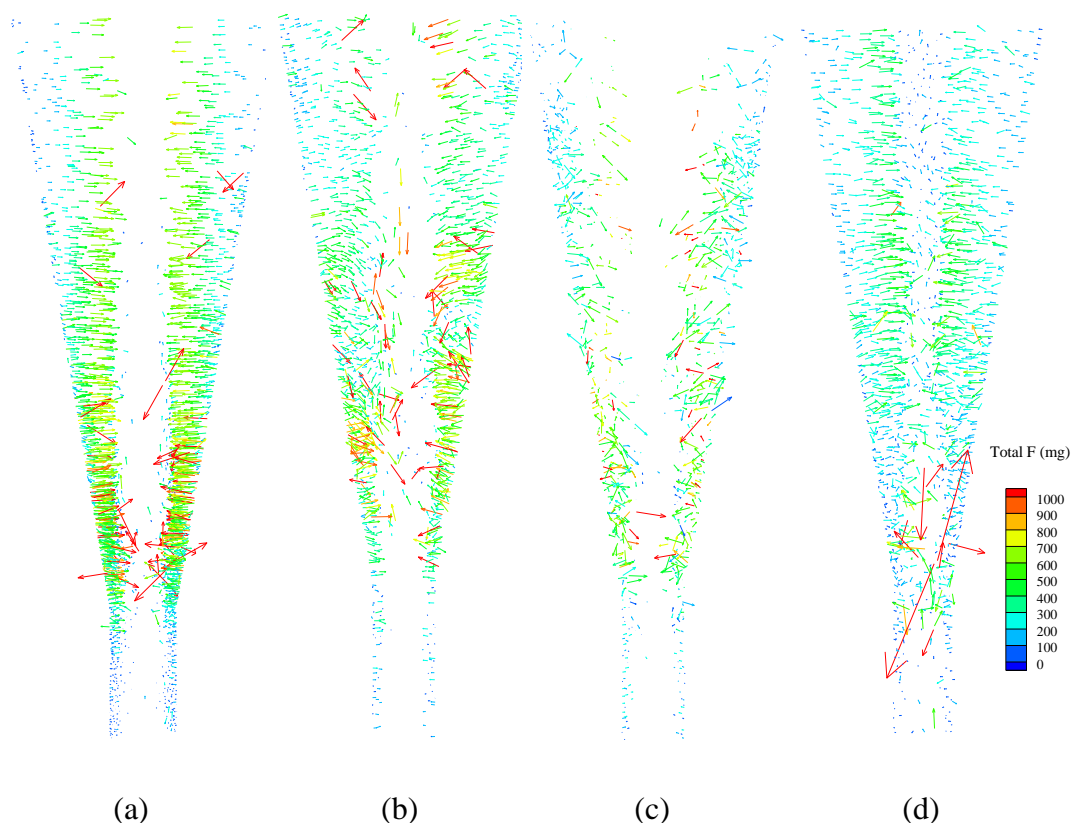


Fig. 3- 15 Total force distributions in 75mm-hydrocyclone at different feed solid concentrations of (a) 1%, (b) 4%, (c) 8% by the CG CFD-DEM model and (d) 8% by CG TFM-DEM

The difference between these two forces can be transformed to the radial acceleration difference ($v^2/r-F/m$) as shown in Fig. 3-16. It can be clearly seen that the radial acceleration difference decreases as the feed solid concentration increases, which means that particles tend to be misplaced, especially for coarser particles, and therefore, the partitions to the underflow decrease. This is consistent with Fig. 3-14 in which coarser particles have a larger radial velocity towards the air-core than fine particles. As the fine particles can easily flow with water, their motions are less dependent on the radial acceleration difference. Furthermore, there is an obvious negative zone in Fig. 3-16(c) when the feed solid concentration is set to 8%. However, when the CG TFM-DEM model is utilized, that obvious negative zone disappears as shown in Fig. 3-16(d). That is to say that the CG CFD-DEM model underestimates

the radial acceleration difference in some areas in the cases of higher feed solid concentrations, leading to an underestimation of partition number to the underflow.

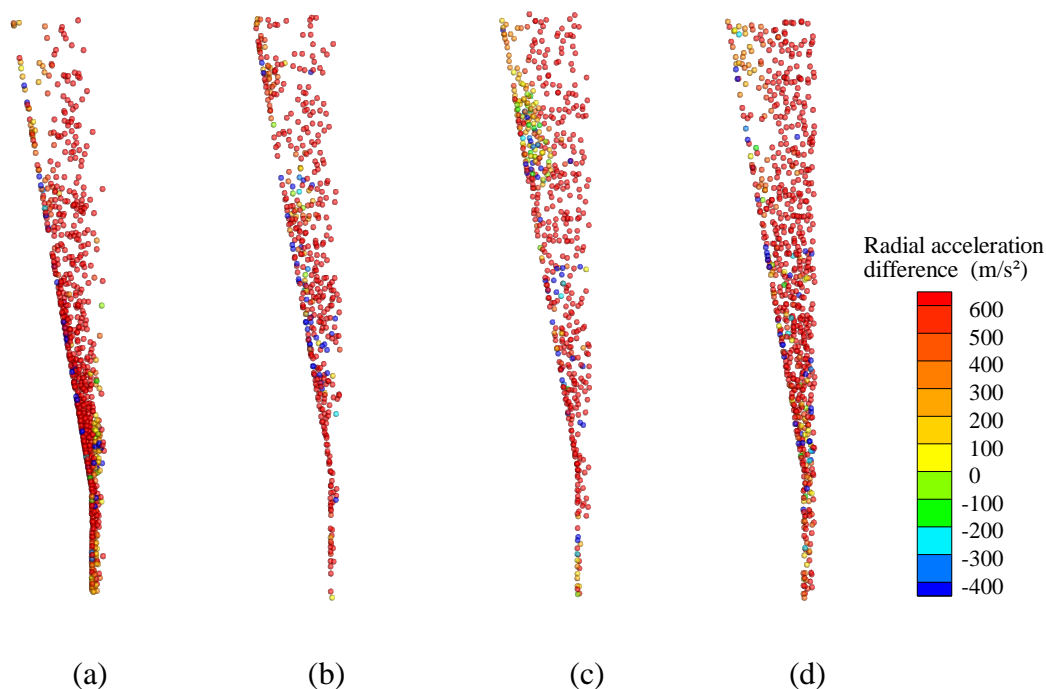


Fig. 3- 16 Radial acceleration difference in 75mm diameter hydrocyclones at different feed solid concentrations of (a) 1%, (b) 4%, (c) 8% by the CG CFD-DEM model, and (d) 8% by the CG TFM-DEM

As for the 100 mm diameter hydrocyclone, flow properties are analyzed with respect to the solid volume fraction on the wall and the radial acceleration difference as well. Figs. 3-17 (a)-(b) compare the solid volume fraction on the wall predicted by the CG CFD-DEM model. For the case of feed solid concentration of 6%, there is an obvious particle “strand” which is similar to that of Fig. 3-8. However, when the solid concentration increases to 10%, this “strand” almost disappears except the slight one in the bottom, which is consistent with the findings on the effect of the solid loading ratio as reported in a previous study on gas cyclones (Chu et al., 2011). Further, the solid volume fraction in the bottom increases with the increase of feed solid concentration. Fig. 3-17(c) demonstrates the effect of the solid volume fraction predicted by the CG TFM-DEM model. It shows that the “strand” is more obvious with a reduced volume fraction, compared with Fig. 3-17(b), which is based on the CG CFD-DEM model.

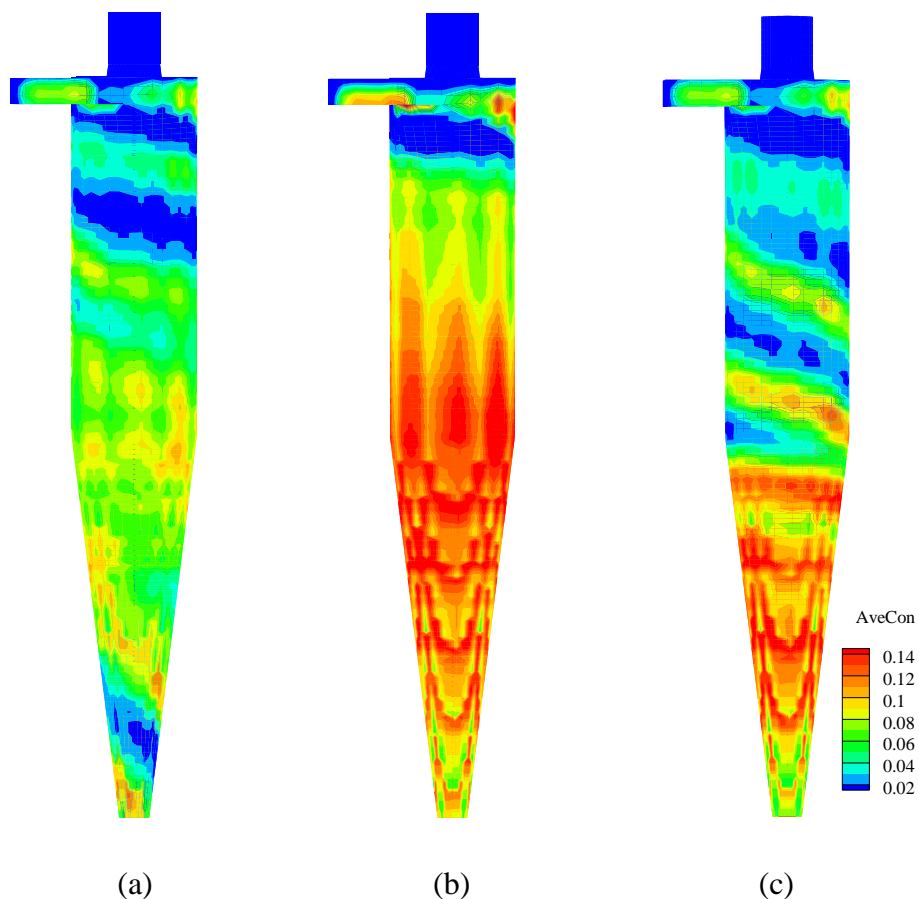


Fig. 3- 17 Solid volume distribution in 100 mm diameter hydrocyclone at feed solid concentrations of (a) 6% and (b) 10% by the CG CFD-DEM model and (c) 10% by the CG TFM-DEM model

The radial acceleration difference in 100 mm diameter hydrocyclone is also investigated here as shown in Fig. 3-18. There is a similar phenomenon to that seen in Fig. 3-16. Specifically, the radial acceleration difference drops noticeably when the feed solid concentration rises from 6% to 10%. However, the radial acceleration difference at 10% feed concentration is improved by employing the CG TFM-DEM model. This phenomenon provides further support for the conclusion that the CG CFD-DEM model under predicts the radial acceleration difference when the size ratio is large at higher feed solid concentrations.

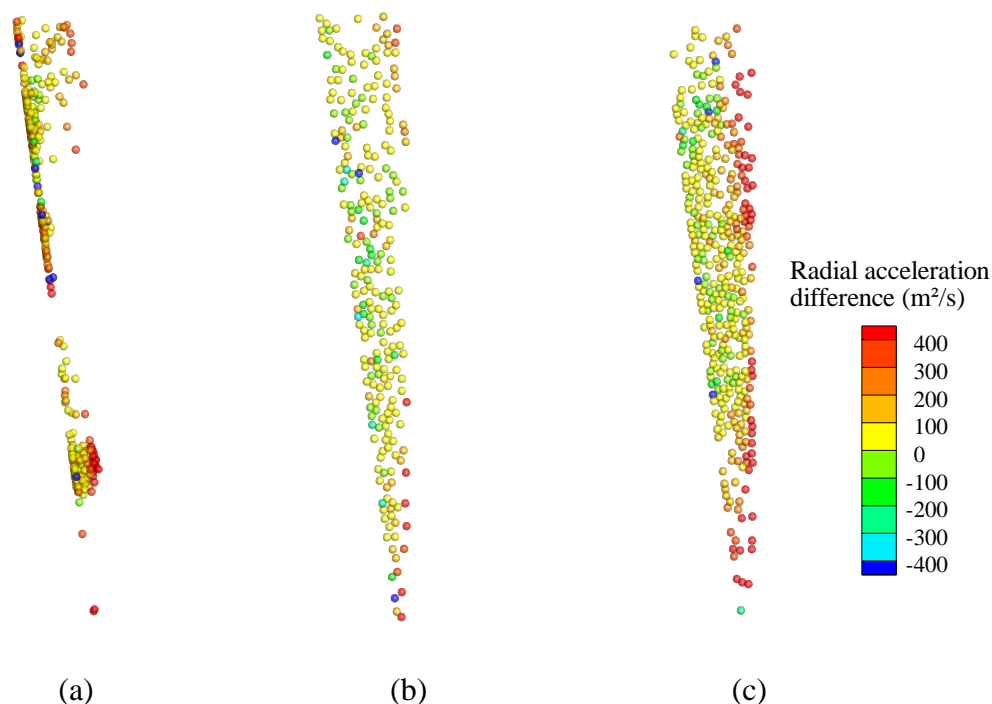


Fig. 3- 18 Radial acceleration difference in 100 mm diameter hydrocyclone at feed solid concentrations of (a) 6% and (b) 10% by the CG CFD-DEM model and (c) 10% by the CG TFM-DEM model

3.5 Conclusions

The multiphase flow at different feed solid concentrations in hydrocyclones is investigated by the CG CFD-DEM and CG TFM-DEM models. These models are validated by comparing with experiments, and they are also compared with the TFM model. The validation and comparison results of the present study are summarized as follows:

- The CG CFD-DEM model is only applicable to dilute flows. When the flow is dense, it underestimates partition numbers due to the underestimation of the particle radial acceleration difference and/or accumulation area. The problem of the CG CFD-DEM model for the dense flow should be caused by the extremely large size ratio of CG particle to real particle. Generally, as the size ratio increases, the prediction will be less accurate especially in the calculation of particle-particle interaction forces, as well as in the radial acceleration difference and solid volume fraction.
- The CG TFM-DEM model is applicable to dense flow but its computational cost is much higher than the CG CFD-DEM model.

- The effects of feed solid concentration predicted by the CG CFD-DEM model qualitatively agree well with experimental data. With the increase of feed solid concentration, the separation efficiency decreases and cut size increases. This is attributed to the more evident particle accumulation and/or reduced radial acceleration. Moreover, particle-particle and particle-wall interactions become stronger for a higher feed solid concentration, which indicates that the wear rate increase.
- The CG TFM-DEM method provides an alternative way to study hydrocyclones at higher feed solid concentrations. Compared with the widely-adopted TFM method, this approach still needs further research on determining the critical particle size below which particles should be considered as a continuum medium. This issue leads to this approach immature when dealing with the particle-fluid flow at higher feed solid concentrations. As both dense and dilute flows are targeted in this thesis, the TFM model is adapted to generate the numerical database because the size/density distributions considered in this thesis are within its handling ability. Considering that the mixture model is not accurate enough to model hydrocyclones which are used to handle different sized particles with a wide density range, the full Eulerian model is adopted to generate the numerical data and to investigate the effects of cyclone size, particle density, inlet feed type, and feed size distribution in the following chapters.

**CHAPTER 4 COMPUTATIONAL ANALYSIS AND
OPTIMIZATION OF HYDROCYCLONE SIZE TO
MITIGATE ADVERSE EFFECT OF PARTICLE
DENSITY**

4.1 Introduction

Hydrocyclones are widely used in the coal industry to upgrade or separate coal fines smaller than 2 mm according to particle size, due to their design simplicity, flexibility of operation, high capacity, and low operation and maintenance costs. An important step in this application is to select a suitable cyclone size, which is characterized by the diameter of cylindrical part. This selection is often done according to the specific requirements on particle cut size, cyclone capacity and separation sharpness or precision under given conditions (Bradley, 1965). It can further be complicated by the presence of a broad particle density distribution, which more or less causes adverse effects on the performance of hydrocyclones and their downstream processes (Firth et al., 1999, O'Brien et al., 2001, Rong, 2007, Atkinson and Swanson, 2008). Specifically, some ultrafine coal particles, either heavy or light, are entrained to the underflow stream and bypass the separation process. This situation leads to the loss of product (light particles) and the deterioration of the subsequent dewatering process, due to the high surface area of the entrained ultrafine particles. On the other hand, some light coarse particles unexpectedly report to the overflow or the upper outlet. Such particles often have a negative impact on the downstream operations like flotation, where the solid recovery drops when particle size is too large. To date, it is not yet clear how cyclone size interacts with particle density. However, this interaction is the key to selecting a suitable cyclone size in the coal industry, particularly for particle misplacement mitigation.

In the past years, various efforts have made to study cyclone size. The results from different investigators are not consistent with each other, though largely based on a uniform particle density. For example, Lynch (1974, 1975) experimentally revealed that for geometrically similar hydrocyclones with sizes ranging from 102 mm to 381 mm, the reduced efficiency curve and resulting cut size do not vary much with the cyclone size for limestone particles of nearly a uniform density. However, other investigators (see, e.g., Refs Bradley, 1965, Arterburn, 1982, Heiskanen, 1993) suggested that cut size is proportional to the cyclone size and is one of the main variables necessary for preliminary sizing and selection of cyclone. This has been found valid to mini-hydrocyclones (5-30 mm) used to handle particles less than 10 μm by different investigators through various experimental measurements (Mognon et

al., 2015, Neesse et al., 2015, Lv et al., 2015). Also, based on physical experiments, some investigators (Young et al., 1994, Lv et al., 2015) suggested that the separation precision of mini-hydrocyclones become worse as the cyclone size increases. Conversely, O'Brien et al. experimentally reported that the sharpness of the partition curve of larger hydrocyclones is equivalent to that of smaller ones. In recent years, some numerical studies have also been carried out to reveal how the cyclone size affects the performance and flows. In particular, the numerical and analytical work of Cilliers (2000) suggested that the diameter of the cylindrical section is the major variable affecting the particle size that can be separated. Delgadillo and Rajamani (2009) found that the air-core diameter increases with the hydrocyclone diameter in their simulations of the water-air mixture. Wang and Yu (2006) numerically showed that when operated in a dilute regime, smaller cyclones are helpful to achieve a higher efficiency and a lower pressure drop, the same as the predictions given by the empirical model of Plitt (1976). Similar numerical results have been obtained by Ghodrat et al. (Ghodrat et al., 2013) who further revealed that the effect of cyclone size significantly varies with the feed solid concentration. Although comprehensive in investigating cyclone size effect, the studies of Wang and Yu (Wang and Yu, 2006) and Ghodrat et al. (Ghodrat et al., 2013) considered only limestone particles of the same density for relatively small (from 18-mm to 300-mm) cyclones. However, particle density distribution is unavoidable and plays an important role for the performance of hydrocyclones used in the coal preparation. Also, the average cyclone size is larger for handling coal particles.

In comparison with the numerous studies of hydrocyclone size, the studies reported for particle density are very few. For example, the experimental works of Firth et al. (Firth et al., 1999) and O'Brien et al. (O'Brien et al., 2001) showed that the particle separation efficiency increases with particle density. Ghadirian et al. (Ghadirian et al., 2015) numerically and experimentally studied the separation behaviours of both light and heavy particles in a 51-mm hydrocyclone operated in a dilute regime, and found that increasing the vortex finder length results in an increased recovery of light particles to the overflow. Recently, Ghodrat et al. (Ghodrat et al., 2016) demonstrated that the misplacement problem associated with particle density can be mitigated using a long or convex-shaped conical section for a 1000 mm diameter hydrocyclone. On

the other hand, extensive studies on the particle density effect have been made in recent years for dense medium cyclones (DMCs) which are also widely used to separate coal particles (see, e.g. Refs (Qi et al., 2015, Wang et al., 2014, Kuang et al., 2014, Narasimha et al., 2007b, Barbee et al., 2005, Chu et al., 2014, Chu et al., 2012a)). However, DMCs function according to the difference of particle density instead of particle size for hydrocyclones, and mainly consider coarse (from 0.5 mm to 50 mm) coal particles. Thus, the DMC-related findings cannot be applied to hydrocyclones. To date, the effects of particle density on the flows and performance of hydrocyclones have not been well addressed. Furthermore, the studies on particle density effect in relation to cyclone size are lacking, in addition to the aforementioned arguable results against cyclone size. Nowadays, two opposite opinions exist in selecting a suitable cyclone size in order to mitigate the adverse effect of particle density in the coal industry, i.e. some investigators suggested large hydrocyclones (e.g. 1000 mm) (O'Brien et al., 2001, Rong, 2007) whereas others recommended mid-range sizes (380 mm- 600 mm) (Atkinson and Swanson, 2008). As such, this paper attempts to clarify the effect of particle density on the flows and performance of hydrocyclones over a wide cyclone size range. This is done based on numerical experiments under well controlled conditions.

Generally speaking, the modelling of hydrocyclones can be discrete- or continuum-based with respect to the treatment of solid phase, which are respectively represented by LPT (Lagrangian Particle Tracking) or TFM (Two-Fluid Model), as reviewed by Nowakowski et al. (Nowakowski et al., 2004) and Narasimha et al. (Narasimha et al., 2007a). The LPT approach ignores the effect of inter-particle interactions as well as reactions of particles on the fluid, and thus is used mainly for operations in a dilute regime or at a low feed solid concentration (see. e.g., Hwang et al., 2012, Wang and Yu, 2006, Wang et al., 2014). The dense discrete phase model which combines LPT with the kinetic theory (Zhou et al., 2016) may be used over a wide range of feed solids concentrations. TFM models in the form of either the so-called mixture model or Eulerian-Eulerian model can in principle be applied to both dense and dilute regimes. The mixture model is essentially a simplified Eulerian-Eulerian model and was found to be inaccurate for predicting the separation performance of hydrocyclones as long as particles have a broad range of sizes and densities (Ghodrat,

2014). The Eulerian-Eulerian approach can be used to overcome the problem associated with the mixture model, as recently demonstrated by Ghodrat et al. (Ghodrat et al., 2016). Therefore, the model of Ghodrat et al. (Ghodrat et al., 2016) is adopted to systematically conduct numerical experiments with respect to particle density and cyclone size. Such studies have not been found in literature, although being highly desired for practical applications. From this study, the interaction between particle density and cyclone size is elucidated in terms of flow and force characteristics. Also, optimum cyclone sizes are suggested to mitigate the adverse effect of particle density.

4.2 Simulation method

4.2.1 Model description

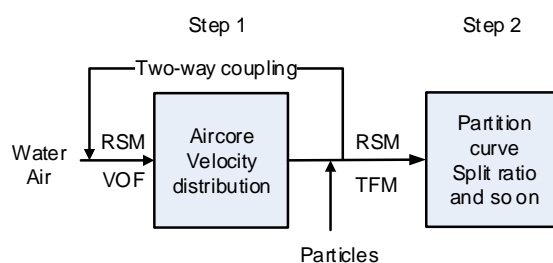


Fig. 4- 1 Steps used in the present modelling.

The present study is based on the computer model reported elsewhere (Ghodrat et al., 2016). The model has been proved valid for hydrocyclone studies, especially in dealing with a broad range of particle densities and sizes. Its framework is developed in three steps as illustrated in Fig. 4-1. This step-by-step implementation not only guarantees the numerical stability, but also facilitates the model validation from simple to complicated cases.

In step 1, only the air and water phases are considered. The turbulent flow of water-air mixture is modelled using the Reynolds stress model (RSM), facilitated by a standard wall function (Launder et al., 1975). The interface between the liquid and air-core is modelled using the Volume of Fluid (VOF) model (Hirt and Nichols, 1981), the same as those widely used elsewhere (see, e.g., Wang and Yu, 2006, Bhaskar et al., 2007,

Mousavian and Najafi, 2009, Azadi et al., 2010, Kuang et al., 2012). In this step, the primary air-core position and the velocity distribution are gained.

In step 2, the simulation starts with the results from the first step, and the VOF approach is changed to the TFM approach in the form of Eulerian-Eulerian model (Gidaspow, 1994). Note that the TFM approach can predict the flows and air-core close to those given by the VOF approach (Ghodrat et al., 2016), and only the former can be used to describe the gas-air-solid flows and separation performance of hydrocyclones. The results obtained here are then used as a part of the initial conditions in the next step.

In step 3, coal particles with different densities and sizes are added to simulate the flows of water, solid and air within the hydrocyclone, as well as to estimate the separation performance by the TFM-RSM approach. In such an approach, both the fluid (liquid and air) and solid phases are treated as interpenetrating continua. Each particle size or density represents one phase. Based on these treatments, a full set of conservative equations with regards to momentum and mass is applied to each phase, combined with the kinetic theory for describing particle-particle interactions. The model formulations and numerical techniques can be found elsewhere (Safa and Soltani Goharrizi, 2014, Ghodrat et al., 2016, Swain and Mohanty, 2013, Davailles et al., 2012), and thus are not detailed here to avoid repeating.

4.2.1 Model applicability

It is necessary to verify the validity of the computer model before its application for numerical experiments. This has been done by comparing the numerical results with the measurements through different applications, involving water-air and water-air-solid flows. The data used in the comparison include: (1) the mean tangential and axial velocities as well as RMS (Root-Mean-Square or turbulent stress) velocities of water, as measured by Hsieh and Rajamani (Hsieh and Rajamani, 1991) within the 75-mm cyclone (water-air flow); (2) the water split and inlet pressure drop, as measured by Hsieh and Rajamani (Hsieh and Rajamani, 1991) and Bicalho et al. (Bicalho et al., 2014) within 75-mm and 15-mm cyclones (water-air flow), respectively; and (3) the separation efficiencies of particles having different sizes and densities, as measured by O'Brien et al. (O'Brien et al., 2001) within a 1000-mm

cyclone operated at the feed solid volume fractions of 7.4% and 15.2% (water-air-solid flow). Overall, all the results obtained thus far from the comparison suggest that the present model can satisfactorily predict the flows and separation performance of hydrocyclones, at least qualitatively. The detailed results can be found elsewhere (Ghodrat et al., 2016). Additionally, we have also qualitatively compared our calculated results with other experimental and numerical observations throughout Chapter 4.4.

4.3 Simulation conditions

Table 4-1 lists the present geometric and operational conditions of hydrocyclones, following the experimental work of O'Brien et al (O'Brien et al., 2001). Fig. 4-2 (a) gives the corresponding geometric profile. Different from the experimental work which considered only a 1000-mm hydrocyclone, eight cyclones are simulated here, whose size varies from 300 mm to 1000 mm. This setup is achieved by simultaneously reducing the dimension of the 1000-mm cyclone in proportion, as done in the works of Ghodrat et al. (Ghodrat et al., 2013) and Wang and Yu. (Wang and Yu, 2006) Such proportional changes guarantee the geometric similarity of the hydrocyclones involved, and are necessary to obtain comparable results in revealing cyclone size effect, as recently highlighted by Zhao and Su (Zhao and Su, 2016) in their study of gas cyclone.

Table 4- 1 Geometric and operational parameters in the present simulation

Parameter	Value
Diameter of the body (D_c), mm	300, 400, 500, 600, 700, 800, 900, 1000
Inlet (involute) (D_i), mm	80, 106, 133, 160, 186, 213, 239, 266
Diameter of vortex finder (D_v), mm	117, 156, 195, 234, 273, 312, 351, 390
Diameter of spigot (D_u), mm	60, 80, 100, 120, 140, 160, 180, 200
Length of cylindrical section (L_c), mm	395, 526, 658, 790, 921, 1053, 1184, 1316
Length of conical section (L), mm	805, 1074, 1342, 1610, 1879, 2147, 2416, 2684
Inlet velocity (u), m/s	3.5

Particle material	Coal
Particles densities (ρ_p), kg/m ³	1275-2200
Feed solid volume fraction	7.4 %
Particle sizes (d), mm	0.045-1.41

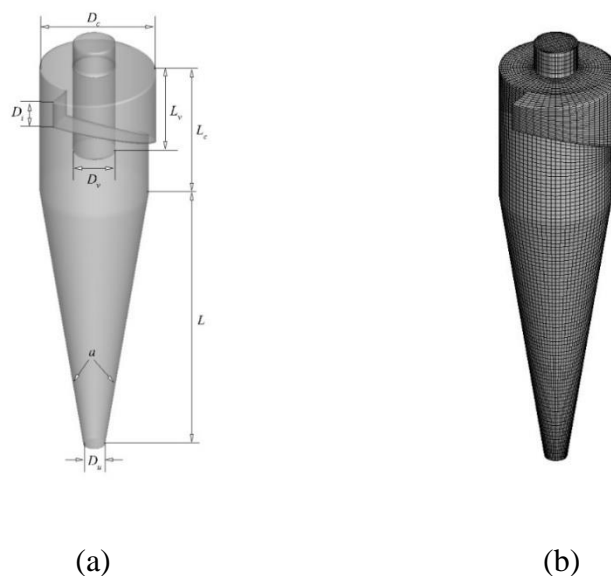


Fig. 4- 2 Geometric profile (a) and mesh (b) of the hydrocyclones simulated.

The whole computational domain of each cyclone simulated is divided by 160122 hexahedral grids. The grid is finer in the vicinity of the walls and vortex finder than in the remainder of the cyclone, as shown in Fig. 4-2 (b). It has been proved that with this grid scheme, the numerical solution is converged and grid-independent for the 1000-mm (largest) cyclone (Ghodrat et al., 2016). In all of the simulations, a “velocity inlet” boundary condition is used at the cyclone inlet, and the “pressure-outlet” condition at the underflow and overflow. The pressure at the two outlets is 1 atm, i.e. the ambient atmospheric pressure. The inlet water velocity and particle velocity are both 3.5 m/s. Corresponding to a normal operation of hydrocyclone in the coal preparation, the feed solid volume fraction is set to 7.4 %, as considered in the experiments (O'Brien et al., 2001).

To carry out a simulation, the particle size/density distribution as used in the experimental work of O'Brien et al. (O'Brien et al., 2001) is divided into a series of size/density intervals, with each represented by a mean size/density in the simulation (see Table 4-2). Note that in this study, the interplay between densities is ignored and

each simulation considers only one density. Accordingly, three simulations are performed to consider the density distribution listed in Table 4-2 for a given cyclone size. The simplifications introduced here are due to the following reasons. One is that the previous study (Ghodrat et al., 2016) suggested that the simulations with and without consideration of the interplay between coal densities give the consistent results in reasonably good agreement with the experimental measurements. And, the latter can reduce the computational time from two months to three weeks, as well as more precisely describe the most concerned partition curves by simulating adequate particle sizes. Another reason is that the present mathematical model can only consider a limited number (up to 20 in ANSYS Fluent) of phases to guarantee numerical stability. In fact, similar treatments have been successfully used for the modelling of dense medium cyclones (DMCs), as reported elsewhere (Kuang et al., 2014, Qi et al., 2015). However, in DMCs the interplay between particle sizes was ignored as particles are separated according to particle densities.

Table 4- 2 Size and density distributions in the simulations

Density \ Size	1275 (kg/m ³)	1500 (kg/m ³)	2200 (kg/m ³)
1.41 mm	20.00%	16.67%	4.00%
0.71 mm	22.50%	5.56%	4.00%
0.42 mm	7.50%	5.56%	4.00%
0.3 mm	7.50%	5.56%	4.00%
0.21 mm	7.50%	5.56%	4.00%
0.15 mm	7.50%	5.56%	4.00%
0.115 mm	7.50%	5.56%	4.00%
0.08 mm	5.00%	5.56%	4.00%
0.045 mm	15.00%	44.44%	68.00%

The simulations are conducted by the unsteady solver in ANSYS Fluent CFD software package (version 14.5) at the National Computational Infrastructure in Australia. 32 CPUs are assigned to each simulation, which lasts for about three weeks to consider the physical time of 40 s. Unless otherwise noted, all the results shown are averaged over the last ten seconds of the physical time, during which the flow simulated can achieve a steady state and thus the macroscopic flow characteristics do not change much with time.

4.4 Results and discussion

4.4.1 Separation performance

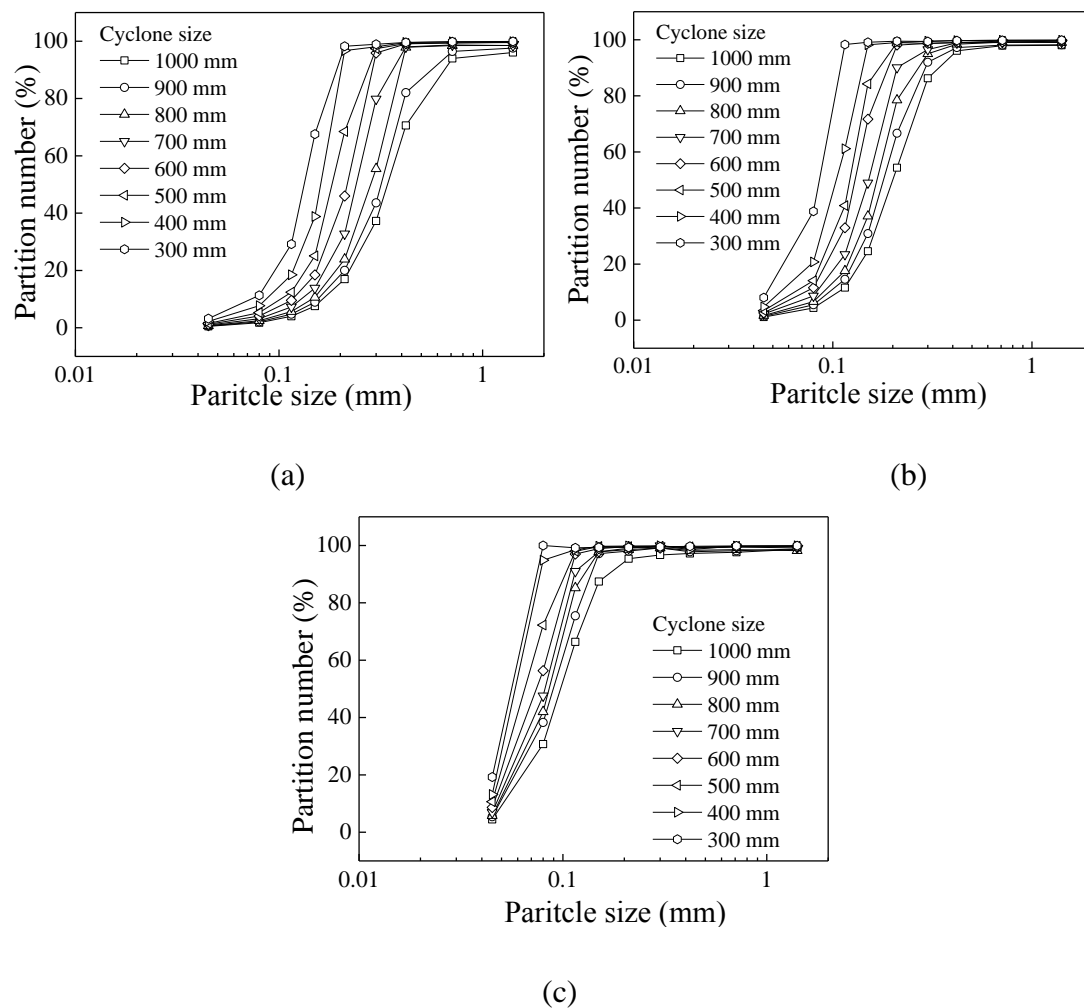


Fig. 4- 3 Effect of cyclone size on the partition curves for the coal density of: (a) 1275 kg/m^3 , (b) 1500 kg/m^3 , and (c) 2200 kg/m^3 .

Fig. 4-3 shows how cyclone size affects the partition curves when processing coal with different densities. Here, the partition number is defined as the volumetric ratio of the particles reported to the underflow to those fed into the cyclone for the same particle size. As seen from this figure, with increasing cyclone size from 300 mm to 1000 mm for a given particle density, the partition curve obviously shifts to the right, and at the same time, the curve sharpness or slope reduces. A similar trend has also been reported by Wang and Yu (Wang and Yu, 2006) and Ghodrat et al. (Ghodrat et al., 2013) in their studies on the separation of limestone particles (density=2700 kg/m³) in hydrocyclones with the size range from 18 mm to 300 mm. Note that for the specific coal particles considered in this work, cyclones smaller than 300 mm should result in a small cut size that is outside the present particle size range, as indicated by Fig. 4-3(c), and thus are not simulated. Notably, Fig. 4-3 also reveals that particle density and cyclone size intensively interact with each other. Generally, the effect of cyclone size is more significant when particles are lighter. Moreover, the partition curve generally becomes steeper with increasing particle density for the same hydrocyclone, similar to those observed in experiments (Firth et al., 1999, O'Brien et al., 2001). Furthermore, under the present conditions, the partition curves do not apparently change for the heaviest particles when the cyclone sizes are relatively small (e.g., 300 and 400 mm here), which is consistent with the experimental observations by Lynch et al. (1974, 1975).

To be quantitative in the analysis, cyclone performance is examined with respect to separation sharpness, cut size, inlet pressure drop and underflow water split. Fig. 4-4 (a) show the cut size d_{50} (corresponding to the separation efficiency of 50% in a partition curve) as a function of cyclone size at different particle densities. The cut size increases with the increase of cyclone size, which is in line with the general observation of hydrocyclones (Bradley, 1965, Arterburn, 1982, Heiskanen, 1993, Lv et al., 2015, Mognon et al., 2015, Neesse et al., 2015). This increase is more significant when particles become lighter.

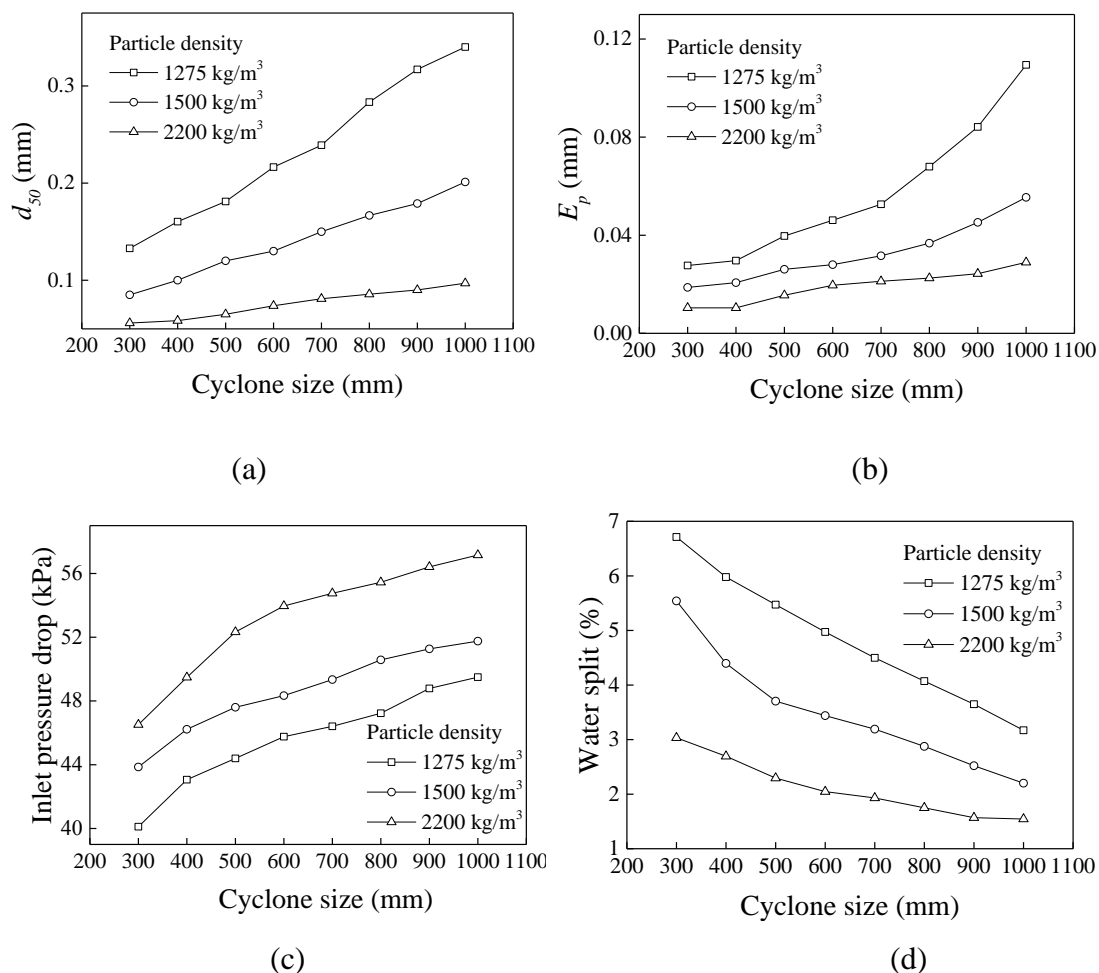


Fig. 4- 4 Effects of cyclone size on performance parameters at different particle densities: (a) cut size, (b) Ecart probable, (c) inlet pressure drop, and (d) water split.

To describe the separation sharpness, the Ecart probable E_p ($= (d_{75} - d_{25}) / 2$) widely used for dense medium cyclones is used in place of the sharpness coefficient determined using the Lynch model (1977). This is because E_p is more robust to identify the difference in sharpness between two partition curves when the data points around the cut size are not dense enough (Ghodrat et al., 2013). By definition, a smaller E_p corresponds to a larger value of sharpness and thus more precise separation. Fig. 4- 4 (b) shows that similar to the trend of cut size, E_p decreases with the decrease of cyclone size or increase of particle density. Furthermore, these variations are more significant for lighter particles or larger cyclones. In other words, the separation precision is reduced in a larger cyclone, particularly for lighter particles. From this viewpoint, a smaller cyclone is preferred. This conclusion is in line with the experimental observation of min-hydrocyclones (Young et al., 1994, Lv et al., 2015). However, O'Brien et al. (O'Brien et al., 2001), reported that the separation sharpness

does not change much for different sized cyclones. It may be due to that in the experimental work of O'Brien et al. (O'Brien et al., 2001), two considered cyclones do not have geometric similarity, which is however necessary to properly reveal the effect of cyclone size (Zhao and Su, 2016). Furthermore, according to the recent semi-mechanistic model of Narasimha et al. (Narasimha et al., 2014), provided that the geometric similarity of hydrocyclones can be maintained, the separation sharpness increases with the increase of the centrifugal acceleration in the radial direction. The present study and others (Ghodrat et al., 2013, Wang and Yu, 2006) suggest that a larger cyclone results in a decreased radial centrifugal acceleration and thus a smaller separation sharpness. Therefore, the present results are consistent with the semi-mechanistic model of Narasimha et al. (Narasimha et al., 2014).

Figs. 4-4 (c) and (d) show the inlet pressure drop and the amount of water split to the underflow, respectively. The former is an index reflecting the energy consumption. The latter is associated with the bypass effect (Slechta and Firth, 1984). That is, coarse particles in the feed stream move along the boundary layer over the outside wall of the vortex finder and directly join the overflow stream within the vortex finder, while ultrafine particles flow with the water flow and report to the underflow. Apparently, the bypass problem is part of the misplacement problem and deteriorated by the presence of particle density distribution. It is shown that as cyclone size or particle density increases, the inlet pressure drop increases (Fig. 4-4 (c)), whereas the water split decreases (Fig. 4-4 (d)). The reason behind is that a higher radial pressure drop forces the water to be discharged to the overflow, leading to a smaller amount of water split into the underflow, similar to those reported elsewhere (Saengchan et al., 2009, Bhaskar et al., 2007). Note that in hydrocyclones, the inlet pressure drop is proportional to the mixture density, cyclone size and tangential velocity (Hararah et al., 2010, Ghodrat et al., 2013). This relationship can also apply to the present results.

The results in Fig. 4-4 manifest that provided that the expected cut size can be achieved, cyclone size needs to be as small as possible to reduce energy consumption and improve separation precision, however, should be large enough to mitigate the deficiencies associated with the bypass effect at the spigot. This result is particularly true for particles having a broad density distribution. When particle density varies, the

separation sharpness changes more significantly for relatively large cyclones, whereas the water split experiences a bigger change for relatively small cyclones.

To further understand the way in which the water split is affected by particle density and cyclone size, the volume fraction and axial velocities of water at the spigot or underflow are examined. Fig. 4-5 (a) shows that when body size or particle density increases, the water volume fraction decreases at the spigot, which means there the solids volume fraction increases, leading to the stronger resistance for the downward water flow. Therefore, the magnitude of downward water flow decreases (Fig. 4-5 (b)). This result suggests that besides the radial pressure drop, the particle accumulation near the spigot also contributes to the variation of water split. That is, it reduces the entrainment effect of water on particles.

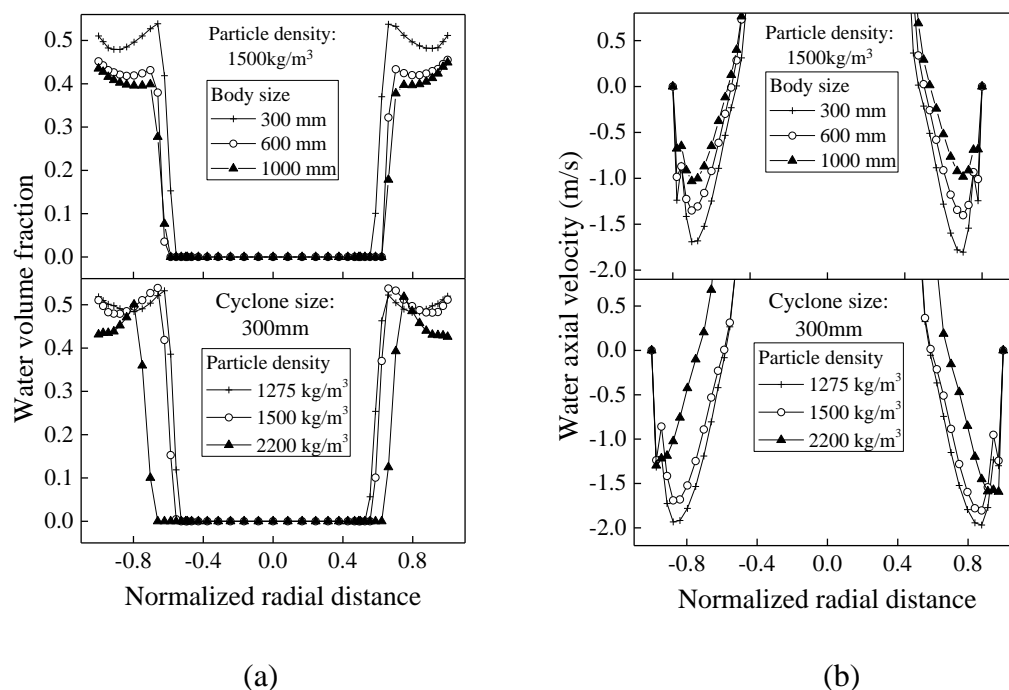


Fig. 4- 5 Profiles of (a) volume fraction and (b) axial velocity at the spigot.

A main concern about hydrocyclone applications in the coal industry is the particle misplacement phenomenon. The misplaced ultrafine particles (e.g. 0.045 mm here) and coarse particles (e.g. 1.41 mm here) are the most problematic for the downstream processes. Here, the separation efficiency of such particles is examined against cyclone size and the results are given in Fig. 4-6. Considering that the downstream flotation process often handles particles below 0.5 mm (Arnold et al., 2007), 0.5 mm particles are also considered in Fig. 4-6. As seen from this figure, when cyclone size

increases, the amount of ultrafine (0.045 m) particles misplaced to the underflow rapidly decreases first and then slows down. This phenomenon is more evident for heavier particles. Conversely, the amount of coarse (0.5 mm and 1.41 mm) particles misplaced to the overflow increases for relatively large cyclones used to handle light particles. All these results suggest that the mid-range cyclone size (e.g. 400-600 here) is useful for mitigating particle misplacement at both the underflow and overflow. Notably, within this range, the separation sharpness is relatively high (see Fig. 4-4(b)). The present recommendation is consistent with the study of Atkinson and Swanson (Atkinson and Swanson, 2008) who, however, drew their conclusion from the comparison of the partition curves of 1000-mm and 480-mm cyclones.

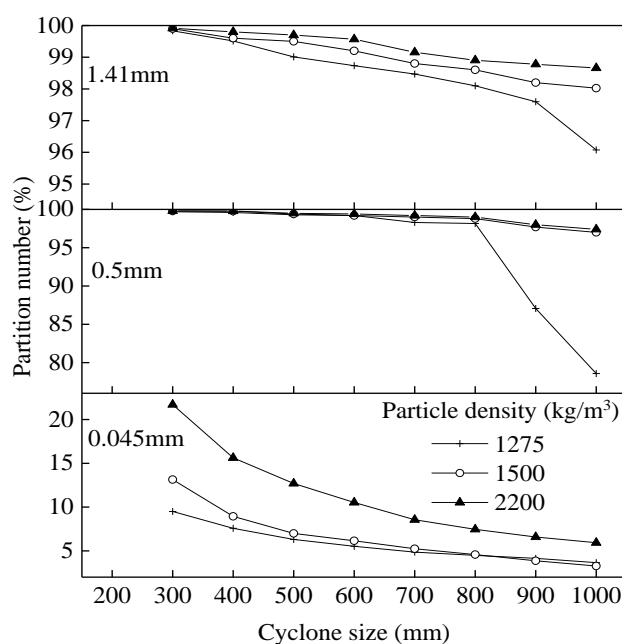


Fig. 4- 6 Partition number of ultrafine and coarse particles as a function of cyclone size at different particle densities.

4.4.2 Flow and force characteristics

The separation performance of cyclone is governed by the multiphase flow and the resultant forces acting on particles. Analysis of this information can generate some insights into this flow system and thus providing a better understanding of the performance. Such analysis is difficult to experimentally achieve, especially for opaque coal slurry. But, it can readily be performed based on the numerical simulations.

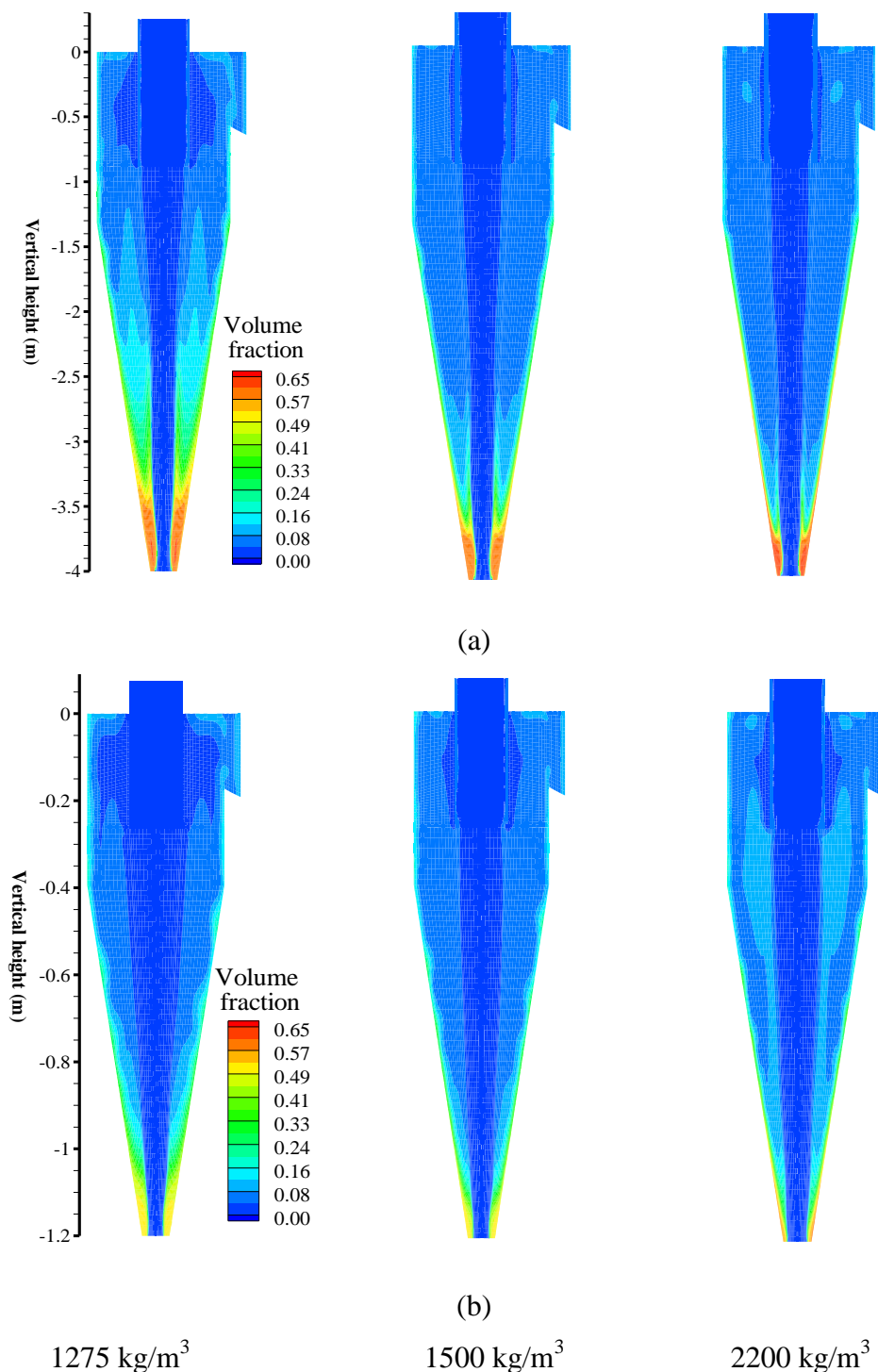


Fig. 4- 7 Spatial distribution of coal volume fraction at the cyclone size of (a) 1000 mm and (b) 300 mm.

Fig. 4-7 demonstrates how cyclone size affects the distributions of solids volume fraction for particles of different densities. Expectedly, the solids volume fraction is higher near the wall for heavier particles. Furthermore, particles are observed to accumulate near the spigot, leading to dense particles there. This accumulation may

block the ways of some coarse light particles towards the wall and lead to their misplacement to the overflow. It also reduces the effective separation space, which hinders particles to move towards the proper flow streams and hence further deteriorates the misplacement problem. It is of interest to note that as cyclone size increases, the particle accumulation area becomes larger near the spigot, which is more evident for light particles. Therefore, light coarse particles are more likely to be misplaced to the overflow in large cyclones.

Fig. 4-8 shows the distribution of water tangential velocities resulting from the strong swirling flow and causing particles to move towards the outer wall. In this figure, the white region in the central region corresponds to the area occupied by the air-core, whose velocities are not shown because the properties of air are very different from those of liquid and solid phases. Such a representation has been used in other studies, and offers a convenience for better showing the flow properties that govern the separation process (Qi et al., 2015, Kuang et al., 2014, Wang and Yu, 2006, Ghodrati et al., 2016). As seen from Fig. 4-8, the tangential velocities increase with the increase of cyclone size, however, largely remains the same for particles with different densities. Notably, the tangential velocities drastically drop near the spigot. This phenomenon has also been experimentally and numerically observed by different investigators (Ghodrati et al., 2016, Davailles et al., 2012, Noroozi and Hashemabadi, 2009, Swain and Mohanty, 2013). It is a result of the intense interactions between water and dense particles near the spigot. It should be pointed out that the tangential velocities alone cannot be used to explain the variation of separation sharpness under the present conditions, although they were mainly considered in most of the previous studies of water-air flows or dilute water-air-solid flows. The distribution of pressure gradient is similar to that of tangential velocities, as shown in Fig. 4-9. However, the pressure gradient decreases with the decrease of particle density or the increase of cyclone size.

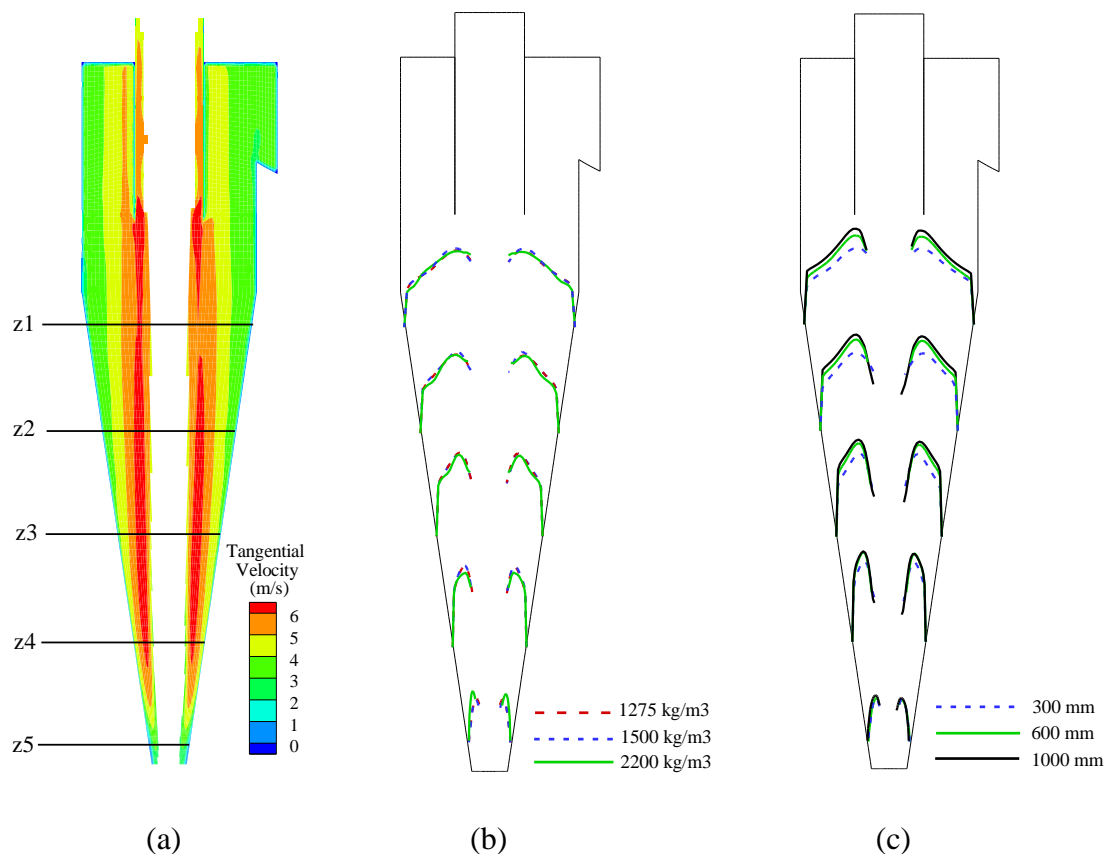


Fig. 4- 8 Distributions of water tangential velocities: (a) representative contour, (b) effect of particle density at the cyclone size of 300 mm, and (c) effect of cyclone size at the particle density of 1275 kg/m^3 .

In hydrocyclones, the separation of particles is mainly governed by the centrifugal, pressure gradient and drag forces in the radial direction (Zhu et al., 2011, Wick, 1977, Bhardwaj et al., 2011). Although the importance of these forces have been well recognised in the separation process of hydrocyclone, their detailed analysis is lacking, particularly for the spatial characteristics. For the first time in literature, we retrieve these three forces from the TFM simulations for analysis via user defined functions (UDF) in ANSYS Fluent. To be comparable, the force-induced radial accelerations are considered.

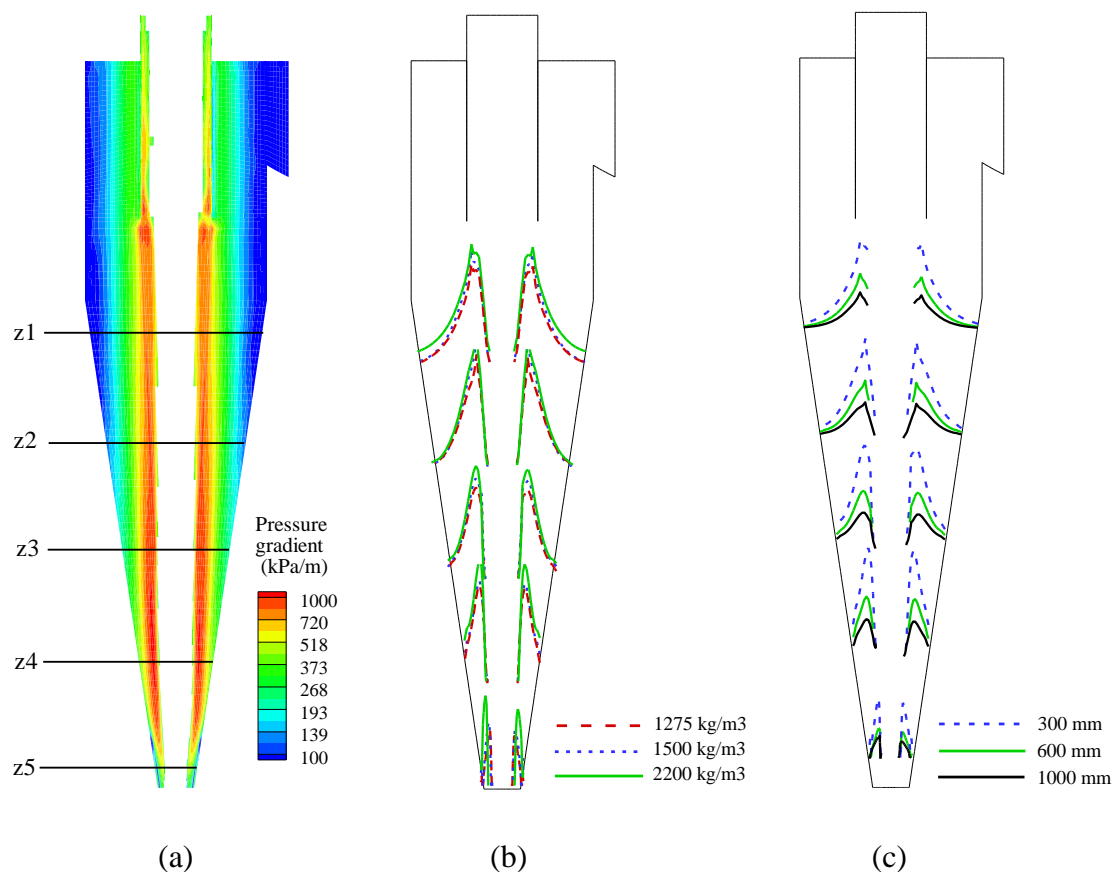


Fig. 4- 9 Distributions of pressure gradient corresponding to Fig. 4-8.

Fig. 4-10 (a) and (b) show the representative distributions of radial accelerations. Expectedly, the accelerations resulting from centrifugal forces are outward (corresponding to positive value), while those due to pressure gradient and drag forces are mainly inward (corresponding to negative value) and shown together for clarity. Basically, the direction of particle motion is affected by the total forces acting on the particle involved. Therefore, the total radial accelerations are first examined against particle size to gain a better understanding of the working principle of hydrocyclone. This can in turn confirm the validity of the present analysis.

Fig. 4-10 (c) compares the total radial accelerations of fine (0.045m) and coarse (1.41m) particles. This is done at five representative heights. Overall, the total accelerations are mainly positive, i.e. towards the outer wall. However, they significantly drop or even become negative near the wall because of the wall effect and the particle segregation there. Also, the total accelerations apparently fluctuate near the center resulting from the air-core. These results can also apply to other

conditions considered, suggesting that the centrifugal forces play a dominating role in hydrocyclones. This is different from dense medium cyclones, where centrifugal and pressure gradient forces may be equally important (Chu et al., 2009), because the particles involved are much coarser and the entrainment effect of dense medium (not water) on particles is much stronger compared to hydrocyclones.

Fig 4-10 (c) also shows that the total accelerations of coarse particles are much larger than those of fine particles, e.g. at lines z3, z4 and z5. This enhances the chance for coarse particles to move towards the outer wall and fall down under the gravity along the wall with the downward flow stream. Because the centrifugal forces less dominate, fine particles are more likely to flow with the water flow. Note that at line z1 which is close to cylindrical section, the total accelerations for coarse and fine particles do not have obvious differences. This result also applies to other locations within the cylindrical part, manifesting that particles are more difficult to separate within the cylindrical part compared to the conical region. This understanding is in line with the previous finding that the cylindrical section plays a minor role in separating particles (Ji et al., 2012, Wang and Yu, 2006).

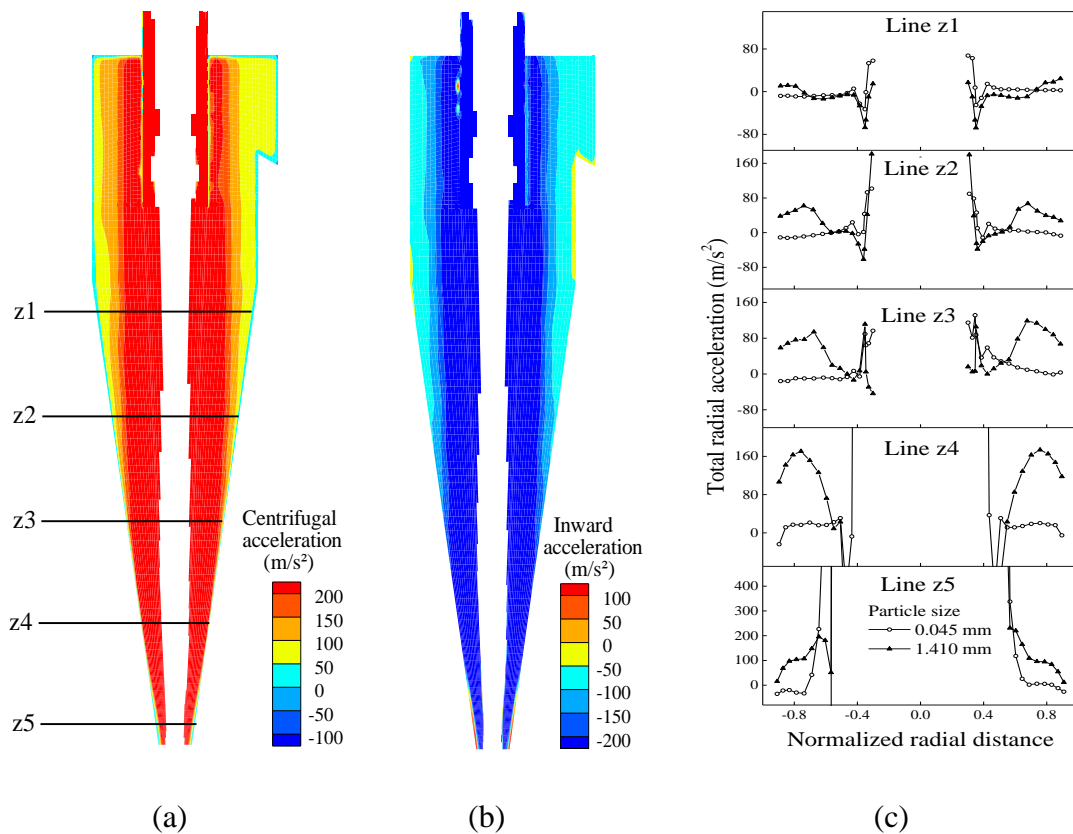


Fig. 4- 10 Distributions of radial accelerations (a) due to centrifugal forces and (b) due to pressure gradient forces and drag forces for 1.41 mm particles, as well as (c) comparison of the total radial accelerations for 1.41 mm and 0.045 mm particles. The particle density and cyclone size considered here are 2200 kg/m^3 and 300 mm, respectively.

Fig. 4-11 shows the distributions of fine and coarse particles within different flow streams. In this figure, LZVV represents the locus of zero vertical or axial velocity of water. It is used to demarcate the upward (near the wall region) and downward (near the center region) water flows. To be comparable, the volume fraction of particles considered is normalised by their own feed. As seen from Fig. 4-11, as expected, most of coarse particles can quickly reach the region near the outer wall once they are fed into the cyclone. Conversely, fine particles can be found from both the downward and upward flow streams. Their volume fractions are apparently larger near the spigot and within the upward flow stream compared to other regions. In fact, only a small portion of fine particles report to the underflow in proportion to the water split. Their majority first come with the downward flow stream to the lower part of cyclone, and then flow with the upward flow streams to the overflow. These results can well support the results from the force analysis via Fig. 4-10.

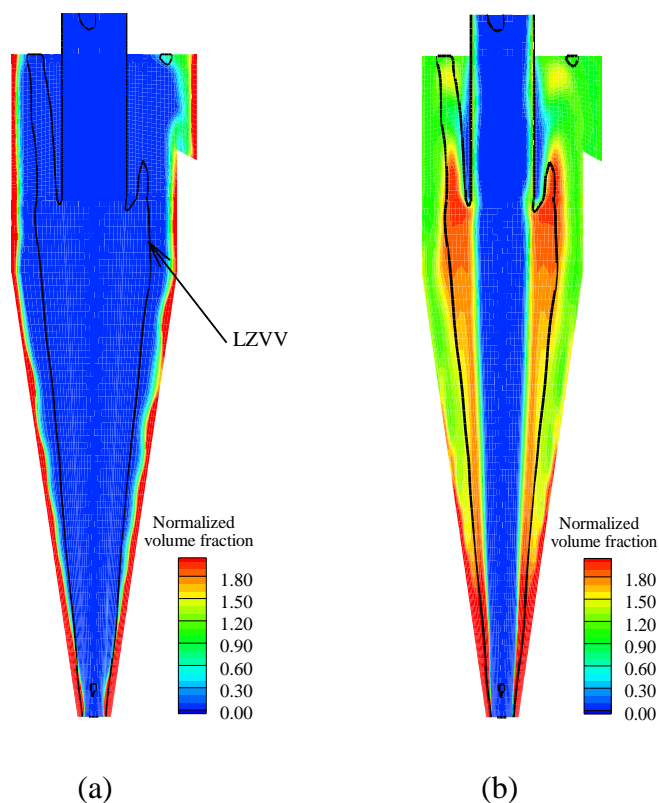


Fig. 4- 11 Distributions of volume fraction for the particles of: (a) 1.41 mm and (b) 0.045 mm, corresponding to Fig. 4-10.

Fig. 4-12 compares the total accelerations of particles of different densities for 300-mm and 1000-mm hydrocyclones. Here, we only consider one particle size for brevity. However, the resulting findings are valid to other particle sizes. As seen from Fig. 4-12 (a), the total radial accelerations are generally smaller within a larger cyclone. Note that a larger cyclone also has an enlarged particle accumulation area near the spigot, which block the ways of some coarse particles towards the outer wall. These two factors collectively account for the reduced separation precision of a larger cyclone, especially when handling light particles which result in a larger accumulation area, as shown in Fig.4-7. Fig. 4-12(a) also shows that as particles become heavier, the total radial accelerations mainly increase within the small cyclone, which does not occur to the large cyclone. Therefore, for a given particle size, particles of different densities have less chance to get separated at the upper part of conical section when they flow down with water within larger cyclones. Such particles are more likely to flow down to the spigot area. Some of them are misplaced once their ways towards the proper flow streams are blocked by the dense particles there. In other words, a large cyclone reduces the difference in the total accelerations for particles of different densities, and in this situation, either the separation precision or the particle misplacement is controlled by the difference in the particle accumulation area. This relationship can well be reflected from the present study.

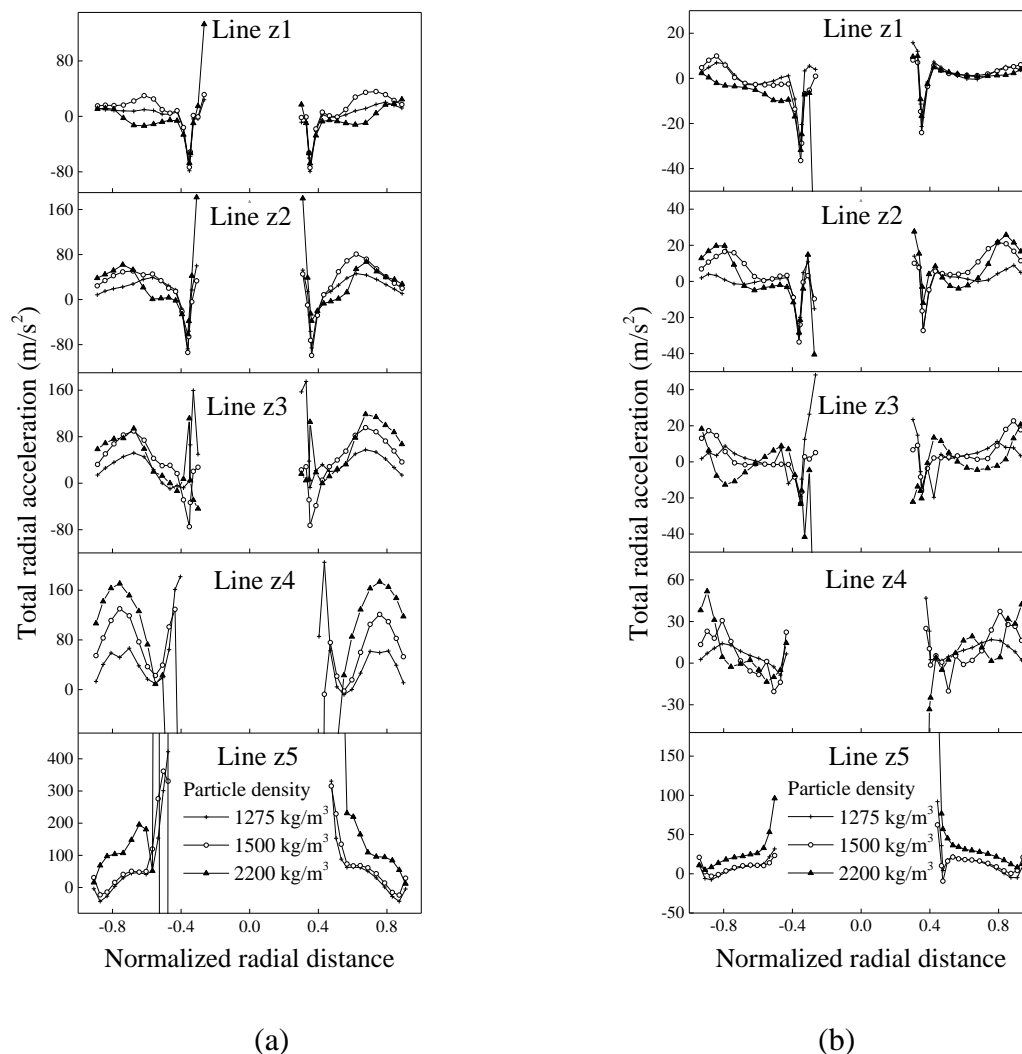


Fig. 4- 12 Comparison of the total accelerations of particles of different densities for (a) 300-mm and (b) 1000-mm hydrocyclones. The particle size is 1.41 mm.

Considering that particle accumulation is of critical importance to cyclone performance, the particle flow behaviors are further examined near the spigot where dense particles are generally present. The result is given in Figs. 4-13 and 4-14. Here, the finest and coarsest particles, which are vulnerable to misplacement, are focused. Overall, particles are found to expectedly flow upwards around the air-core but downwards near the wall region. For the coarse (e.g. 1.41 mm) particles, when cyclone size increases or particle density decreases, the magnitudes of radial velocities, by which particles return from the upward flow stream to the downward flow stream, become smaller (Figs. 4-13 (a) and 4-14 (a)). This is attributed to the decrease of total radial accelerations or/and the increase of particle accumulation area. Notably, within the area close to the spigot, the radial velocities from the downward

flow stream to the upward flow stream is much stronger for the large cyclone or light coarse particles. This result well corresponds to the aforementioned misplacement behaviors of coarse light particles. On the other hand, for the fine (e.g. 0.045 mm) particles, the downward flow at the spigot is much stronger for a smaller cyclone. Such particles are entrained by water, which of amount increases with the decrease of cyclone size, companying with the increase of total radial accelerations.

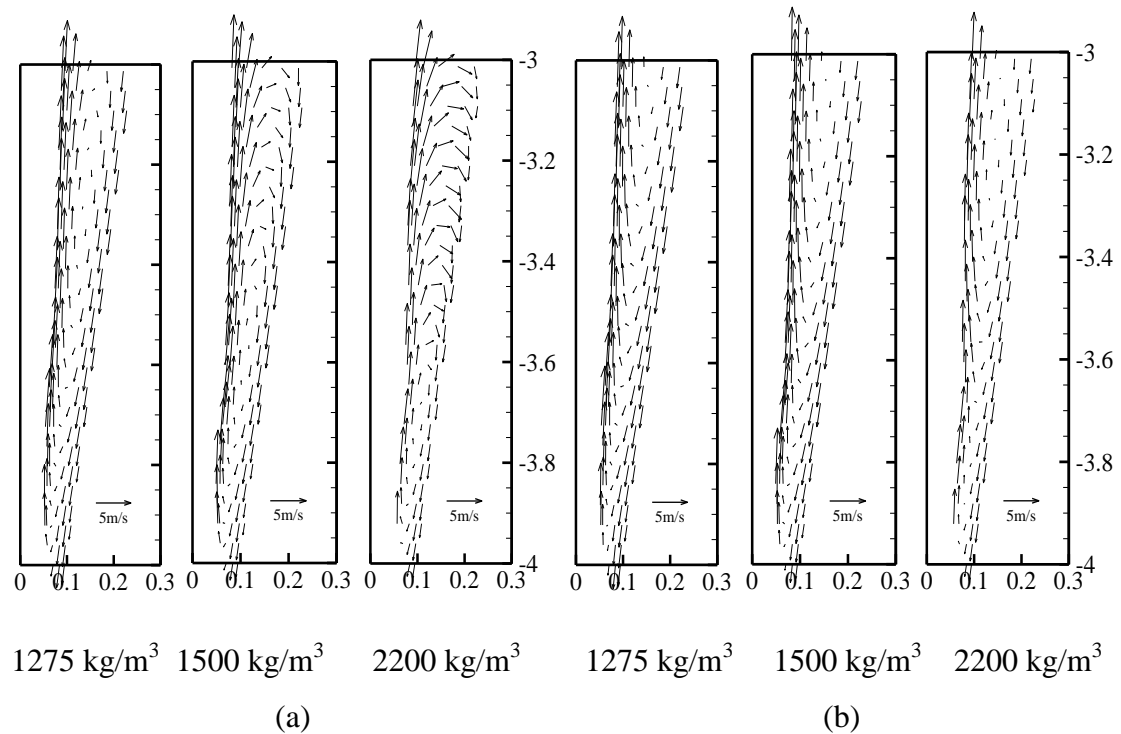


Fig. 4- 13 Flow fields within the lower part of 1000-mm hydrocyclone for (a) 1.41 mm and (b) 0.045 mm particles

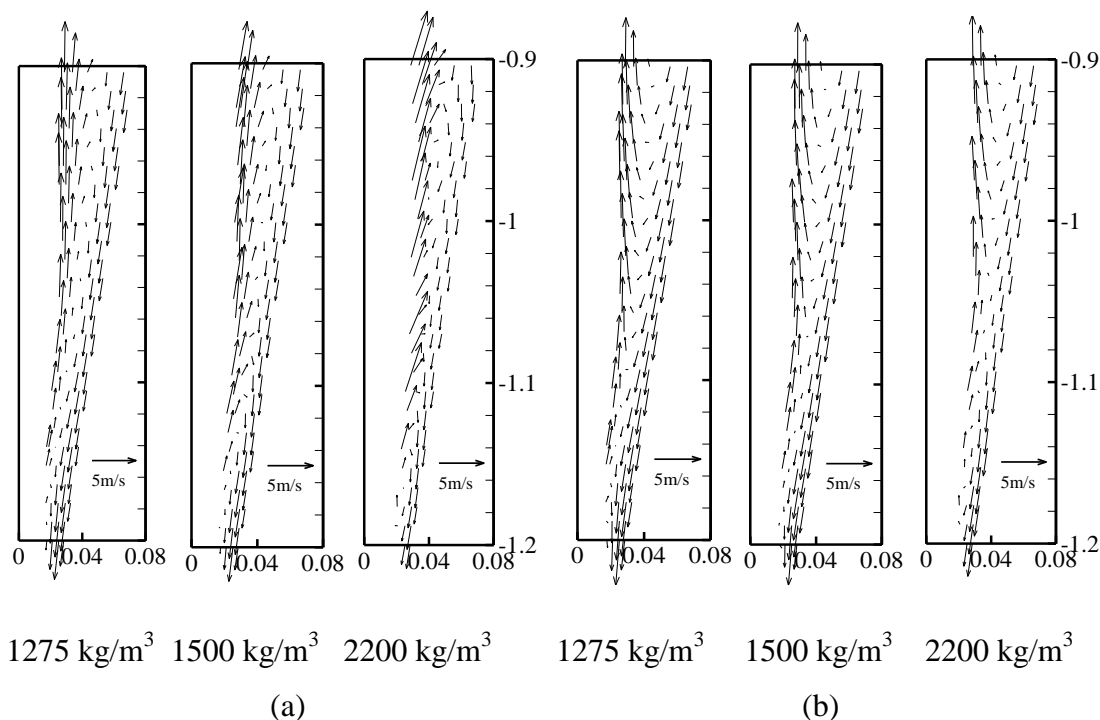


Fig. 4- 14 Flow fields within the lower part of 300-mm hydrocyclone for (a) 1.41 mm and (b) 0.045 mm particles.

4.5 Conclusions

There are opposite opinions on selecting hydrocyclone size to mitigate the adverse effect of particle density in the coal industry. To this end, in this study the effects of particle density on the flows and performance of hydrocyclones are fully studied with respect to cyclone size by the recently developed Two-fluid Model. The major findings from the present study can be summarised as follows:

(1) When particle density varies, the separation sharpness changes more significantly for relatively large cyclones, whereas the water split experiences a bigger change for relatively small cyclones. When cyclone size changes, the separation sharpness and water split vary more dramatically for light particles. Therefore, particle density effect needs to be considered for selecting cyclone size.

(2) More ultrafine particles are misplaced to the underflow in smaller cyclones, which is pronounced for heavier particles. On the other hand, more particles which are coarse and light, unexpectedly report to the overflow in larger cyclones. Moreover, larger cyclones handling lighter particles have weakened separation precision and increased cut size. In order to obtain good separation sharpness and mitigate particle

misplacement at the same time, a mid-range cyclone size is recommended to be employed on the condition that the expected cut size can be achieved.

(3) The centrifugal forces are mostly stronger than the total drag and pressure gradient forces in the radial direction but mainly inside the conical part of hydrocyclones. Thus, the total radial accelerations of the particles there are mainly outward. The larger total radial accelerations of coarser particles enhance their chance of moving towards the outer wall. Accordingly, more fine particles are entrained by the water flow, distributed between the downward and upward flow streams near the spigot, and then report to the underflow and overflow with the water flow. This entrainment effect of water can be mitigated by the particle accumulation near the spigot.

(4) The outward total radial accelerations increase with increasing particle density for relatively small cyclones, which however does not apparently occur to relatively large cyclones. The particle accumulation near the spigot blocks the ways of particles for separation and reduces the cyclone separation space. Its area increases as cyclone size increases or particle density decreases. These variations of total radial acceleration and particle accumulation account for the reduced separation precision for larger hydrocyclones handling lighter particles.

**CHAPTER 5 NUMERICAL STUDY OF THE EFFECT OF
INLET FEED TYPE ON THE MULTIPHASE FLOW AND
PERFORMANCE OF HYDROCYCLONES**

5.1 Introduction

Hydrocyclones are widely used in the mineral and chemical processing industry. The flow in a hydrocyclone is very complex because of the existence of swirling turbulence, air-core and segregation involving gas, liquid, and solid phases. Researchers have dedicated much effort on investigating the effect of geometrical, material and operational parameters on the separation performance of hydrocyclones. Among the geometrical conditions, inlet design has been considered an important factor and its effects studied carefully as summarized below. Geometrical parameters related to a hydrocyclone inlet include the inlet feed type, inlet diameter, aspect ratio (ratio of length to width) and number of inlets. Studies on the inlet diameter (Rao et al., 1976, Jiang et al., 2007, Kfuall, 1953, Huang et al., 2014), aspect ratio (Ioziya and Leith, 2007, Hsu, 2014, Rakesh et al., 2014) and number of inlets (Yoshida et al., 2008, Tue Nenu and Yoshida, 2009, Zhao et al., 2006) have been conducted in recent years. The effect of inlet feed type, such as how the tangential and involute (spiral) inlet types affect the separation performance of a hydrocyclone as well as gas cyclones and dense medium cyclones is reported in literature (Zhao et al., 2006, Yoshida et al., 2004, Noroozi and Hashemabadi, 2009, Zhang et al., 2013, Zhang et al., 2017, Wang, 2009). Note that there is a new inlet feed type named as a ‘spiral and slope’ inlet which is being increasingly used in the industry (O'Brien et al., 2001). Even though it is claimed that this ‘spiral and slope’ inlet is superior to previous inlet types in the separation performance according to industry advertisements, its working mechanisms have not been fully understood. Note that a helical inlet has a similar shape to the ‘spiral and slope’ inlet as reported by Hong et al. (Hong et al., 2005). This study suggested that electro cyclones with inlets of this shape are advantageous in the collection efficiency over those with tangential and involute inlets. However, this study is based on electronic gas cyclones which have a different working mechanism to that of a hydrocyclone in addition to the fact that they process ultrafine particles with diameters between 0.3 to 6 μ m. In this chapter, this new inlet feed type is studied and compared with the involute one with respect to the effect on separation performance of hydrocyclones.

Apart from the inlet feed type, the hydrocyclone separation efficiency is significantly affected by the material properties such as the particle density and feed solid

concentration. However, systematic studies on these two parameters, especially the density effect, have only been conducted in recent years. As such, this chapter attempts to clarify the differences between the involute inlet and ‘spiral and slope’ inlet with respect to the effect of particle density and feed solid volume fraction. This is done based on numerical experiments under well-controlled conditions.

Generally speaking, the modelling of hydrocyclones can be discrete- or continuum-based depending on the treatment of the solid phase, which is represented by either Lagrangian Particle Tracking (LPT), or Discrete Element Method (DEM) in the discrete-based treatment, or by Two-Fluid Model (TFM) in the continuum-based treatment (Nowakowski et al., 2004) . The LPT approach ignores the effect of inter-particle interactions as well as reactions of particles on the fluid, and thus is used mainly for operations in a dilute regime or at a low feed solid concentration (see. e.g., Hwang et al., 2012, Wang and Yu, 2006, Wang et al., 2014). The dense discrete phase model which combines the LPT with the kinetic theory (Zhou et al., 2016) may be used over a wide range of feed solids concentrations. The CFD-DEM or TFM-DEM approach coupled with CG concept was adopted to model the fluid-particle flow in hydrocyclones in Chapter 3. However, the CG CFD-DEM approach is found to underestimate the separation performance when the feed solid concentration is high. On the other hand, the CG TFM-DEM model is applicable but needs further research on determining the critical particle size below which particles should be considered as a continuum medium. TFM models in the form of either the so-called mixture model or Eulerian-Eulerian model can in principle be applied to both dense and dilute regimes. The mixture model is essentially a simplified Eulerian-Eulerian model and was found to be inaccurate for predicting the separation performance of hydrocyclones as long as particles have a broad range of sizes and densities (Ghodrat, 2014). The Eulerian-Eulerian approach can be used to overcome the problem associated with the mixture model, as recently demonstrated by Ghodrat et al. (Ghodrat et al., 2016, Ji et al., 2017). Therefore, the model of Ghodrat et al. (Ghodrat et al., 2016) is adopted to systematically conduct numerical experiments to study the effect that is brought about by the involute and ‘spiral and slope’ type inlets. Such studies have not been reported in literature, although they are highly relevant for practical applications. From this study, the effects are elucidated in terms of flow and

force characteristics. Also, a superior inlet feed type is suggested with regards to improving the separation precision and eliminating particle misplacement.

5.2 Simulation method and conditions

5.2.1 Model Description

The present study is based on the computer model reported elsewhere (Ghodrat et al., 2016, Ji et al., 2017). The model has been proved to be valid for hydrocyclone studies, especially in dealing with a broad range of particle densities and sizes. Its framework is developed in three steps as illustrated in Fig. 5-1 because of the complexity of the flows inside a hydrocyclone. This step-by-step implementation not only guarantees the numerical stability, but also facilitates the model validation from simple to complicated cases.

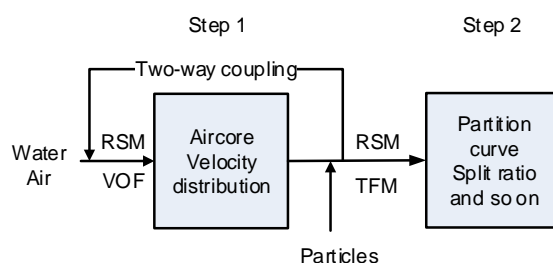


Fig. 5- 1 Modelling Steps used in the present work

In step 1, only the air and water phases are considered. The turbulent flow of water-air mixture is modelled using the Reynolds stress model (RSM), facilitated by a standard wall function (Launder et al., 1975). The interface between the liquid and air-core is modelled using the Volume of Fluid (VOF) model (Hirt and Nichols, 1981), the same as those widely used elsewhere (see, e.g., Wang and Yu, 2006, Bhaskar et al., 2007, Mousavian and Najafi, 2009, Azadi et al., 2010, Kuang et al., 2012). In this step, the primary air-core position and the velocity distribution are obtained.

In step 2, the simulation starts with the results from the first step, and the VOF approach is changed to the TFM approach in the form of Eulerian-Eulerian model (Gidaspow, 1994). Note that the TFM approach can predict the flows and air-core close to those given by the VOF approach (Ghodrat et al., 2016), and only the former can be used to describe the gas-air-solid flows and separation performance of

hydrocyclones. The results obtained here are then used as a part of the initial conditions in the next step.

In step 3, coal particles with different densities and sizes are added to simulate the flows of water, solid and air within the hydrocyclone, as well as to estimate the separation performance by the TFM-RSM approach. In such an approach, both the fluid (liquid and air) and solid phases are treated as interpenetrating continua. Each particle size or density represents one phase. Based on these treatments, a full set of conservative equations with regards to momentum and mass is applied to each phase, combined with the kinetic theory for describing particle-particle interactions. The model formulations and numerical techniques can be found elsewhere (Nowakowski et al., 2000, Safa and Soltani Goharrizi, 2014, Ghodrat et al., 2016, Davailles et al., 2012, Swain and Mohanty, 2013), and thus are not detailed here to avoid repetition.

5.2.1 Model Applicability

It is necessary to verify the validity of the computer model before its application for numerical experiments. This has been done by comparing the numerical results with the measurements through different applications, involving water-air and water-air-solid flows. The data used in the comparison include: (1) the mean tangential and axial velocities as well as RMS (Root-Mean-Square or turbulent stress) velocities of water, as measured by Hsieh and Rajamani (Hsieh and Rajamani, 1991) within the 75-mm cyclone (water-air flow); (2) the water split and inlet pressure drop, as measured by Hsieh and Rajamani (Hsieh and Rajamani, 1991) and Bicalho et al. (Bicalho et al., 2014) within 75-mm and 15-mm cyclones (water-air flow), respectively; and (3) the separation efficiencies of particles having different sizes and densities, as measured by O'Brien et al. (O'Brien et al., 2001) within a 1000-mm cyclone operated at the feed solid volume fractions of 7.4% and 15.2% (water-air-solid flow). Overall, all the results obtained thus far from the comparison suggest that the present model can satisfactorily predict the flows and separation performance of hydrocyclones, at least qualitatively. The detailed results can be found elsewhere (Ghodrat et al., 2016).

5.2.3 Simulation conditions

Table 5-1 lists the present geometric and operational conditions of hydrocyclones,

following the experimental work of O'Brien et al (O'Brien et al., 2001).

Table 5- 1 Geometrical and operational conditions of 1000 mm diameter hydrocyclone

Parameter	Value
Inlet feed type	Involute, Spiral
Diameter of the body (D_c)	1000 mm
Diameter of inlet (D_i)	266 mm
Diameter of vortex finder (D_v)	390 mm
Diameter of apex (D_u)	200 mm
Length of cylindrical part (L_c)	1316 mm
Length of vortex finder (L_v)	2684 mm
Included angle (α)	20°
Inlet velocity (u)	3.5 m/s
Particle material	coal
Particle density (ρ_p)	1275,1500,2200 kg/m ³
Particle size	0.045-1.41 mm
Feed solid concentration (ρ_{feed})	7.4,15.2 %

Fig. 3-2(a) gives the corresponding geometric profile. Unlike the experimental work which considered only hydrocyclones with the 'spiral and slope' inlet, here hydrocyclones with the involute and the 'spiral and slope' inlet are simulated and compared. All the conditions are kept the same for the simulations cases of these two hydrocyclones except the difference in the inlet feed type. The number of hexahedral grids for each cyclone simulated is around 160,000. Moreover, it has been proved that with this grid scheme, the numerical solution is converged and grid-independent both for the cyclone with the 'spiral slope inlet' and involute inlet. The grid is finer in the

vicinity of the walls and vortex finder than in the remainder of the cyclone, as shown in Fig. 5-2(b). In all of the simulations, a “velocity inlet” boundary condition is used at the cyclone inlet, and the “pressure-outlet” condition at the underflow and overflow. The pressure at the two outlets is 1 atm, i.e. the ambient atmospheric pressure. The inlet water velocity and particle velocity are both 3.5 m/s. Corresponding to the normal operation of a hydrocyclone in the coal preparation, the feed solid volume fractions are set to 7.4 % and 15.2%, as considered in the experiments (O'Brien et al., 2001).

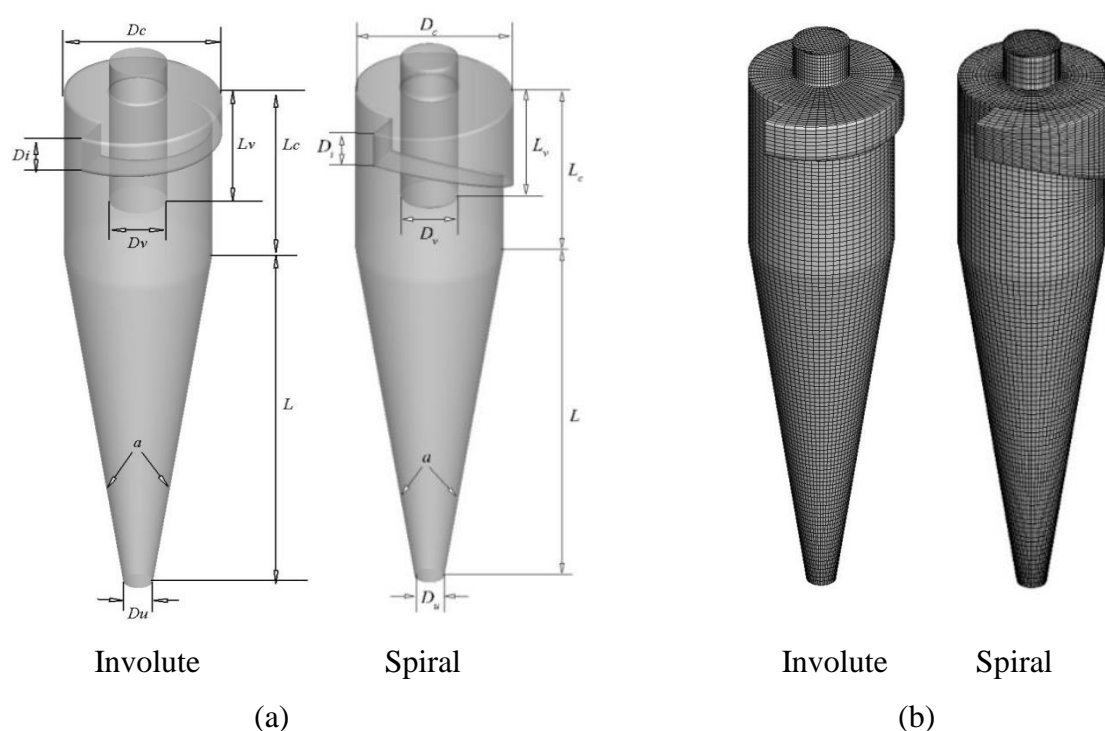


Fig. 5- 2 (a) Geometry and (b) mesh representation of simulated hydrocyclones

To carry out a simulation, the particle size/density distribution as used in the experimental work of O'Brien et al. (O'Brien et al., 2001) is divided into a series of size/density intervals, with each represented by a mean size/density in the simulation (see Table 5-2). Note that in this study, the interplay between densities is ignored and each simulation considers only one density as in previous works (Ghodrat et al., 2016). Accordingly, three simulations are performed to consider the density distribution listed in Table 5-2 for a given cyclone. The reasons for the simplifications of interplay are demonstrated in details in Chapter 4.

Table 5- 2 Size and density distributions in the simulations

Size	Density	1275	1500	2200
		(kg/m ³)	(kg/m ³)	(kg/m ³)
1.41 mm		20.00%	16.67%	4.00%
0.71 mm		22.50%	5.56%	4.00%
0.42 mm		7.50%	5.56%	4.00%
0.3 mm		7.50%	5.56%	4.00%
0.21 mm		7.50%	5.56%	4.00%
0.15 mm		7.50%	5.56%	4.00%
0.115 mm		7.50%	5.56%	4.00%
0.08 mm		5.00%	5.56%	4.00%
0.045 mm		15.00%	44.44%	68.00%

5.3 Results and discussion

Fig. 5-3 shows the effect of inlet type on the partition curves when dealing with coal with different densities under different feed solid concentrations. The ‘spiral and slope’ inlet is called here as ‘spiral’ for brevity in all the figures in this chapter. The partition number is defined as the volumetric ratio of the particles reported to the underflow to those fed into the cyclone for the same particle size. From Fig. 5-3, it can be clearly seen that the partition curves for the ‘spiral and slope’ inlet are generally sharper than those for the involute inlet. Note that the sharper the partition curve, the more accurate the separation. That is to say, that the separation of hydrocyclones with the ‘spiral and slope’ inlet is more efficient than those with the involute inlet. Notably, the effect of inlet feed type is more obvious at a higher feed solid concentration of 15.2%, compared to the slight effect at a feed solid concentration of 7.4%. This means hydrocyclones with the ‘spiral and slope’ inlet are more desirable when dealing with the denser flow with respect to obtaining a sharper separation. Moreover, the effect of feed solid concentration on the partition curve is more evident when processing light materials. For the heavy materials as shown in Fig. 5-3 (c), the variation of partition curves with the feed solid concentration is not as obvious as that shown in Figs. 5-3 (a) and (b), especially for hydrocyclones with the ‘spiral and slope’ inlet. Actually, this

phenomenon can also be observed in the previous work, but it has not been analysed in details. On the other hand, the trend that the partition number increases with the particle density, as reflected in Fig. 5-3, has been studied comprehensively in Chapter 4.

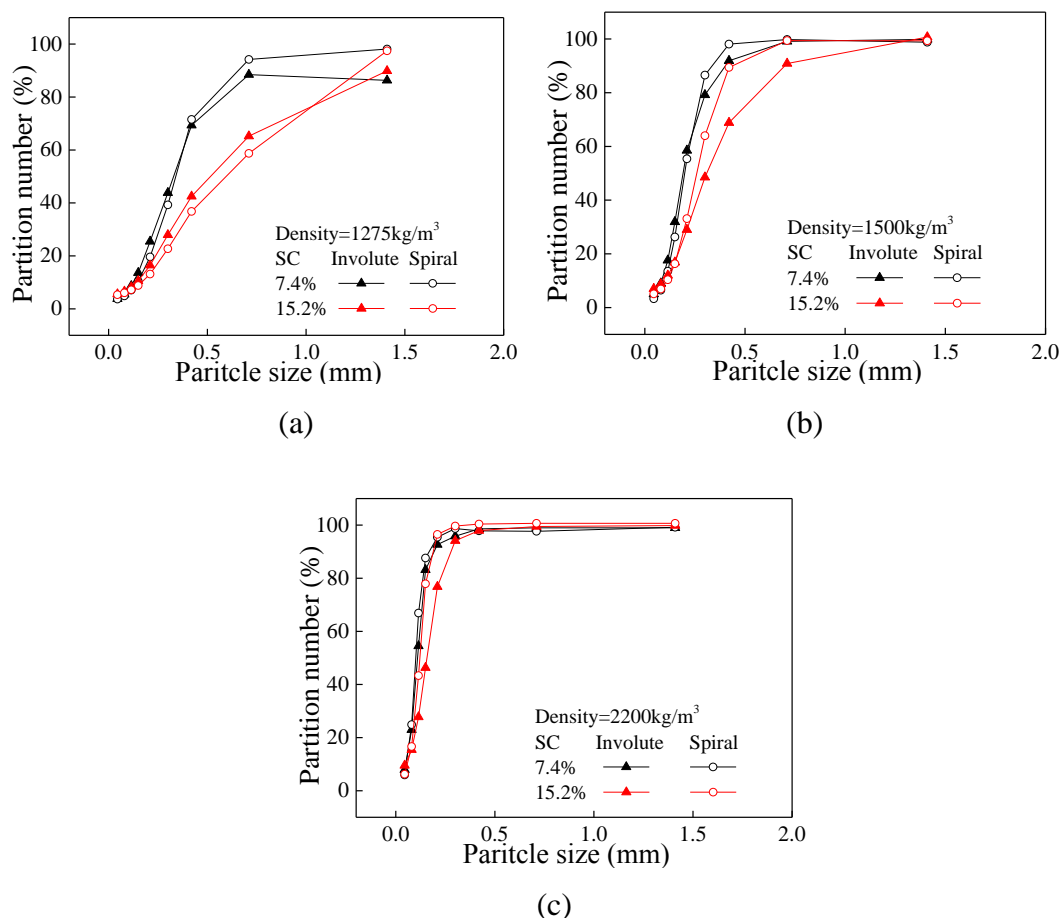
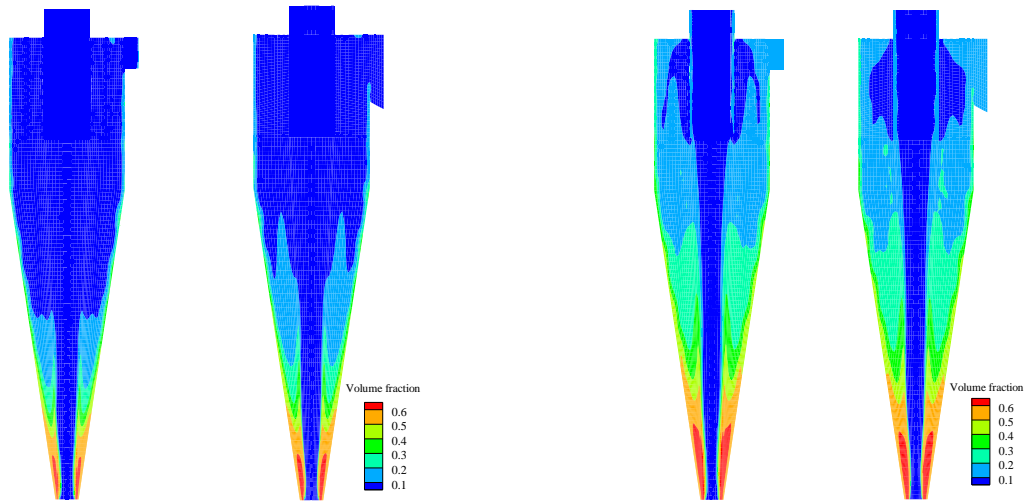


Fig. 5- 3 Effects of inlet type on the partition curves for the coal density of: (a) 1275 kg/m³, (b) 1500 kg/m³, and (c) 2200 kg/m³.

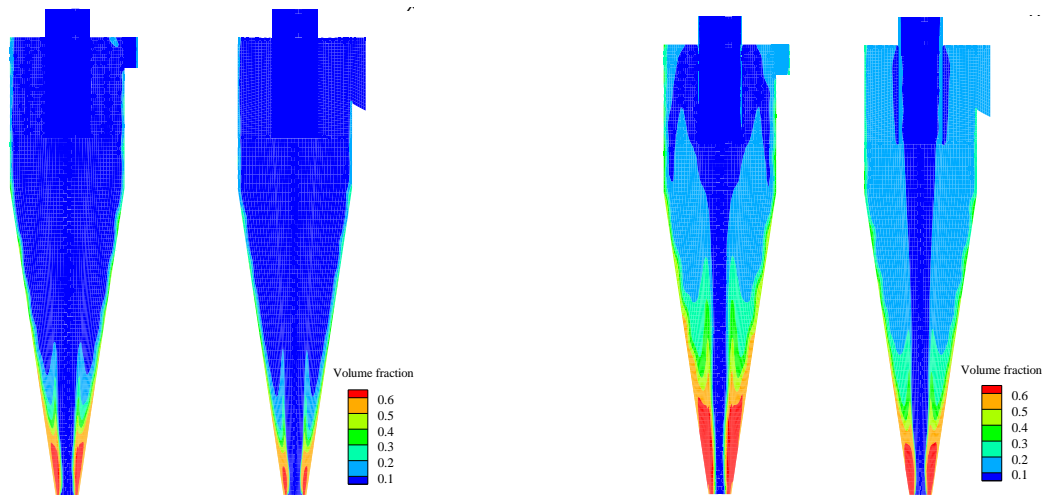
Apart from the effect on the separation sharpness, the inlet feed type and feed solid concentration can also affect the particle misplacement. Specifically, more coarse particles are misplaced to the underflow in the hydrocyclones with the involute inlet, which is more significant in the case of a denser flow. On the other hand, the amount of fine particles discharged to the underflow can also be reduced in the hydrocyclones with a ‘spiral and slope’ inlet. That is to say that the ‘spiral and slope’ inlet is beneficial for eliminating the particle misplacement.

Fig. 5-4 demonstrates how the inlet feed type affects the distributions of solid volume fraction for particles of different densities at different feed solid concentrations. It is believed that a larger accumulation area near the spigot area leads to more misplaced

particles and a worse separation efficiency (Ghodrat et al., 2016, Ji et al., 2017). As shown in Fig. 5-4, the accumulation area is generally larger for hydrocyclones with the involute inlet, which is intensified for a denser flow. However, this phenomenon is not so obvious for light particles. The same trend observed in previous works (Ji et al., 2017, Ghodrat et al., 2016), namely light particles tend to result in a larger particle accumulation area, can also be concluded in Fig. 5-4.



(a)



(b)

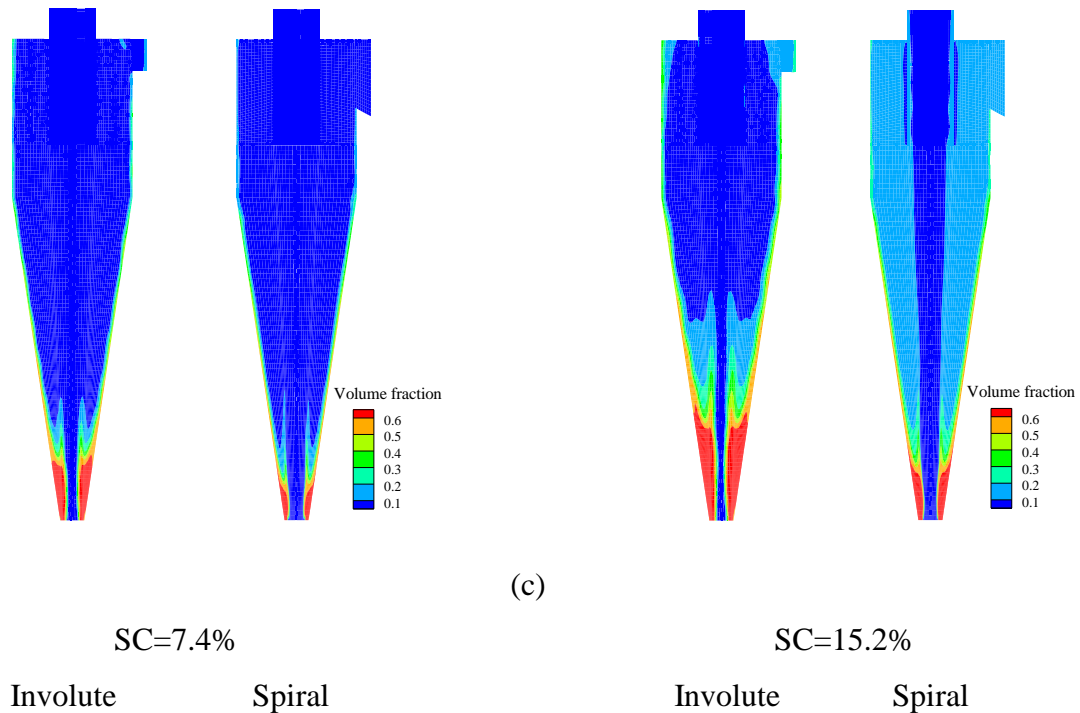


Fig. 5- 4 Spatial distributions of coal volume fraction with densities of (a) 1275 kg/m³, (b) 1500 kg/m³ and (c) 2200 kg/m³(where SC is the feed solid concentration)

Fig. 5-5 compares the distribution of axial velocity of water in hydrocyclones with different types of feed inlets. Here the axial distributions of water in the case of a particle density of 1500 kg/m³ under 7.4% feed solid concentration are considered as an example. Note that particles of different densities at different feed solid concentrations have the same variation trend with inlet feed type. An eddy flow region labelled as A in Fig. 5.5 exists in the region between the outer wall of vortex finder and the wall of the body as reported previously (Wang et al., 2007, Bradley, 1965). Currently, understanding of this eddy flow is quite limited. It is believed that this eddy flow is caused by the inability of the overflow to cope with the upward flow (Wang et al., 2007), and it could lead to an inefficient hydrocyclone particle classification (Dlamini et al., 2005). From Fig. 5-5, it can be clearly observed that the eddy flow in the region A is stronger in the hydrocyclones with the involute inlet. That is to say that the ‘spiral and slope’ inlet contributes to reducing the eddy flow, which is beneficial for improving the separation efficiency.

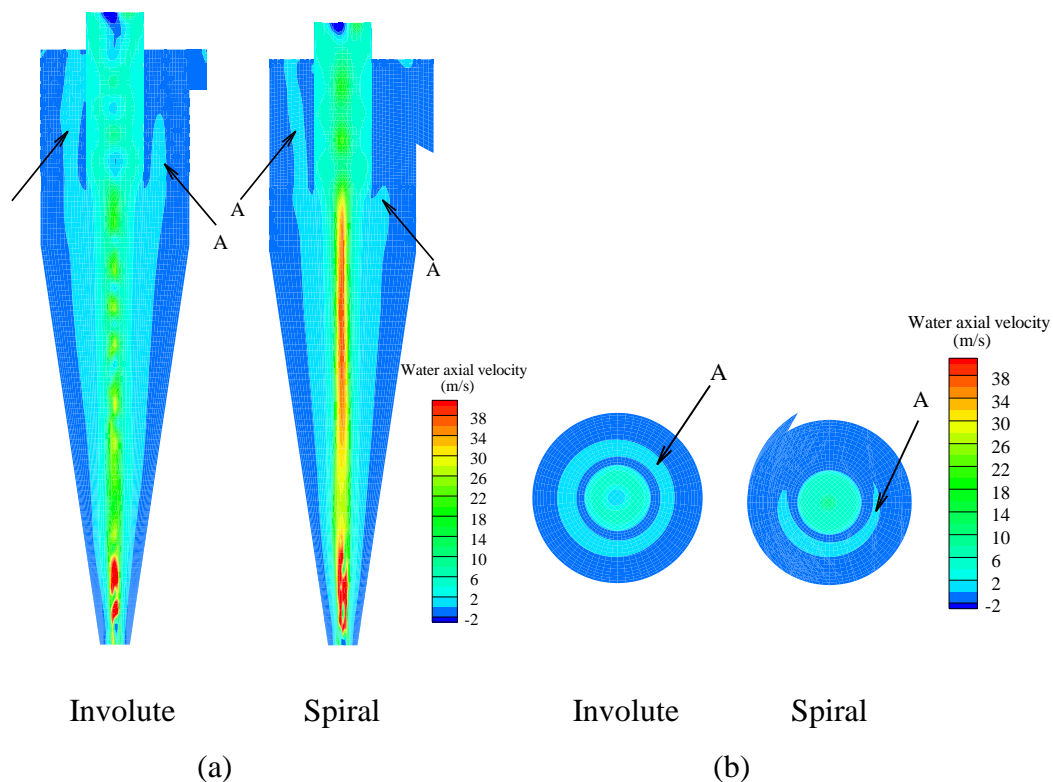


Fig. 5- 5 Distributions of water axial velocity at particle density of 1500 kg/m^3 under 7.4% feed solid concentration in (a) vertical central slice and (b) horizontal slice at 100 mm above the bottom of overflow outlet

Fig. 5-6 compares the total radial accelerations of particles due to the pressure gradient force, drag force and centrifugal force. This is done at five representative heights. Here, only one particle size of 1.41mm is considered for brevity. However, the resulting findings are valid to other particle sizes. As seen from Fig 5-6, the total radial acceleration is generally larger in hydrocyclones with the ‘spiral and slope’ inlet at a low feed solid concentration, which, however, is not so evident for particles with a density of 1275 kg/m^3 . When the feed solid concentration increases to 15.4%, the differences in the total radial acceleration due to the inlet feed type are more significant. Besides, the total radial acceleration generally decreases with the increase of feed solid concentration, which is not so obvious for coal particles having a density of 2200 kg/m^3 . Note that hydrocyclones with an involute inlet or under high feed solid concentrations have an increased particle accumulation area near the spigot as shown in Fig. 5-4. This factor coupled with the weakened total radial acceleration could collectively account for the reduced separation precision, as the conclusion obtained in Chapter 4, especially for hydrocyclones with the involute inlet at higher feed solid concentration.

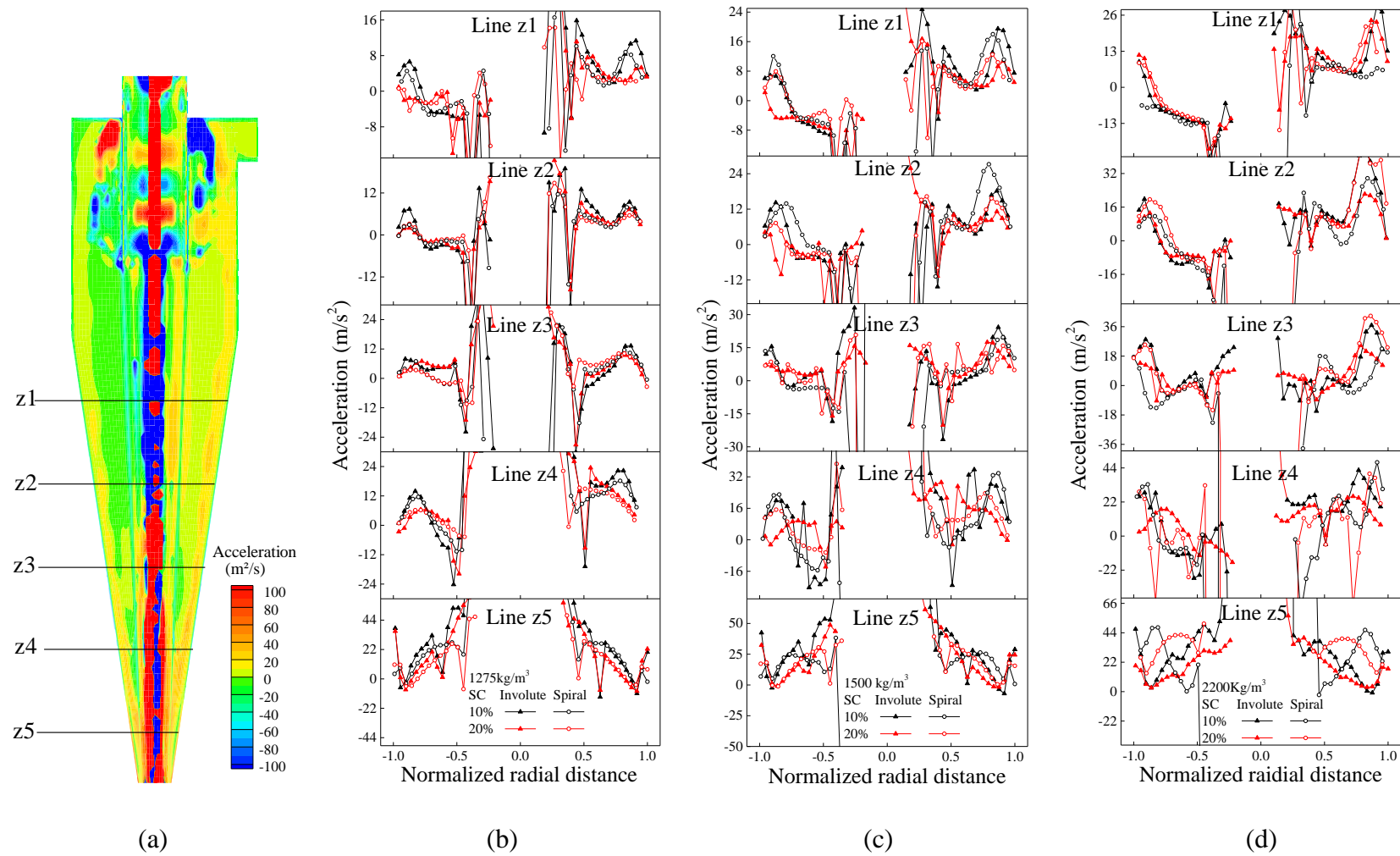


Fig. 5- 6 Distributions of total radial acceleration of 1.41mm diameter particles (a) representative contours, and radial acceleration with different inlet types at different feed solid concentrations of particles of density: (a) 1275 kg/m³, (b) 1500 kg/m³ and (c) 2200 kg/m³

Fig. 5-7 compares the flow properties within these two different inlets in a plane 100 mm from the top of the inlet. Note that all the particles have the same flow properties in the corresponding inlets, here only flow properties of water are taken as an example. It can be clearly seen that there is an obvious flow pointing to the wall in the ‘spiral and slope’ inlet as shown in Fig. 5-7 (b). However, this outward trend is not observed in the involute inlet. This is to say, that when a mixture of particles and water is fed into the inlet, the mixture tends to move towards to the wall in the ‘spiral and slope’ inlet, which could be beneficial for eliminating the short-circuited flow. This should be one of the reasons for the larger separation precision for coarse particles in the hydrocyclones with the ‘spiral and slope’ inlet as shown in Fig. 5-3.

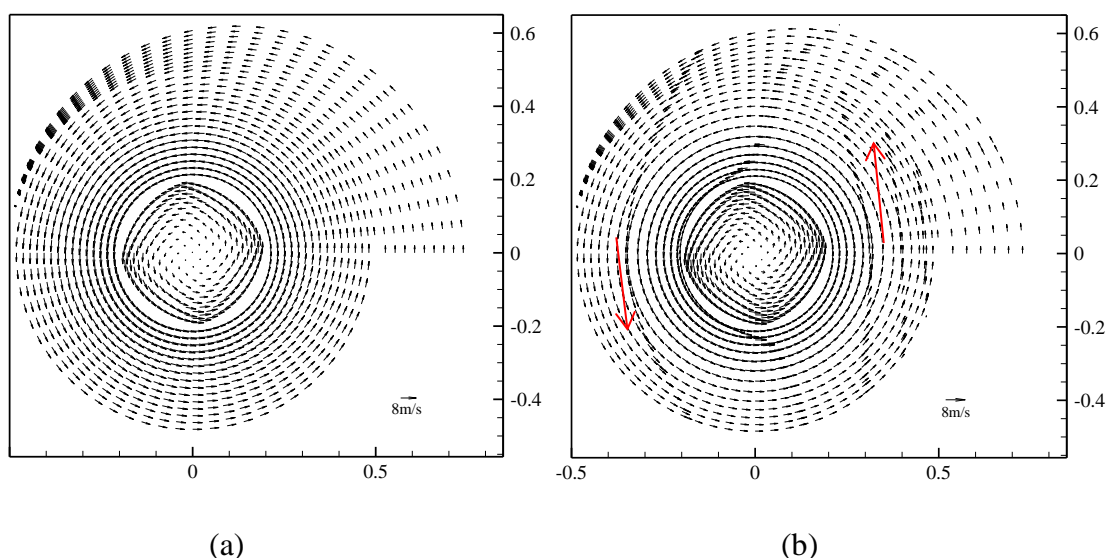


Fig. 5-7 Flow field of water within the inlet of (a) involute type and (b) ‘spiral and slope’ type at particle density of 1500 kg/m^3 under 7.4% feed solid concentration

The particle flow behaviors near the spigot where particles accumulate are further examined. The results are shown in Figs. 5-8 and 5-9. Here, the finest (e.g. 0.45 mm) and coarsest (e.g. 1.41 mm) particles, which are vulnerable to the misplacement, are focused. Overall, particles are found to flow upwards around the air-core but downwards near the wall region as expected, which is the same as the findings in Chapter 4. For the coarse particles in hydrocyclones with the ‘spiral and slope’ inlet or at lower feed solid concentration, the magnitude of radial velocity from the upward flow stream to the downward flow stream, is larger (Fig. 5-8) than that with an involute inlet or at a higher feed solid concentration. This is due to the enlarged total radial acceleration or/and the reduced particle accumulation area in the hydrocyclones

with the ‘spiral and slope’ inlet or at a lower feed solid concentration. Besides, near the bottom of the spigot, radial velocity from the downward flow stream to the upward flow stream is weaker for the ‘spiral and slope’ inlet or at lower feed solid concentration. These two phenomena correspond well with the results as shown in Fig. 5-3. For fine particles, the downward flow at the spigot is stronger in hydrocyclones with the ‘spiral and slope’ inlet or at a low feed solid concentration. This is attributed to the strengthened total radial acceleration or/and the weakened particle accumulation area. However, the fine particles are also entrained by water. Note the amount of water to the underflow is smaller in hydrocyclones with the ‘spiral and slope’ inlet or at a low feed solid concentration, which indicates a weak fine particle entrainment. This compensates for the greater possibility of fine particles being misplaced to the underflow due to the higher total radial acceleration, which could explain the slightly smaller partition number of fine particles for the ‘spiral and slope’ inlet or low feed solid concentrations.

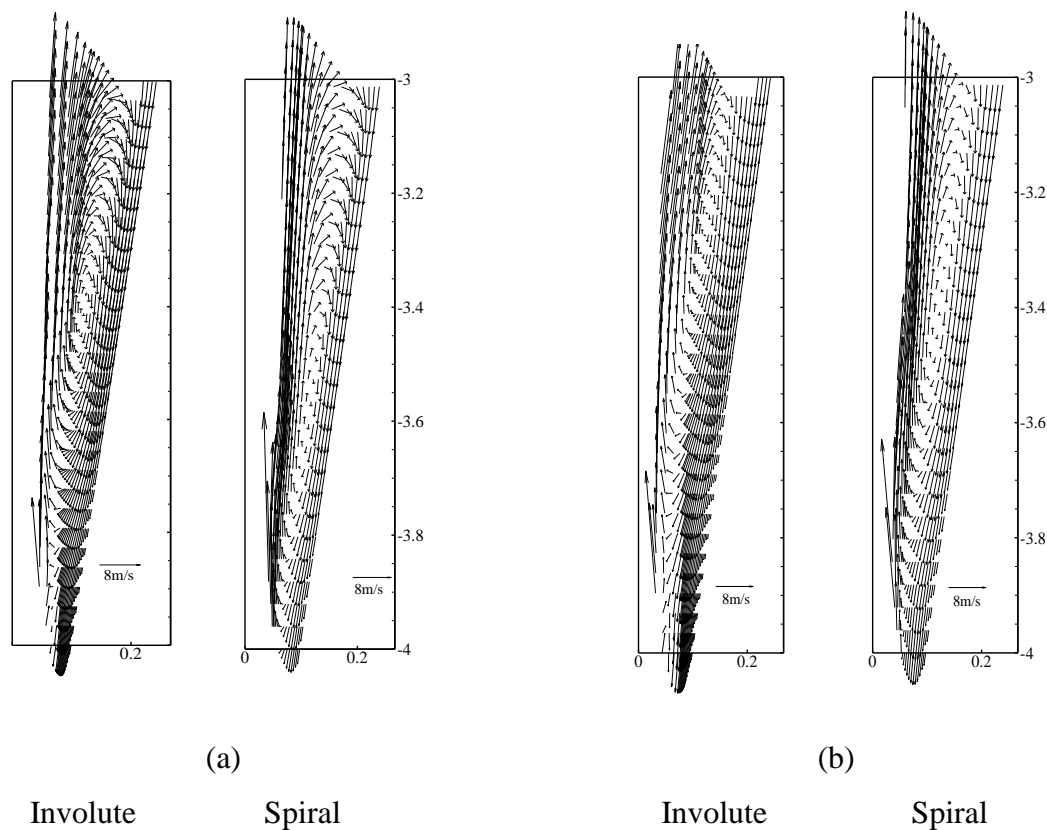


Fig. 5-8 Flow field within the lower part for 1.41 mm diameter particles in hydrocyclones with different inlet types at feed solid concentrations of (a) 7.4% and (b) 15.2%

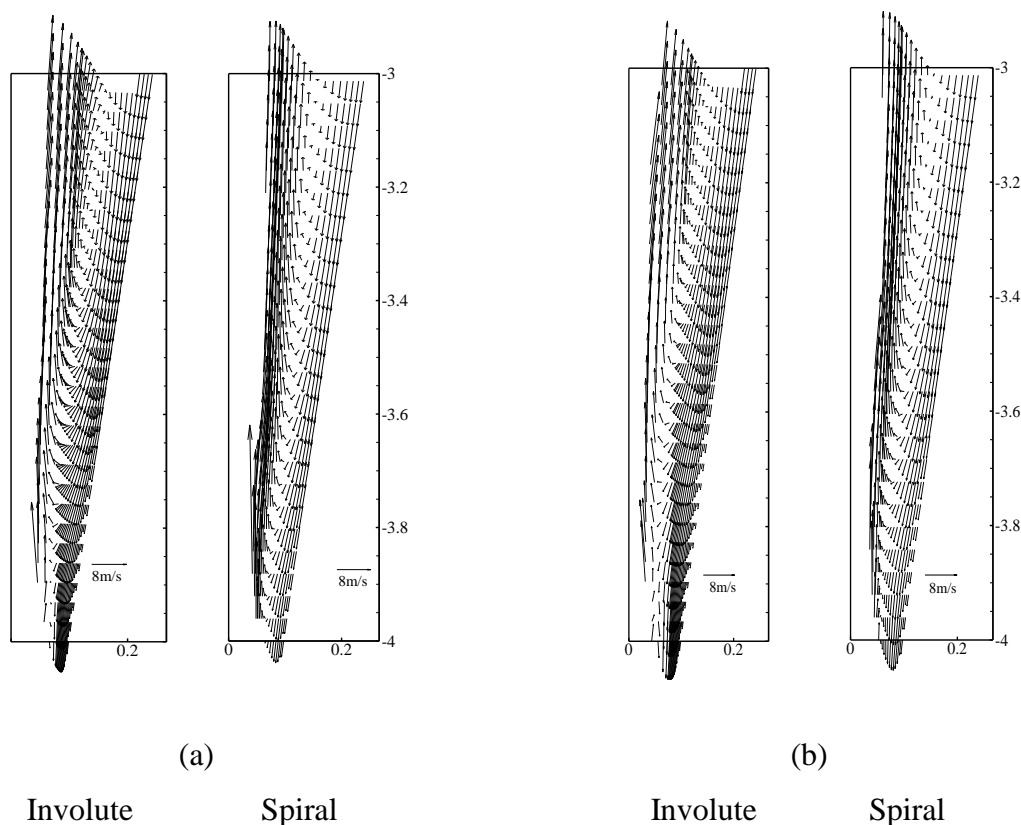


Fig. 5- 7 Flow field within lower part for 0.45 mm diameter particles in hydrocyclones with different inlet types at feed solid concentrations of (a) 7.4% and (b) 15.2%

5.4 Conclusions

Hydrocyclones with the ‘spiral and slope’ inlet are studied and compared with those with an involute inlet in terms of the separation precision and particle misplacement. The effect of inlet feed type is investigated coupled with the effect of feed solid concentration and particle density by a recently developed Two-fluid Model. The major findings from the present study can be summarised as follows:

- Partition curves of hydrocyclones with the ‘spiral and slope’ inlet are generally sharper than those for the involute inlet. The difference due to the inlet feed type becomes more evident when the feed solid concentration is high.
- More coarse particles are misplaced to the underflow in hydrocyclones with the involute inlet, which is pronounced for a denser flow. On the other hand, the amount of ultrafine particles discharged to the underflow can also be reduced in the hydrocyclones with the ‘spiral and slope’ inlet. The difference in the particle misplacement due to the inlet feed type is more significant at high feed solid concentrations. In order to obtain a shaper separation and mitigate the particle

misplacement, hydrocyclones with the ‘spiral and slope’ inlet are recommended for use, especially for denser flows.

- The total radial accelerations are generally larger in the hydrocyclones with the ‘spiral and slope’ inlet or at a low feed solid concentration. The particle accumulation near the spigot blocks the paths of particles available for the separation and reduces the space of the cyclone available for the separation. The accumulation area decreases for the ‘spiral and slope’ inlet or more dilute flows. These variations of the total radial acceleration and particle accumulation contribute to the increased separation precision for hydrocyclones with the ‘spiral and slope’ inlet. Further, the decreased eddy flow between the vortex finder and wall as well as the outward flow to the wall within the ‘spiral and slope’ inlet could also be beneficial for improving the separation efficiency and eliminating the particle misplacement.

**CHAPTER 6 COMPUTATIONAL STUDY OF THE
EFFECT OF FEED SIZE DISTRIBUTION ON THE
SEPARATION PERFORMANCE OF HYDROCYCLONES**

6.1 Introduction

Hydrocyclones in industrial applications usually face the challenges of dealing with feed materials having a wide range of size distributions, which testifies to the importance of understating the effect of feed size distribution on the hydrocyclone performance. However, to date, the understanding of the effects of feed size distribution is that different size distributions result in different cut sizes, which is quite limited. Further, there are some uncertainties about the effect of feed size distribution reported in literature. Specifically, an earlier study by Slechta and Firth (Slechta and Firth, 1984) shows that the classification capability of a hydrocyclone is not affected by the increased amount of near-sized material, which however, leads to an increase in the amount of misplaced material. Plitt once proposed that the effect of feed size analysis is not evident and can be neglected for normal situations. However, he later reported the conclusion that the increase of the cut size with the decrease of particle size can be drawn from his empirical equation (Plitt, 1976). Nageswararao believed that it is logical to get different cut sizes if the size distribution of the feed is different even though all other parameters are kept the same (Nageswararao, 1978). Instead of systematically studying the effect of feed size distribution, some researchers adopted a simplified approach because it is too complex to properly describe the feed material effect (Nageswararao et al., 2004, Flintoff and Plitt, 1987, Narasimha et al., 2014). The simplified approach uses material-specific constants to describe the feed material characteristic which includes the size distribution. However, as mentioned in Chapter 2, the determination of these material-specific constants relies on previous surveys or test data of desired materials, which significantly affect the applicability of this approach. Further, this approach would not contribute to the fundamental understanding of effects of feed size distribution. In conclusion, the understanding of the effects of feed size distribution on the separation performance of a hydrocyclone is quite limited, and thus, a study is necessary.

Even though there have been only a very limited number of studies on the effect of feed size distribution on the hydrocyclone performance, there are several studies on the trajectory or distribution of a single particle or a group of particles within hydrocyclones. Specifically, distributions of different-sized particles within a hydrocyclone were investigated by using a high-speed probe by Renner and Cohen

(Renner and Cohen, 1978). A similar study on the size distribution of dispersed phase within a hydrocyclone was conducted by using Phase Doppler Particle Analyser (PDPA) (Yang et al., 2011). Further, trajectories of different-sized particles in hydrocyclones were investigated numerically by Wang et al. (Wang et al., 2007). These studies may be helpful for analysing the effect of the feed size distribution on the separation performance of hydrocyclones. Note that the effect of feed size distribution on the separation performance of DMCs was systematically studied by Chen et al. (Chen et al., 2016), which may provide some reference for similar studies on hydrocyclones even though DMCs deal with much coarser particles according to the density difference of particles.

Generally speaking, the modelling of hydrocyclones can be discrete- or continuum-based depending on the treatment of the solid phase, which is represented by either Lagrangian Particle Tracking (LPT), or Discrete Element Method (DEM) in the discrete-based treatment, or by Two-Fluid Model (TFM) in the continuum-based treatment. The LPT approach ignores effects of inter-particle interactions as well as reactions of particles on the fluid, and thus is used mainly for operations in a dilute regime or at a low feed solid concentration (Wang and Yu, 2006, Wang et al., 2014, Hwang et al., 2012). The dense discrete phase model (DDPM) which combines LPT with the kinetic theory (Zhou et al., 2016) may be used over a wide range of feed solid concentrations. The CFD-DEM or TFM-DEM approach coupled with CG concept was adopted to model the fluid-particle flow in hydrocyclones in Chapter 3. However, the CG CFD-DEM approach is found to underestimate the separation performance when the feed solid concentration is high; on the other hand, the CG TFM-DEM model is applicable but it needs further research on determining the boundary size. TFM models in the form of either the so-called mixture model or Eulerian-Eulerian model can in principle be applied to both dense and dilute regimes. The mixture model is essentially a simplified Eulerian-Eulerian model and was found to be inaccurate for predicting the separation performance of hydrocyclones as long as particles have a broad range of sizes and densities (Ghodrat, 2014). The Eulerian-Eulerian approach can be used to overcome the problem associated with the mixture model, as recently demonstrated by Ghodrat et al. (Ghodrat et al., 2016, Ji et al., 2017). Therefore, the model developed by Ghodrat et al. (Ghodrat et al., 2016) is adopted to systematically conduct numerical experiments to study the effect of feed

size distribution. In this study, the effects are elucidated in terms of flow and force characteristics.

6.2 Simulation method and conditions

6.2.1 Model description

The present study is based on the computer model reported elsewhere (Ghodrat et al., 2016, Ji et al., 2017). The model has been proved to be valid in hydrocyclone studies, especially in dealing with a broad range of particle densities and sizes. The turbulent flow of water-air mixture is modelled using the Reynolds stress model (RSM), facilitated by a standard wall function (Launder et al., 1975). The interface between the liquid and air-core is modelled using the Volume of Fluid (VOF) model (Hirt and Nichols, 1981), the same as those widely used elsewhere (Bhaskar et al., 2007, Mousavian and Najafi, 2009, Azadi et al., 2010, Kuang et al., 2012, Wang and Yu, 2006). Different sized particles, water, and air within the hydrocyclone are simulated by the TFM approach in the form of Eulerian-Eulerian model. Based on these treatments, a full set of conservative equations with regards to momentum and mass is applied to each phase, combined with a kinetic theory for describing particle-particle interactions. The model formulations and numerical techniques can be found elsewhere (Ghodrat et al., 2016), and thus are not detailed here to avoid repetition.

6.2.1 Model applicability

The model validation has been done by comparing the numerical results with the measurements through different applications involving water-air and water-air-solid flows. The data used in the comparison include: (1) the mean tangential and axial velocities as well as RMS (Root-Mean-Square or turbulent stress) velocities of water, as measured by Hsieh and Rajamani within a 75-mm cyclone (water-air flow); (2) the water split and inlet pressure drop, as measured by Hsieh and Rajamani and Bicalho et al. (Bicalho et al., 2014) within 75-mm and 15-mm cyclones (water-air flow), respectively, and (3) the separation efficiencies of particles having different sizes and densities, as measured by O'Brien et al. within a 1000-mm cyclone operated at the feed solid volume fractions of 7.4% and 15.2% (water-air-solid flow). Overall, all the results obtained thus far from the comparison suggest that the present model can

satisfactorily predict the flows and separation performance of hydrocyclones, at least qualitatively. The detailed results can be found elsewhere (Ghodrat et al., 2016).

6.2.3 Simulation conditions

Fig. 6-1(a) gives the corresponding geometric profile of the hydrocyclone used in this work. To obtain comparable results with experiments, the geometrical and operational conditions, the number of hexahedral grids for each cyclone simulated is around 160000. Moreover, it has been proved that with this grid scheme, the numerical solution is converged and grid-independent both for the cyclone with spiral slope inlet and involute inlet. The grid is finer in the vicinity of the walls and vortex finder than in the remainder of the cyclone, as shown in Fig. 6-1 (b). In all of the simulations, a “velocity inlet” boundary condition is used at the cyclone inlet and the “pressure-outlet” condition at the underflow and overflow. The pressure at the two outlets is 1 atm, i.e. the ambient atmospheric pressure.

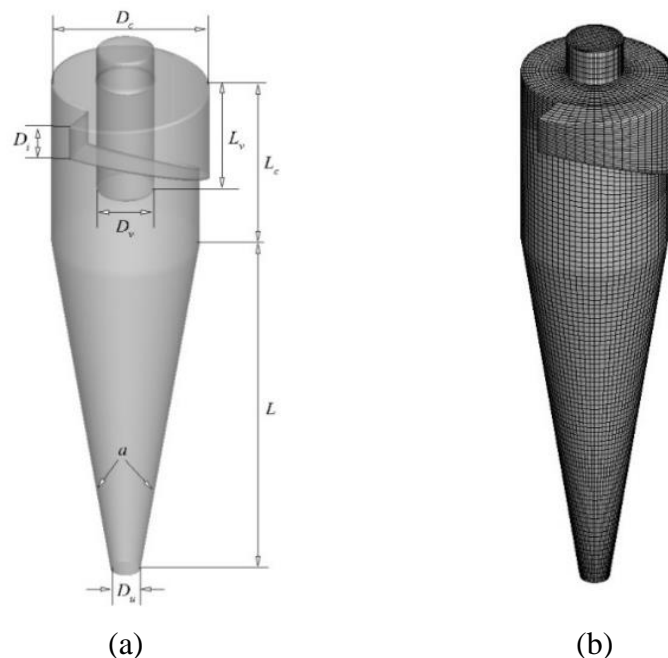


Fig. 6- 1 (a) Geometry and (b) mesh representation of simulated hydrocyclones

In this work, Johnson’s SB function was used as the general function to represent the size distribution of feed materials as suggested in the earlier studies (Yu and Standish, 1990, Yu, 1994). Note that Chen et al. (Chen et al., 2016) once conducted a systematic study on the effect of feed size distribution on the separation performance

of DMCs by employing Johnson's SB function. The probability density distribution function (PDF) of the size distribution is given by:

$$f_{SB}(d) = \frac{d_{max} - d_{min}}{(d - d_{min})(d_{max} - d)} \times \exp \left\{ -\frac{\sigma_j^2}{2} \left[\ln \left(\frac{d - d_{min}}{d_{max} - d} \right) - \ln \left(\frac{d_{0.5} - d_{min}}{d_{max} - d_{0.5}} \right) \right]^2 \right\} \quad (2-8)$$

where $d_{min} \leq d \leq d_{max}$, $d_{0.5}$ represents the particle median size, and σ_j describes the spread of the particle size distribution. Johnson's SB function can be reduced to a two-parameter function because d_{min} and d_{max} may be determined from measurements or other physical considerations.

In this work, three size distributions are investigated with different values of σ_j (i.e., 0.5, 1, and 2) while the median size is at a fixed value for these three distributions. Note that a larger σ_j represents a larger amount of particles of the median size in this case. Therefore the effect of feed size distribution is transformed to establishing that of parameter σ_j or amount of median particles. The median size is kept at 0.3 mm and the size range is 0.045-1.41 mm, which are same with those of the original size distribution in the experiment (O'Brien et al., 2001) shown in Table 4-2 in Chapter 4.

Fig. 6-2 shows the PDF and mass fractions for different size distributions.

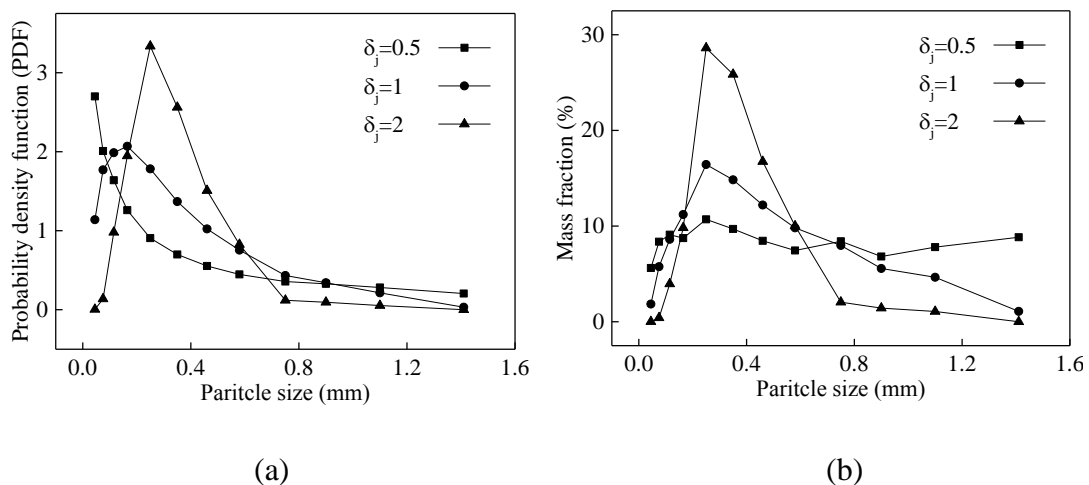


Fig. 6- 2 Distributions of (a) the probability density function, and (b) mass fraction with different values of σ_j

Table 6-1 lists the present geometric and operational conditions of hydrocyclones, following the experimental work of O'Brien et al. (O'Brien et al., 2001). All the

conditions are kept the same for the simulations cases except the differences in the size distribution parameter σ_j . The inlet water velocity and particle velocity are both set to 3.5 m/s. As in normal operation of a hydrocyclone in coal preparation, the feed solid volume fraction is set to 7.4 %, following the experiments (O'Brien et al., 2001). The material considered in this work is coal with a density of 1275 Kg/m³ as in the experiment.

Table 6- 1 Geometrical and operational conditions of the hydrocyclone

Parameter	Value
Diameter of the body (D_c)	1000 mm
Diameter of inlet (D_i)	266 mm
Diameter of vortex finder (D_v)	390 mm
Diameter of apex (D_u)	200 mm
Length of cylindrical part (L_c)	1316 mm
Length of vortex finder (L_v)	2684 mm
Included angle (a)	20°
Inlet velocity (u)	3.5 m/s
Particle material	coal
Particle density (ρ_p)	1275 kg/m ³
Particle size	0.045-1.41 mm
Size distribution (σ_j)	0.5, 1, and 2
Feed solid concentration (ρ_{feed})	7.4 %

6.3 Results and discussion

Fig. 6-3 compares partition curves for the material with different size distributions. It can be clearly seen that partition numbers reported to the underflow decrease significantly for intermediate-sized particles with the increase of σ_j . This indicates that the separation is deteriorated as σ_j increases. While the effect of σ_j on partition of fine and coarse particles is minor. Further, an increase in the parameter σ_j leads to an increase in the cut size, which is consistent with the previous finding that different cut sizes are logically obtained if the size distribution of the feed is different even though all other parameters are kept the same (Nageswararao, 1978). Moreover, there are also some differences in the partition curves. Specifically, for the size distribution where σ_j equals 0.5, the shape of the partition curve is normal with a sharp separation. For the size distribution where σ_j equals 1, the partition curve is not perfectly normal because the increase in partitions due to the increase in the particle diameter from 0.35 mm to 0.46 mm is not so obvious. For the size distribution where σ_j equals 2, even the partition number for particles of 0.35 mm diameter is almost the same as that of particles of 0.25 mm diameter. That is to say that the partition difference between two intermediated-sized particles may become smaller as the parameter σ_j increases, which is not beneficial for a classification. In conclusion, the increase of the fraction of median particles leads to a significantly deteriorated separation of intermediate-sized particles and an obvious increase of the cut size. The reason for this deteriorated separation can be explained by the following analysis.

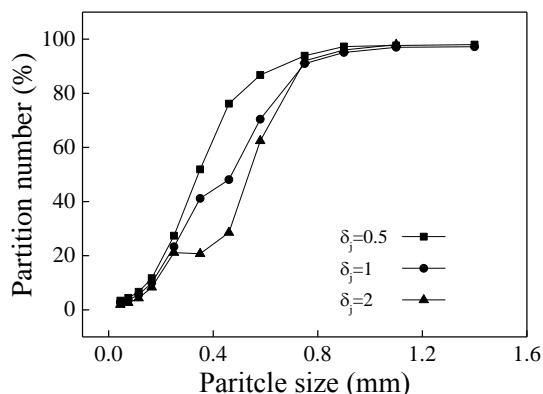
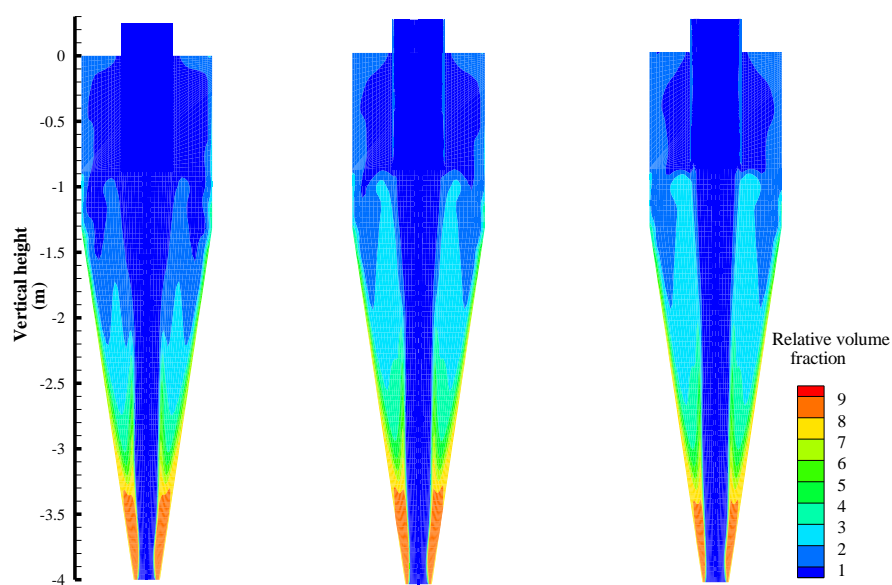


Fig. 6- 3 Partition curves for materials with different size distributions

Fig. 6-4 demonstrates how the size distribution affects the distributions of the volume fractions of total solids and intermediate-sized particles of 0.35 mm and 0.46 mm

diameters. Note that a relative volume fraction is adopted here by dividing the real volume fraction by the corresponding feed volume fraction. It can be clearly seen from Fig. 6-4 (a) that an increase in the value of σ results in a significant increase in the relative volume fraction of total solids in the area extending from the vortex finder to middle cone. This is due to the significant increase in the relative volume fraction of intermediate-sized particles in the same area, as shown in Figs. 6-4 (b) and (c). Note that relative volume fractions of particles of other sizes in this area are not found to increase as σ_j increases; corresponding figures are not shown here for brevity. That is to say that a larger amount of median particles leads to a more obvious particle accumulation which mainly contains intermediate-sized particles. As particles of the intermediate sizes tend to have a stronger stochastic motion and a longer residence time within hydrocyclones (Wang et al., 2007), a more evident particle accumulation should be caused if the fraction of these particles increases. Unlike the strengthened particle accumulation in the area extending from the vortex finder to middle cone, the accumulation near the spigot does not show an obvious increase. It may be concluded that an increase in the fraction of median particles leads to a more obvious accumulation of intermediate-sized particles in the area extending from the vortex finder to middle cone. As the particle accumulation is believed to deteriorate the separation by blocking the way to the wall and reducing the separation space (Ghodrat et al., 2016), the separation performance of intermediate-sized particles is reduced more significantly as shown in Fig. 6-3.



(a)

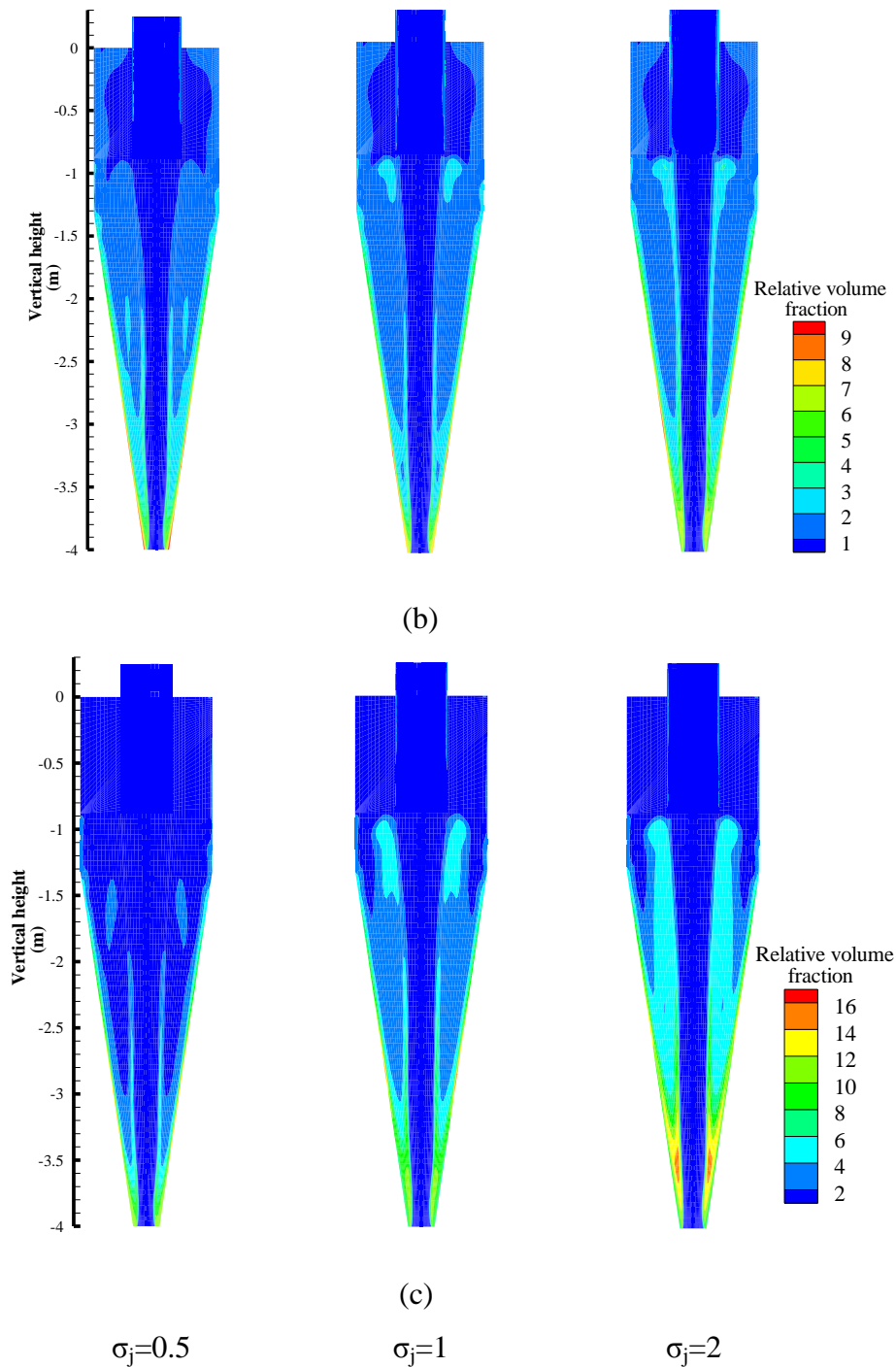


Fig. 6- 4 Spatial distributions of relative volume fraction for the (a) total solids, (b) 0.35 mm diameter particles and (c) 0.46 mm diameter particles with the parameter $\sigma_j=0.5, 1, \text{ and } 2$

Fig. 6-5 compares the radial velocity distributions for different-sized particles with the size distribution parameter σ_j equal to 0.5. In this figure, the white region in the central region corresponds to the area occupied by the air-core, whose velocities are not shown because the properties of air are very different from those of liquid and solid phases. Such a representation has been used in Chapter 4 and offers a convenient

and better way of representing flow properties that govern the separation process. Particles with diameters of 0.045 mm, 0.25 mm, 0.35 mm, 0.46 mm, and 1.1 mm are considered as an example. It can be clearly seen that the magnitude of the outward radial velocity increases and that of the inward one decreases with the increase of particle diameter, which indicates that larger particles tend to move outward and then have higher partitions to the underflow. This is consistent with the finding in Chapter 4 where the total radial acceleration was used to explain this trend. Even though the radial velocity of particles with σ_j equals 0.5 is only shown here as an example, these trends are still valid to other size distributions.

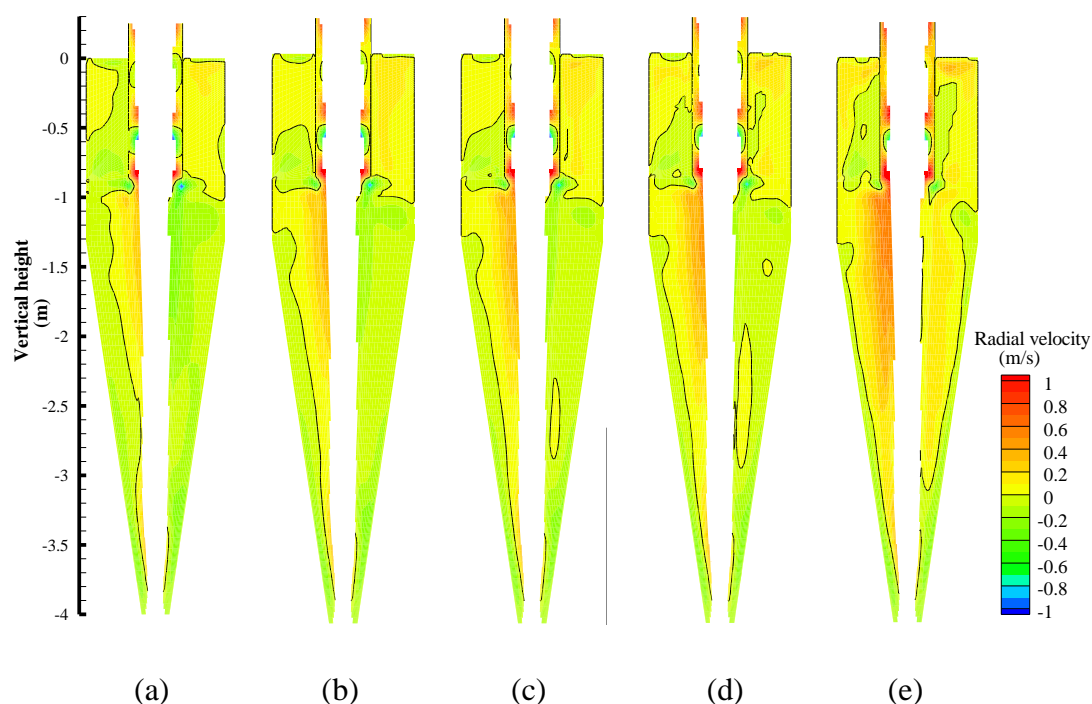


Fig. 6- 5 Distributions of radial velocity for particles having diameters of (a) 0.045 mm, (b) 0.25mm, (c) 0.35, (d) 0.46 mm, and (e) 1.1 mm when the parameter $\sigma_j=0.5$

To further investigate the effect of size distribution on the hydrocyclone performance, distributions of drag force for different size distributions are compared as shown in Fig. 6-6. Only one particle size 1.1 mm is taken as an example for brevity. However, the resulting findings are valid to other particle sizes. Note that the drag force with the negative value has the inward direction pointing to the central axis, while that with the positive value has the outward direction pointing to the wall. It is observed that the value of inward drag force increases as the parameter σ_j increases. More importantly, for the distribution of drag force with σ_j equal to 1 or 2, there are some small zones in which the magnitude of drag force becomes suddenly magnified compared to their

neighbouring zones. Further, an increase in the value of σ_j results in an increase in the number of the zones, which indicates that the fluctuations of the drag force become stronger because of presence of a larger amount of median particles. Note that these zones are located above the middle part of the cone where more intermediate-sized particles accumulate as shown in Fig. 6-4. That is to say that the drag force tends to be unstable in the upper to middle conical part due to the increased amount of median particles, which is consistent with the finding by Wang et al. (Wang and Yu, 2009) that the drag force of particles with a cut size has a stronger fluctuation in the middle of the conical part. Note that this work by Wang et al. is tracking the trajectory of a single particle by the CFD-LPT approach for a dilute flow. Actually, an increase in the amount of median particles also leads to an increase in the magnitude of the pressure gradient force and centrifugal force but not an increase in the intensification of force fluctuations. They are not shown here for brevity.

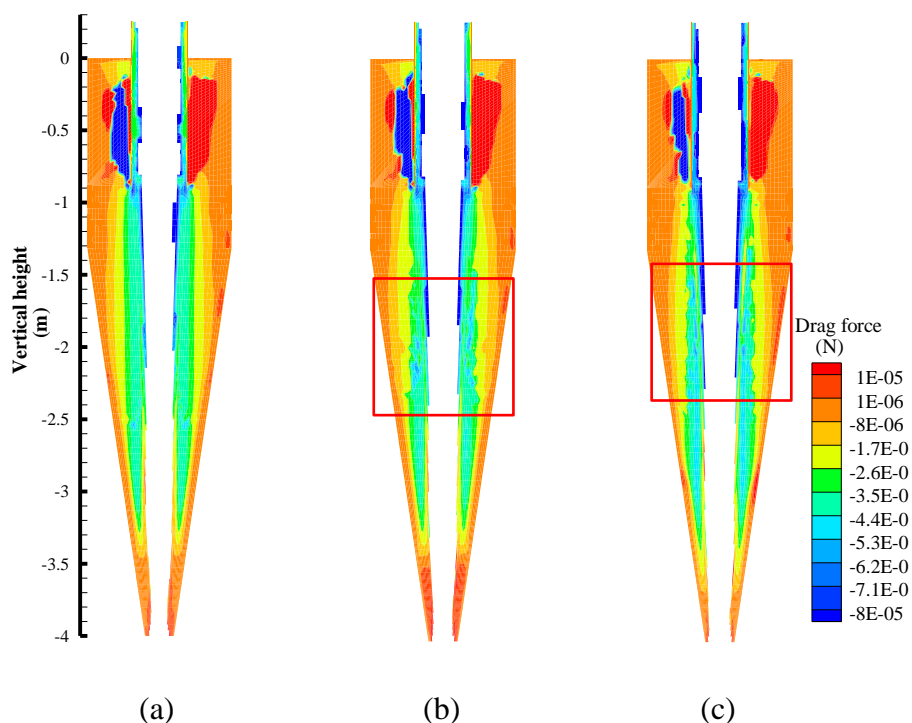


Fig. 6- 6 Distributions of drag force for materials with: (a) $\sigma_j=0.5$, (b) $\sigma_j=1$, and (c) $\sigma_j=2$

The total radial acceleration due to the drag force, pressure gradient force, and centrifugal force is compared as shown in Fig. 6-7. The black line in Fig. 6-7 represents the locus of zero radial acceleration. Similarly, the total radial acceleration with the negative value has the inward direction pointing to the central axis, while that

with the positive value has the outward direction pointing to the wall. Corresponding to the fluctuation of drag force shown in Figs. 6-6 (b) and (c), the total radial acceleration has the similar fluctuation in the same location with the direction always changing between the inward and outward directions, which can be seen from Figs. 6-7 (b) and (c). It can be concluded that it is the fluctuation of the drag force that leads to the direction fluctuation of the total force. Coarse particles, which have a larger radial acceleration, tend to move along the wall, and the fluctuation of radial acceleration direction located near the air-core above the middle conical part would not affect these coarse particles significantly. In the case of fine particles, which have a smaller radial acceleration and already have the tendency to flow with water, this fluctuation would not obviously affect them either. However, in the case of intermediate-sized particles which have a stochastic characteristic, the fluctuation of radial acceleration affect them significantly and further deteriorates their separation.

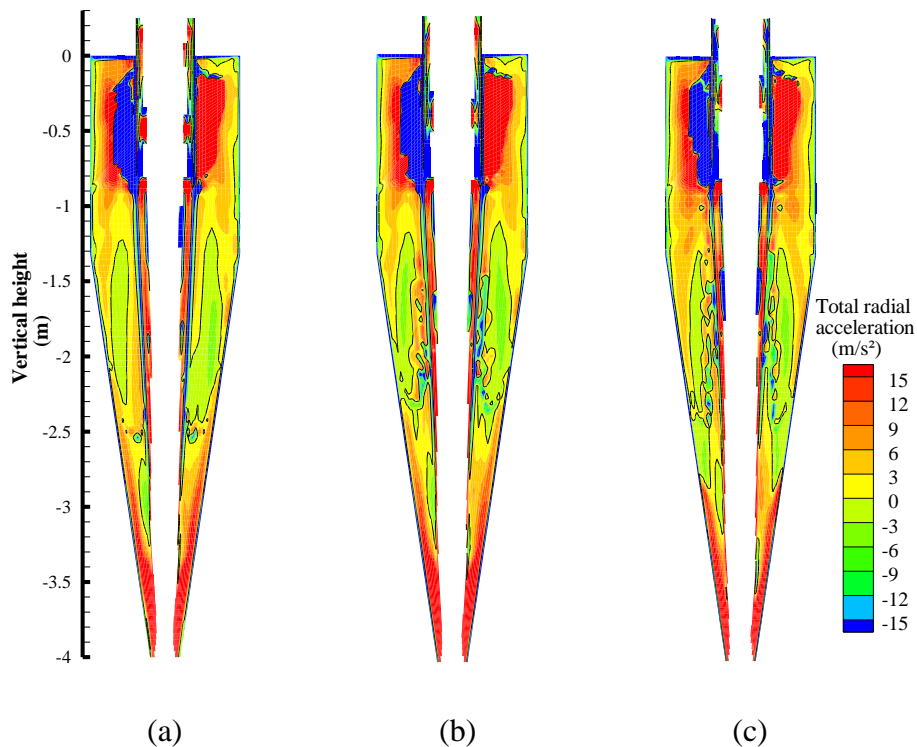


Fig. 6- 7 Distributions of total radial acceleration for materials with : (a) $\sigma_j=0.5$, (b) $\sigma_j=1$, and (c) $\sigma_j=2$

Fig. 6-8 compares the total radial acceleration of particles with intermediate diameters of 0.25 mm, 0.35 mm, and 0.46 mm for different size distributions along five representative lines. It can be clearly seen that the total radial acceleration of larger particles is generally higher than that of smaller particles for the size distribution with

σ_j equal to 0.5 along all representative lines. However, the difference of total radial acceleration due to particle size difference is not obvious at z_4 and z_5 for the size distribution with σ_j equal to 1, and not obvious at z_3 , z_4 , and z_5 for the size distribution with σ_j equal to 2. This indicates that an increase in the amount of median particles leads to a smaller difference in the radial acceleration due to the particle size difference, and thus a smaller difference in the partition to the underflow as shown in Fig. 6-3. The direction fluctuation of radial acceleration shown in Figs. 6-7 (b) and (c) can also be observed at z_1 , z_2 , and z_3 in Figs. 6-8 (b) and (c).

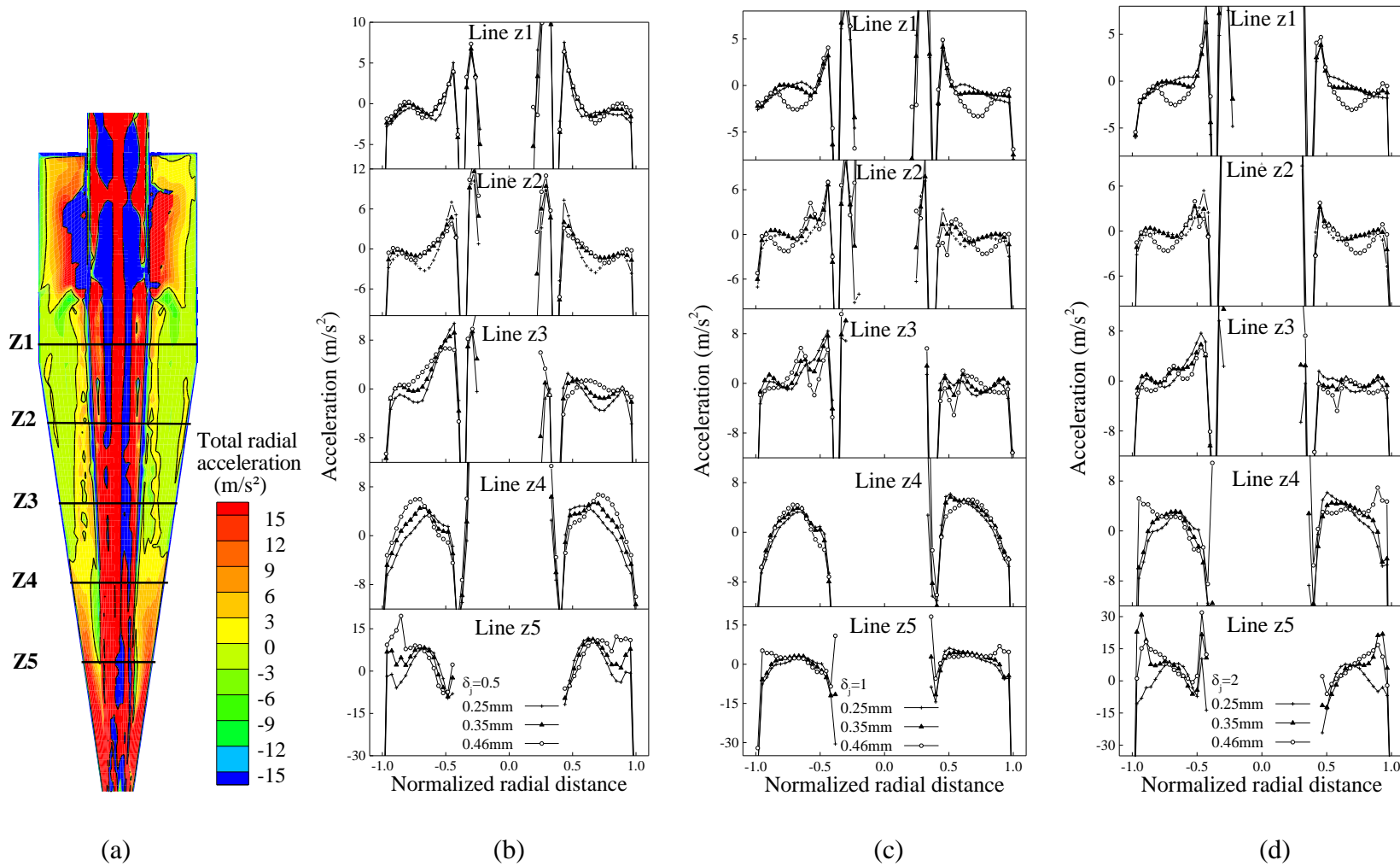


Fig. 6- 8 Distributions of total radial acceleration: (a) representative contours in the longitudinal section; and those along lines z1 to z5 for the material with (b) $\sigma_j=0.5$, (c) $\sigma_j=1$, and (d) $\sigma_j=2$

6.4 Conclusions

The effect of size distribution on the flow and separation performance of hydrocyclones is studied by the recently developed Two-fluid Model. The major findings from the present study can be summarised as follows:

- An increase in the amount of median particles leads to a reduction in partition numbers of intermediate-sized particles, an increase in the cut size, and a smaller difference in partitions between two intermediate-sized particles. However, the effect of the fraction of median particles on separations of fine and coarse particles is not significant.
- It is found that an increase of the fraction of median particles leads to a more obvious accumulation of intermediate-sized particles in the area extending from the vortex finder to middle cone. The particle accumulation is believed to deteriorate the particle separation by blocking the flow path to the wall and reducing the separation space, and therefore, the separations of intermediate-sized particles reduce significantly for the size distribution with a larger σ_j value.
- The direction of total radial acceleration (force) of particles located in the upper to middle conical part always changes between the inward and outward when the amount of the median particles is large, which is attributed to the fluctuation of the drag force in the same area. As intermediate-sized particles have a stochastic motion and a longer residence time within hydrocyclones, the fluctuation of the radial acceleration direction further deteriorates their separations in hydrocyclones.
- An increase in the amount of median particles leads to a smaller difference in the radial acceleration between two intermediate-sized particles and thus, a further smaller difference in the partition number.

**CHAPTER 7 PREDICTION OF SEPARATION
PERFORMANCES OF HYDROCYCLONES BY A
NEWLY DEVELOPED MODEL**

7.1 Introduction

Hydrocyclones are widely used in the mineral and chemical processing industry. The flow in a hydrocyclone is very complex because of the existence of swirling turbulence, air-core and segregation involving gas, liquid, and solid phases. There have been several research methods to study hydrocyclones, namely, the experimental approach, empirical approach, and numerical approach. Experimental methods (Neesse and Dueck, 2007, Scheid et al., 2012, Dai et al., 1999, Hsieh and Rajamani, 1991, Narasimha et al., 2012) contribute to the insight into the multiphase flow in hydrocyclones, but those experiments are expensive. Thus, researchers (Asomah and Napier-munn, 1997, T.C.Rao et al., 1976, Dietz, 1981, Cilliers and Hindet, 1991, Schubert, 2007, Narasimha et al., 2012, Narasimha et al., 2014, Plitt, 1976) have focused on collecting the experiment data to develop empirical models to predict the hydrocyclone performance. This empirical approach is fast, portable and easily applied in the industry. However, these previously developed empirical models are weak in the applicability because they are generally limited to the experimental conditions used in the modelling. Therefore, it is desirable and more reliable to develop a mathematical description of the fundamentals which govern the multiphase flow of hydrocyclones. Further, the empirical models have failed to consider variables comprehensively; for example, the effect of particle density which is important in hydrocyclone studies (Ji et al., 2017, Ghodrat et al., 2016) was ignored. The numerical method provides a lower-cost and more flexible way to study the multiphase flow in hydrocyclones. Further, it can be also used to understand the underlying fundamentals in hydrocyclone studies compared with the empirical approach. Unavoidably, the numerical model has disadvantages as well. For example, it is not suitable to be used as an industrial tool because of the time-demanding computation as reported in Chen's work (Chen et al., 2012). In this chapter, a PC-based model based on the numerical data is developed, aiming to develop a mathematical description of the underlying fundamentals of hydrocyclone operations. That is to say that this model can meet the industrial requirements and contribute to explaining the underlying fundamentals related to the effect of each variable. Here the "PC-based model" means the model can be readily run by a personal computer (PC) under any operation systems instead of a super computer.

There have been some previously developed empirical models. Among them is the Lynch and Rao model (T.C.Rao et al., 1976) which proposed equations for the reduced partition number, water split, classification size, and throughput. Another model which has a wider usage as found from literature is Plitt model (Plitt, 1976, Plitt, 1979). However, the earlier models have considered only a limited number of variables because of the restrictions on collecting the experimental data. Much effort has been spent on including more factors. For instance, material-specific constants were introduced to describe the effect of material properties on the hydrocyclone performance in Nageswararao model (Nageswararao et al., 2004, Nageswararao, 1978) and Flintoff model (Flintoff and Plitt, 1987). However, the determination of these constants relies on previous surveys or test data of desired materials. Even though a source the material-specific constants was developed to enable users to select their values, it is suggested caution should be exercised to use the simulation results based on these selected values (Nageswararao et al., 2004). The similar approach of using the application-dependent system constants was also adopted in Narasimha's work recently (Narasimha et al., 2014). To determine these constants, a refitting to each set of data is necessary. As a result, the applicability of these models is affected dramatically. Other models such as Cilliers's model (Cilliers and Hindet, 1991), Svarovsky model (Svarovsky and Thew, 1992), and Kawatra model (Kawatra et al., 1996) have not taken the material properties into consideration in their models. Note that the particle density is also found in some empirical models like Plitt model. However, the particle density was not considered as an independent variable; instead, it was first introduced in the equation of particle forces and then included in the performance equations of hydrocyclones. Apart from the weakness on considering a comprehensive range of variables, the previous models only cover hydrocyclones with a body diameter between 75 and 760 mm except that of Nageswararao and Narasimha, which includes large hydrocyclones with a diameter of 1200 mm. However, Nageswararao and Narasimha models rely on the specific constants as mentioned before. Further, it is found that the Nageswararao model was developed only based on higher feed solid concentrations i.e. 38-73% (by weight) (Nageswararao, 1978). This deficiency on considering the limited feed solid concentrations can be overcome by the Narasimha model which extends it to low to moderate ones (Narasimha et al., 2014). However, the fact that the application-

dependent system constants used in the Narasimha model needs to be refitted to each set of data limits its applicability. Note that the ranges of the body diameter and feed solid concentration that the model covers are also important factors to evaluate the model applicability. Therefore, hydrocyclones with a wide range of body diameter operated under different feed solid concentrations are included in this work to guarantee a wider applicability of this model. Further, the material property, i.e. the density effect of feed material is fully considered as an independent variable; thus, the model can predict the separation performance without relying on the specific constants. In conclusion, the developed model in this work is based on the numerical data and considers more comprehensive variables, which enables it to have a better applicability.

This predictive model is developed based on the extensive numerical data which needs to be generated in advance. Numerical methods to generate data include the TFM model (the full Eulerian multiphase approach and simplified Eulerian approaches such as the Mixture and VOF models), the combined approach of computational fluid dynamics and Lagrangian particle tracking method (CFD-LPT), and the combined approach of CFD and discrete element method (CFD-DEM). The TFM model has been widely adopted in hydrocyclone studies (Davailles et al., 2012, Brennan, 2006, Kuang et al., 2012, Nowakowski and Dyakowski, 2003, Nowakowski et al., 2000, Ji et al., 2017, Ghodrati et al., 2016). The CFD-LPT approach provides a direct way to describe particle flow in hydrocyclones by tracking the motion of individual particles (Murthy and Bhaskar, 2012, Wang et al., 2007, Wang and Yu, 2006, Xu et al., 2012). However, this method is only applicable to dilute flows because of the omission of the particle-particle and particle-fluid interactions. The CFD-DEM approach accounting for the collision between particles and reactions of particles on the fluid has been adopted to model the fluid-particle flow in dense medium cyclones (Chu et al., 2012a, Chu et al., 2012b, Chu and Yu, 2008), gas cyclones (Chu et al., 2011), fluidized bed (Alobaid and Epple, 2013, Alobaid et al., 2013, Cello et al., 2009, Fries et al., 2013) and so on. But it is found that the CFD-DEM approach is difficult to deal with millions of particles found in hydrocyclones. To overcome this problem, coarse-grain (CG) CFD-DEM and CG TFM-DEM models are utilized as demonstrated in Chapter 3. However, the CG CFD-DEM approach is

found to underestimate separation performance when the feed solid concentration is high. On the other hand, the CG TFM-DEM model is applicable, but it needs further research on determining the critical size. As both dense flows and dilute flows are targeted in this work, the TFM model, which has a wider range of applications, is adapted to generate a considerably large database of numerical data.

7.2 Model development

7.2.1 Strategy and database

The strategy for developing the predictive model is shown in Fig. 7-1. It is divided into four steps. The TFM database based on our ten years of simulation work is used to develop the preliminary predictive model, which comprises step one. Then the numerical data from literature are employed to validate this preliminary model, constituting step two. The experimental data which are collected from published journal papers or thesis and industry reports are split into two groups. One is for correcting the preliminary predictive model because there are systems errors between the simulated data and experimental data. Correcting the preliminary model is considered as step three, which is followed by the fourth step where the other sets of experimental data are used to validate the corrected predictive model.

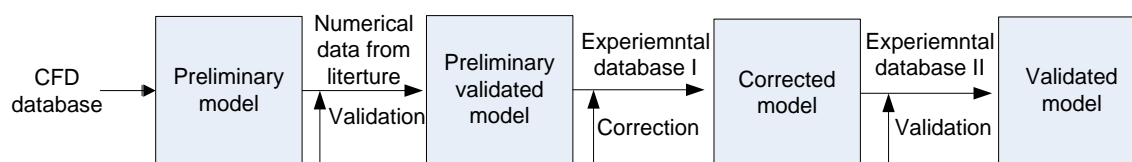


Fig. 7- 1 Strategy for the development of a predictive model

The geometrical, operational, and material variables considered are listed in Table 7-1. The operational variables considered are mainly two, namely, the inlet feed flowrate and feed solid concentration. The variation of inlet diameter results in different inlet areas, and further different inlet velocities which are reflected in the flowrate variation. Therefore the inlet feed flowrate is considered as an independent variable here. As a material property variable, only the material density is currently considered. Even

though effects of inlet feed type and size distribution are investigated in Chapters 5 and 6, respectively, the corresponding data are difficult to be included in the database. Because the numerical data on the effect of feed size distribution is not enough to develop a model, an efficient method to describe the inlet feed type has not been found yet. We are still carrying out the simulation work on the effect of size distribution and seeking an efficient way to describe the inlet feed type.

Table 7- 1 Independent variables in the database

Variable	Factors	Symbol	Value
X ₁	Body diameter	D_c	0.075-1 m
X ₂	Ratio of vortex finder diameter to body diameter	D_v/D_c	0.13-0.66
X ₃	Ratio of spigot diameter to body diameter	D_u/D_c	0.13-0.33
X ₄	Ratio of vortex finder length to body diameter	L_v/D_c	0.33-2
X ₅	Ratio of conical length to body diameter	L_c/D_c	0.47-2.68
X ₆	Flowrate	Q	0.001-0.2 m ³ /s
X ₇	Cone shape	S	0.3-3
X ₈	Ratio of Material density to water density	ρ_p	1.275-3.6
X ₉	Feed solid concentration	ϕ	0.01-0.3

In principle, the “PC-based” model is applicable with the variable range shown in Table 7-1. Actually, these ranges cover all the common conditions of those nine variables encountered in the hydrocyclone studies.

To avoid the effect on the fitting accuracy due to differences in the order of magnitude of different independent variables (Chen et al., 2012), the values of these independent variables are normalized by using ratios. The multiphase flow in hydrocyclones is quite complicated and it is thus challenging to derive dimensionless numbers to describe this process. Even though dimensionless parameters are not used,

the geometrical parameters are normalized by dividing the body diameter of hydrocyclone, similar to the prediction models reported for hydrocyclones in the literature (Plitt, 1976, Plitt, 1979) . In fact, the way used here has been proved valid for the prediction of dense medium cyclone performance through different applications (Chen et al., 2012). The geometrical parameters listed in Table 7-1 are also correspondingly shown in Fig. 7-2.

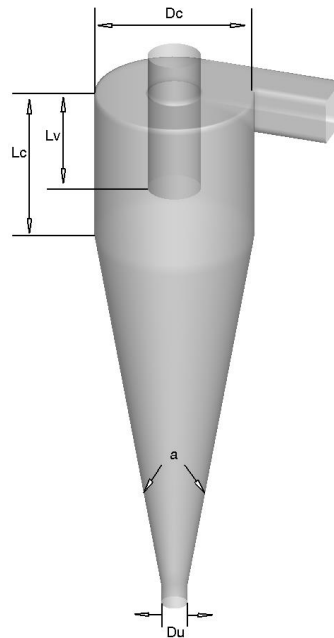


Fig. 7- 2 Hydrocyclone geometrical representations

Four dependent variables as listed in Table 7-2 are included in this work to describe the hydrocyclone performance.

Table 7- 2 Dependent variables in the database

Variable	Factors	Symbol
Y_1	Cut size	d_{50}
Y_2	Separation sharpness	E_p
Y_3	Pressure drop	P
Y_4	Water split	R_f

The definitions of the terms used in Table 7-2 are as follows:

Cut size d_{50} : the size at which the partition number to underflow is 50%;

Sharpness: represented by the Ecart probable E_p ($= (d_{75} - d_{25})/2$), a smaller E_p corresponds to a larger value of sharpness and thus a more precise separation;

Inlet pressure drop P : the difference between the inlet pressure and outlet pressure, a parameter reflecting energy consumption; and

Water split R_f : the water fraction report to underflow, associated with the bypass effect.

7.2.2 Model fitting

The function form is shown in Eq. (7-1):

$$Y_i = aX_1^{a_1} X_2^{a_2} \dots X_9^{a_9} \quad (7-1)$$

where, X_1, X_2, \dots, X_9 are the independent variables; Y_i ($i = 1, 2, 3, 4$) are the dependent variables; a, a_1, a_2, \dots, a_9 are the fitting parameters. This function form is the same as that of the DMC predictive model in Chen's work (Chen et al., 2012). It is found that this function form is more powerful compared to others such as the linear, exponential and polynomial forms.

As shown in Fig. 7-1, the third step of the modelling strategy uses the experimental data to correct the preliminary function shown in Eq. (7-1). Therefore, the correction parameter, b, b_1, b_2, \dots, b_9 are introduced into each prediction function. The corrected function form for the cut size, pressure drop, and water split can be described as in Eq. (7-2):

$$Y_i = bX_1^{b_1} X_2^{b_2} \dots X_9^{b_9} \quad (7-2)$$

The corrected function form of the separation sharpness includes the material density in the exponent, which is slightly different to those of other dependent variables. The function form of the separation sharpness is shown as in Eq. (7-3):

$$Y_2 = bX_1^{b_1 - X_8} X_2^{b_2} \dots X_9^{b_9} \quad (7-3)$$

7.2.3 Fitting accuracy

Fig. 7-3 shows an overall comparison between the calculated and simulated hydrocyclone separation performances. The correlation coefficient R^2 is generally introduced to describe the fitting accuracy. It can be clearly seen from Fig. 7-2 that these predicted results are in good agreement with the simulated ones with high correlation coefficients. Specifically, the correlation coefficients for the cut size, sharpness, pressure drop are all over 0.9 except the water split which has a slightly lower value, indicating that the predictive model is formulated correctly

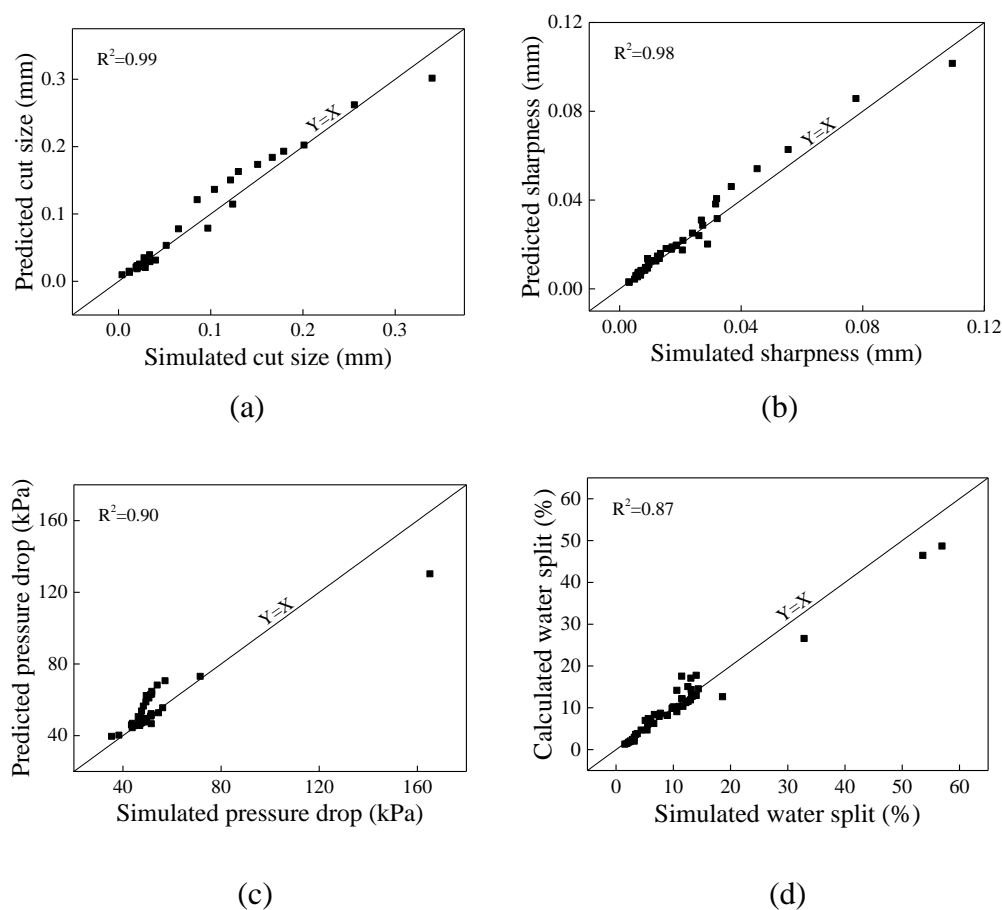


Fig. 7- 3 Comparisons between the calculated and simulated separation performance: (a) cut size, (b) sharpness, (c) pressure drop, (d) water split

To further check the fitting accuracy of the model, the predicted and simulated results are further compared with regards to predicting the effect of material density, as shown in Fig. 7-4. Note that this set of experimental data of density is from the industry report C6047 (O'Brien et al., 2001) at a feed solid concentration of 7.4% (by volume). It is seen that the effect of material density can be described by the

developed predictive model with a high correlation coefficient, except the water split which has a slightly lower correlation coefficient.

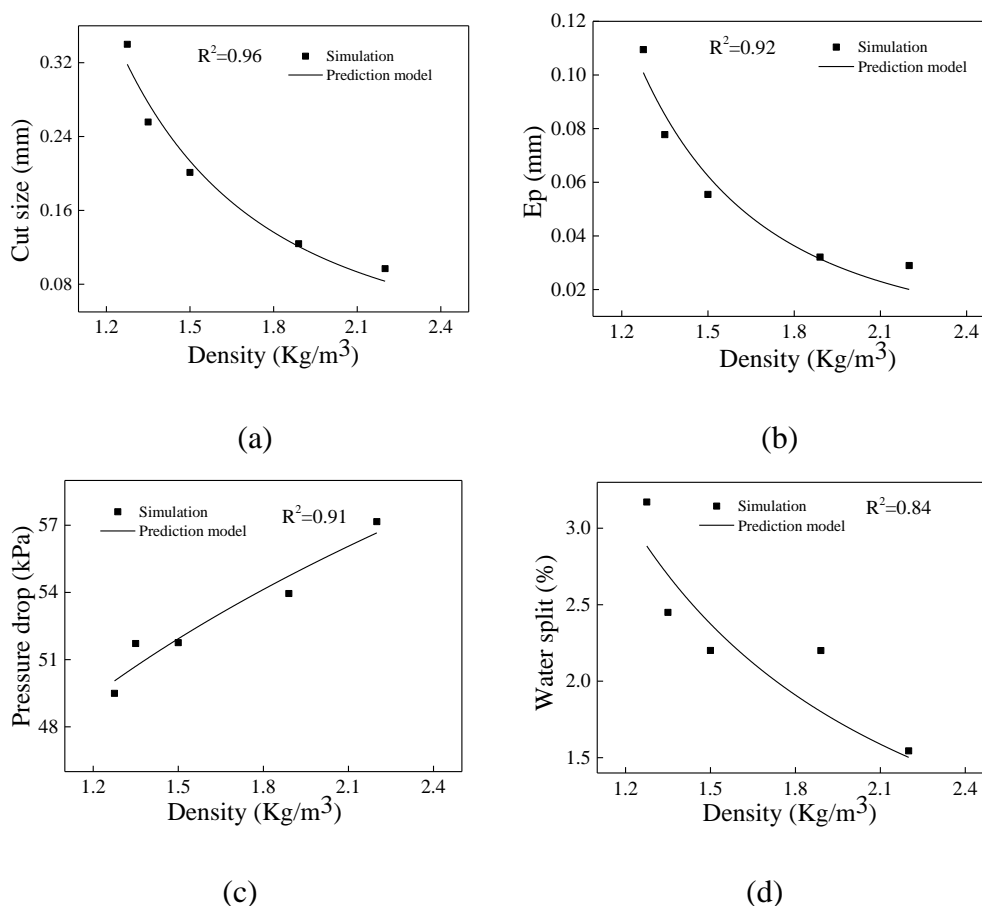


Fig. 7- 4 Comparisons between the calculated and simulated separation performance as a function of material density: (a) cut size, (b) sharpness, (c) pressure drop, (d) water split

The newly developed preliminary model is further checked by comparing the predicted results with the simulated ones obtained from literature (Wang et al., 2007, Wang and Yu, 2006, Wang, 2009) as shown in Fig. 7-5. It can be seen that the errors between the predicted ones and simulated ones are generally within $\pm 30\%$, which further supports the conclusion that the developed model is applicable. However, these comparisons with the simulated data can only be used to check the fitting accuracy; on the other hand, comparisons with the experimental data should be used for the validation which can be found in the section as follows.

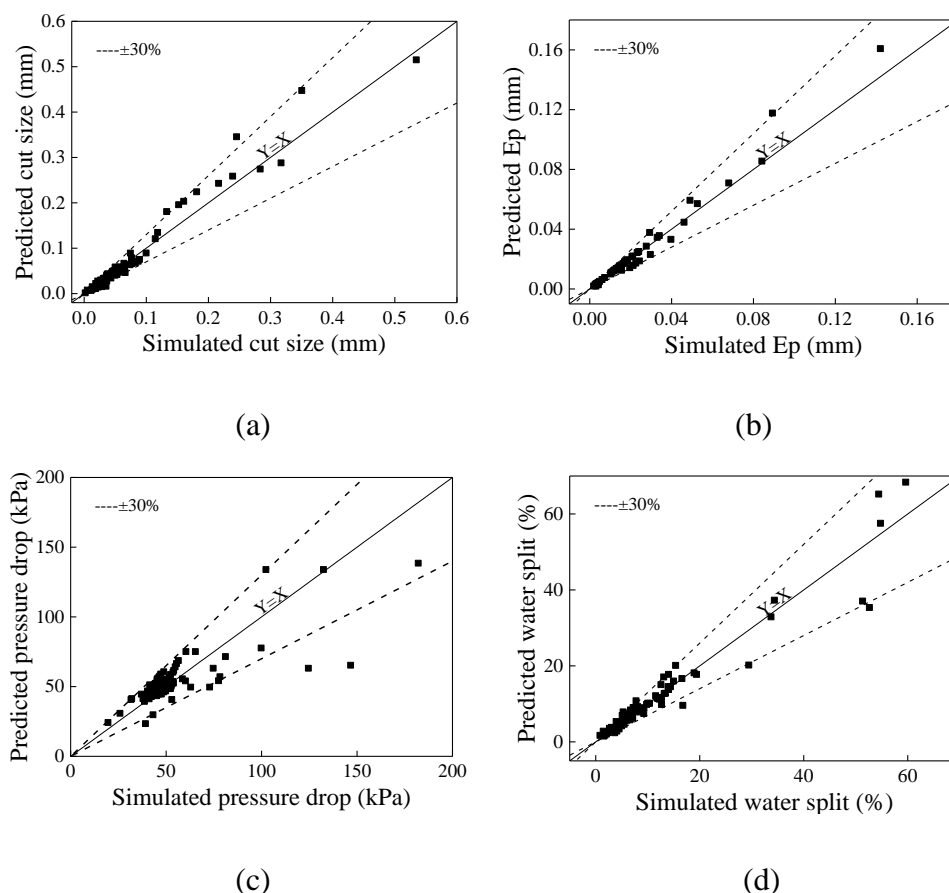


Fig. 7- 5 Comparisons between the predicted and simulated separation performances obtained from literature (Wang, 2009, Wang and Yu, 2006, Wang et al., 2016): (a) cut size, (b) sharpness, (c) pressure drop, (d) water split

7.3 Model validation

As there are some errors between the numerical results and experimental data, it would cause large errors if the predictive model based on the numerical results is directly used to predict the results for the experimental conditions. To avoid this problem, the predictive model is corrected by the experimental data before being applied. As mentioned previously, the collected experimental data are separated into two groups, one group being for correcting the model, and the other being for validating the corrected model. The corrected function forms are shown as shown in Eqs. (2) and (3).

Fig. 7-6 compares the predicted and experimental separation performances. The experimental data has been obtained from industry reports, published papers and thesis (Firth et al., 1999, O'Brien et al., 2001, Rajamani and Milan, 1992, Davailles et

al., 2012, Muzanenhamo, 2014). It can be seen that the predicted results agree well with the experimental ones within $\pm 30\%$ error margins, which indicates that this corrected predictive model is reasonably valid.

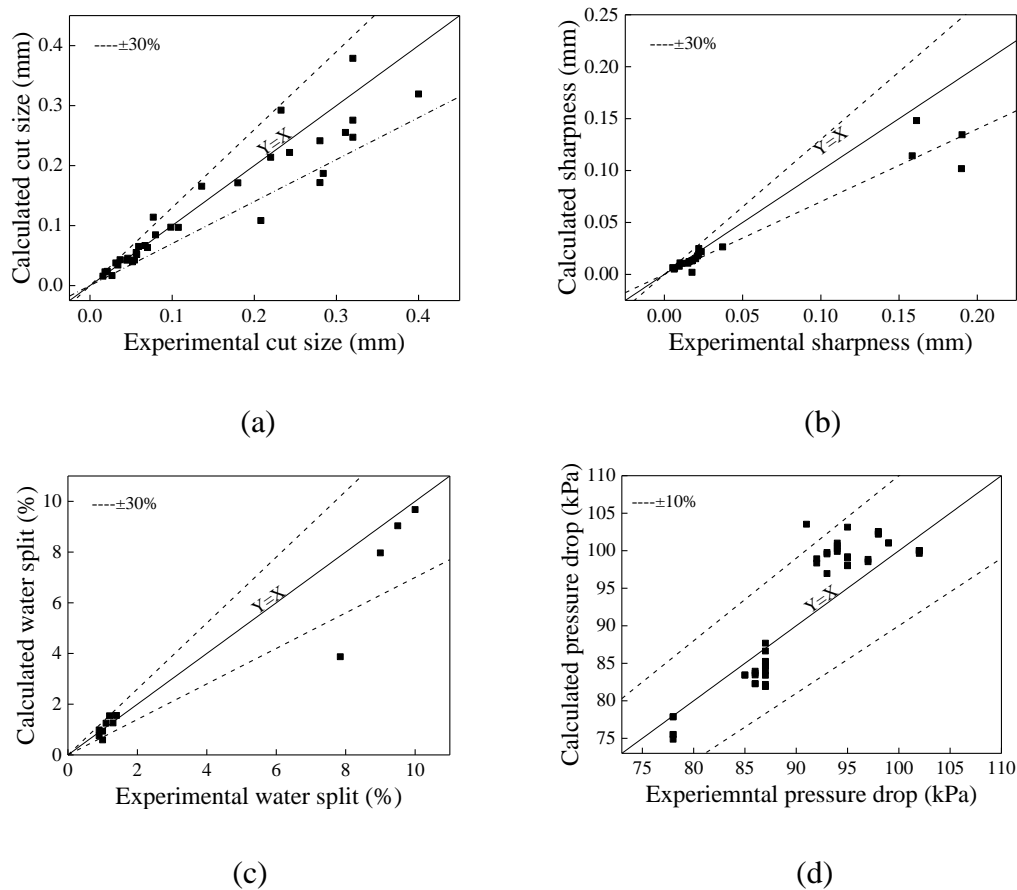


Fig. 7- 6 Comparisons between the predicted and experimental separation performances obtained from literature: (a) cut size, (b) sharpness, (c) pressure drop, and (d) water split

Figs. 7-7 and 7-8 compare the predicted and experimental cut size as a function of material density and feed solid concentration, respectively. The experimental data in Fig 7-7 are from industry reports (Firth et al., 1999, O'Brien et al., 2001). For Fig. 7-8, the experimental data are from Rajamani's study (Rajamani and Milin, 1992) and Muzanenhamo's thesis (Muzanenhamo, 2014). It can be clearly seen that an increase in the material density or a reduction in the feed solid concentration leads to a decrease in the cut size, which is consistent with both the experimental and numerical findings on the effect of the two variables: material density (O'Brien et al., 2001, Firth et al., 1999, Ghodrat et al., 2016) and feed solid concentration (Davailles et al., 2012, Kuang et al., 2012, Braun and Bohnet, 1990, Cilliers, 2000, Rajamani and Milin,

1992). Furthermore, the predicted data points agree well with the corresponding experimental ones.

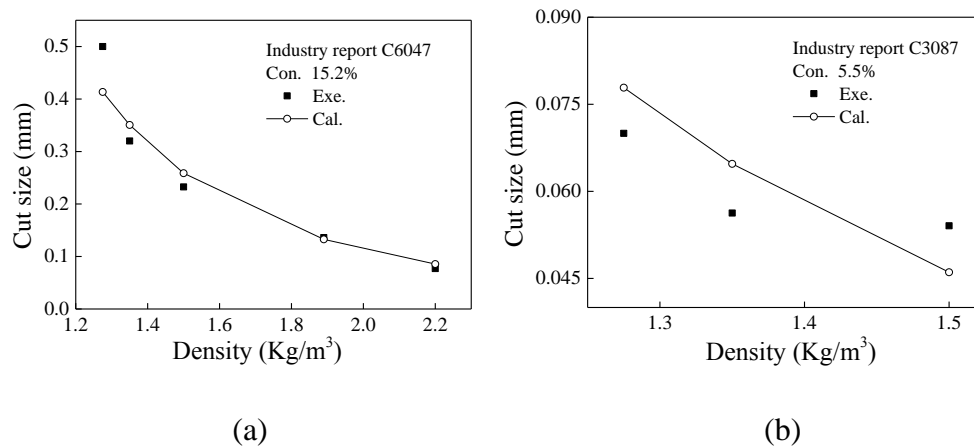


Fig. 7- 7 Comparisons between the predicted and experimental results of cut sizes versus material density for: (a) 1000 mm diameter hydrocyclone at a feed solid concentration of 15.2% cited in the industry report C6047 (O'Brien et al., 2001) and (b) 250 mm diameter hydrocyclone at a feed solid concentration of 5.5% cited in the industry report C3084 (Firth et al., 1999)

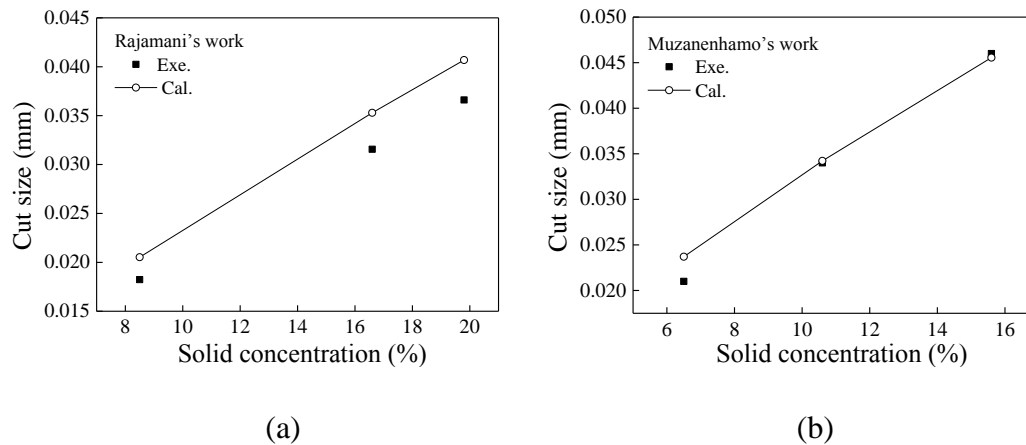


Fig. 7- 8 Comparisons between the predicted and experimental results of cut sizes versus solid concentration for the hydrocyclones in the works of: (a) Rajamani (Rajamani and Milin, 1992), and (b) Muzanenhamo (Muzanenhamo, 2014)

The predicted and experimental effects of the material density and feed solid concentration on the separation sharpness are shown in Figs. 7-9 and 7-10, respectively. Note that a smaller E_p value represents a sharper separation. It can be seen that the separation sharpness increases with the increase of material density or decrease of feed solid concentration, which is the same as the finding of previous studies (Firth et al., 1999, O'Brien et al., 2001, Davailles et al., 2012, Kuang et al.,

2012, Ghodrati et al., 2016). Further, the predicted values reasonably agree well with the experimental ones.

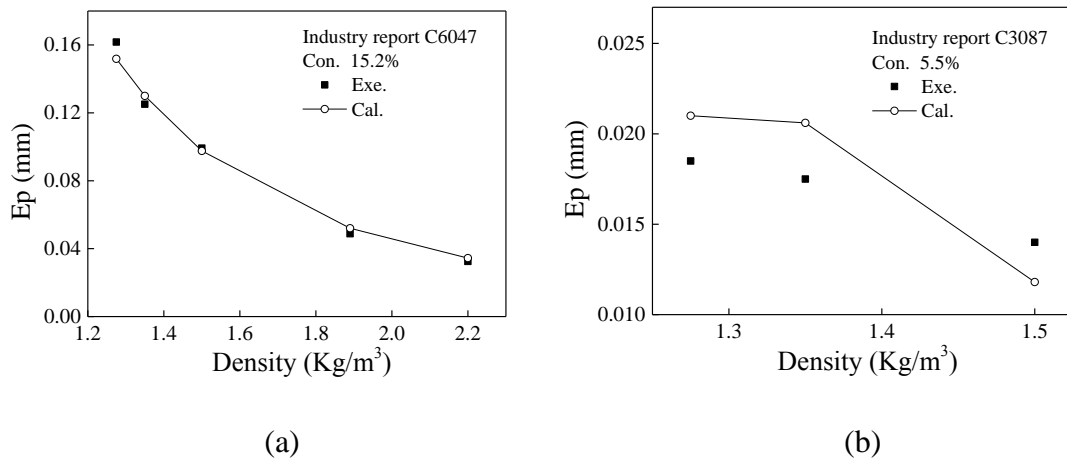


Fig. 7- 9 Comparisons between the predicted and experimental results of separation sharpness versus material density for: (a) 1000 mm diameter hydrocyclone at a feed solid concentration of 15.2% cited in the industry report C6047 (O'Brien et al., 2001) and (b) 250 mm diameter hydrocyclone at a feed solid concentration of 5.5% cited in the industry report C3084 (Firth et al., 1999)

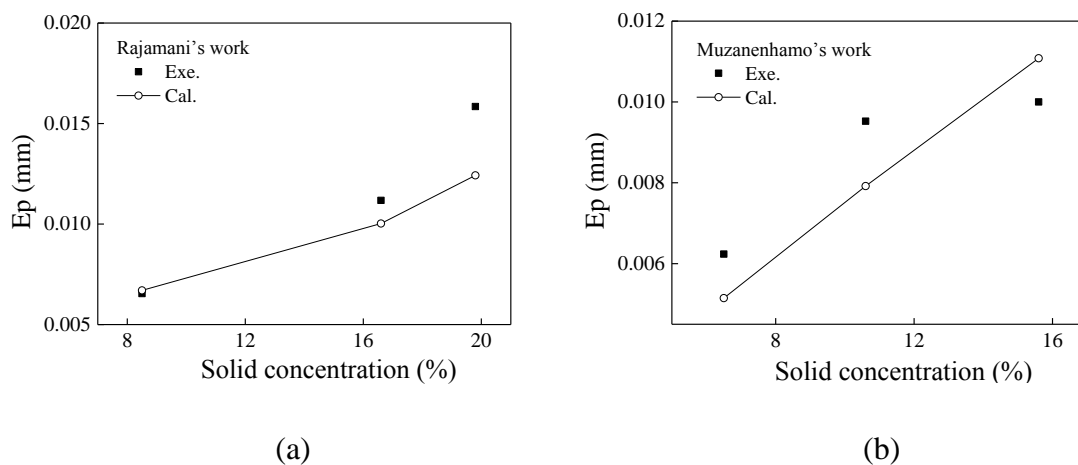


Fig. 7- 10 Comparisons between the predicted and experimental results of sharpness versus solid concentration for hydrocyclones in the works of (a) Rajamani's paper (Rajamani and Milin, 1992), and (b) Muzanenhamo's thesis (Muzanenhamo, 2014)

Plitt model has been used to validate new models due to its wider applicability (Chen et al., 2000, Nageswararao et al., 2004, Kawatra et al., 1996, Wang and Yu, 2006), and recently proposed Narasimha model is shown to have a higher accuracy (Narasimha et al., 2014). Therefore, Plitt and Narasimha models are compared with the new predictive model here. Note that the parameters such as the water split and pressure drop are not always available in the experiments reported in literature; on the

other hand, partition curves can be found easily. Therefore, the prediction accuracy for partition curves is used to evaluate these three models. Note that the partition number of the finest particle is considered as the value of water split for the experiment in the absence of water split data. Further, all of the experimental data used for the validation are independent of the data used for developing this model. Fig. 7-11 compares the experimental partition curves with the predictions based on the newly developed model, Plitt model, and Narasimha model. It can be observed from Fig. 7-11(a) that Plitt model is not suitable to predict the separation performance of materials with different densities because all the partition curves are close to each other. Comparatively, the newly developed predictive model can describe the effect of particle density on the partition curves with a much higher accuracy. From Fig. 7-11(b), it can be seen that Narasimha model can predict the partition curves with a slightly lower accuracy than the new model. However, as mentioned in Section 7.1, the application of Narasimha model must be facilitated with refitting the application-dependent system constants, which significantly limits its model applicability. To utilize the Narasimha model in this work, these specific constants are calculated based on the experimental data at a lower feed solid concentration of 7.4%.

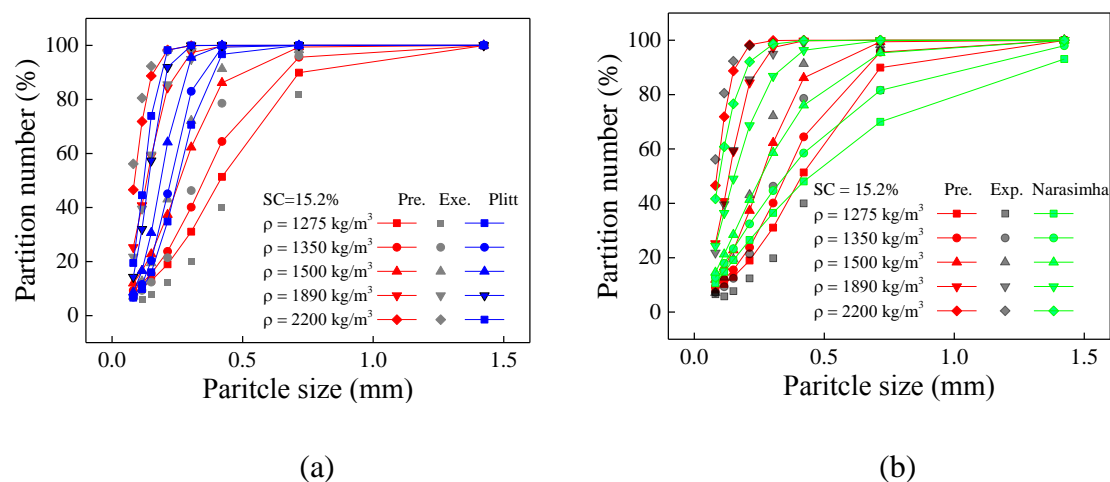


Fig. 7- 11 Partition curves for 1000 mm diameter hydrocyclone at the feed solid concentration of 15.2% cited in the industry report C6047 (O'Brien et al., 2001) based on (a) the present predictive model and Plitt model, and (b) the present predictive model and Narasimha model

Fig. 7-12 compares the predicted partition curves at a feed solid concentration of 5% with experimental ones for materials with different densities reported in the industrial report C3084 (Firth et al., 1999). Similar to Fig. 7-11, the experimental data at the

feed solid concentration of 10% are used to determine the specific constant for the Narasimha model. It is seen from Fig. 7-12 that Plitt model is still weak to estimate the effect of particle density on the partition curve. By contrast, the results predicted by the newly developed model and Narasimha model are closer to the experimental ones.

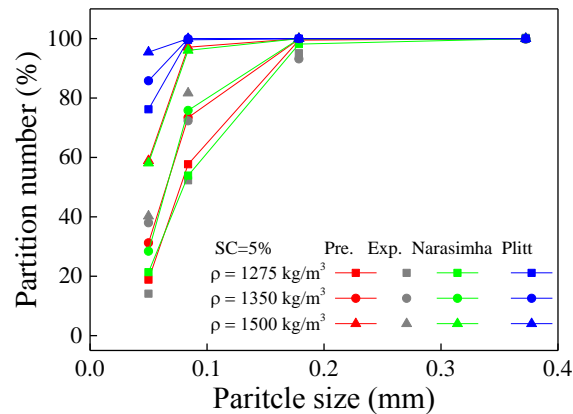


Fig. 7- 12 Comparisons of partition curves for different models with the experimental ones at a feed solid concentration of 5% reported in the industry report C3087 (Firth et al., 1999)

Fig. 7-13 shows the predicted and experimental partition curves under different feed solid concentrations. The specific constant for the Narasimha model is calculated based on the experimental data at a feed solid concentration of 4% reported in Hsieh's work (Hsieh and Rajamani, 1991). It can be observed that Plitt model underestimates separation performance, while the other two can give more comparable results with experiments ones. As mentioned before, the Narasimha model has a limited applicability due to the refitting of the application-dependent system constants. However, the predictive model proposed in this work can overcome this deficiency because it is based on the numerical results and considers comprehensive variables. Therefore, the newly developed model is more suitable for industrial uses with a wider range of applicability.

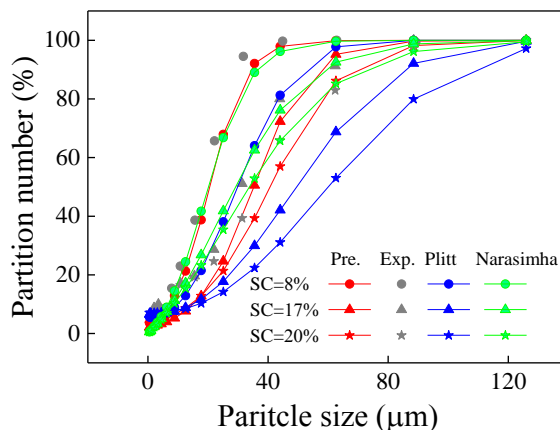


Fig. 7- 13 Partition curves predicted by different models for the conditions in Rajamani's experiments (Rajamani and Milin, 1992)

7.4 Conclusions

The major findings from the present study can be summarised as follows:

- A PC-based model based on the acquired extensive numerical results is developed in this study to predict the hydrocyclone performance, aiming to develop a mathematical description of the underlying fundamentals of hydrocyclone operations. That is, this model can meet the industrial requirements and contribute to explaining the underlying fundamentals of hydrocyclone operations.
- The effects of material density and the particle-fluid flows under a wide range of feed solid concentrations are considered in this new model, which overcome the deficiency of the previously developed models on considering comprehensive variables.
- The new model is validated against the experiments with regards to predicting the cut size, separation sharpness, pressure drop and water split. The predicted results agree well with the experimental ones within $\pm 30\%$ error margins, indicating that this newly developed predictive model is reasonably valid.
- The new model is further compared with the famous Plitt model and the recently-proposed Narasimha model with regards to predicting the partition curves. The results show that the Plitt model is not suitable to predict the separation performance of materials with different densities. Comparatively, the newly developed predictive model can describe the effect of particle density on the

partition curves with a much higher accuracy. Even though the Narasimha model somehow predicts the partition curves reasonably, the application of Narasimha model must be facilitated by refitting the application-dependent system constants, which significantly limits its model applicability. In conclusion, the new model can give more accurate predictions and it has wider model applicability because it is developed based on the numerical results and considers comprehensive variables such like the material density.

CHAPTER 8 CONCLUSIONS AND FURTHER WORKS

8.1 Conclusions

The thesis assesses the applicability of numerical approaches in modelling the multiphase flow in hydrocyclones at a wide range of feed solid concentrations. Based on the selected numerical approach, the effects of material density and its interactions with the cyclone body size and inlet feed type are investigated. Further, the effect of feed size distribution on the multiphase flow and performance of hydrocyclones is studied. Finally, the numerical results, including those generated in this PhD projects and other PhD projects, are then included in the numerical database based on which a PC-based predictive model is developed. The followings are the main conclusions drawn from this research.

(1) The TFM model, which has a wider range of applications, is adapted to generate numerical results under a wide range feed solid concentrations. Considering the limitation of this approach in handling different material types, an effort is also made to develop a DEM-based model for hydrocyclones. It is found that the CG CFD-DEM underestimates the separation performance when the feed solid concentration is high. This is caused by the extremely large size ratio of a CG particle to a real particle. Generally, as the size ratio increases, the prediction will be less accurate especially in the calculation of particle-particle interaction forces, as well as in the radial acceleration difference and solid volume fraction. The CG TFM-DEM model is applicable to the dense flows because it can significantly reduce the size ratio. However, it needs further research for determining the critical particle size below which particles should be considered as a continuum medium.

(2) The effects of particle density on the flow and performance of hydrocyclones are comprehensively studied with respect to cyclone size by the selected TFM model. The results show that particle density effect needs to be considered in selecting cyclone size. It is found that more ultrafine particles are misplaced to the underflow in smaller cyclones, which is pronounced for heavier particles. On the other hand, coarse light particles are more likely to report to the overflow in larger cyclones. Moreover, the handling of lighter particles gives rise to a decreased separation precision and an increased cut size. This result is consistent with the experimental observations and pronounced in large hydrocyclones.

The inner flows and the forces acting on particles have been analyzed in details. It is shown that the particle separation behaviors against particle density and cyclone size mainly attribute to two factors. One is the relative importance of the radial accelerations due to the centrifugal, pressure gradient and drag forces acting on particles, respectively. These accelerations collectively determine the radial motion of particles and thus their chance of entering the proper flow streams for separation. Another factor is the extent of particle accumulation near the spigot. Such accumulation reduces the separation space of hydrocyclone and blocks of the ways of particles for separation, although it mitigates to some extent the water entrainment effect on ultrafine particles.

Based on the results from this study, a mid-range cyclone size is recommended to mitigate the adverse effect of particle density and obtain a relatively precise particle separation on the condition that the expected cut size can be achieved.

(3) The study on the effect of material density has been extended to its interactions with the inlet feed type and feed solid concentration. It is found that hydrocyclones with the ‘spiral and slope’ inlet are superior to those with the traditional involute one for improving the separation precision and eliminating particle misplacement. The differences in the separation precision and particle misplacement between these two feed types are pronounced for the dense flows. Moreover, the effect of feed solid concentration on the separation precision is more evident when processing light materials. The larger total radial acceleration and smaller area of particle accumulation contribute to the increased separation precision for hydrocyclones with the ‘spiral and slope’ inlet. Further, the decreased eddy flow within the ‘spiral and slope’ inlet could also be beneficial for the improvement of separation efficiency and elimination of particle misplacement. Therefore, hydrocyclones with the ‘spiral and slope’ inlet are recommended for industrial uses, especially for handling dense flows.

(4) The effect of feed size distribution on the multiphase flow and performance of hydrocyclones is also studied. The results show that an increase in the amount of median particles leads to a deteriorated separation of intermediate-sized particles, an increase in the cut size, and a smaller difference in partitions between two intermediate-sized particles. It is found that the accumulation of intermediate-sized

particles above the middle cone is more obvious for the size distribution with a larger number of median particles. Further, there are obvious direction fluctuations of total radial acceleration (force) which is attributed to the fluctuations of the drag force. As intermediate-sized particles have a stochastic motion and a longer residence time within hydrocyclones, the fluctuations of the radial acceleration direction further deteriorate their separations. An increase in the amount of median particles also leads to a smaller difference in the radial acceleration between two intermediate-sized particles and thus, a further smaller difference in the partition number.

(5) A PC-based predictive model based on the numerical results is developed in this work to predict the hydrocyclone performance. This model can not only meet the cost expectation and user convenience from the industrial perspective, but also provide a platform to scientifically explain the underlying fundamentals of hydrocyclone operations. The effects of material density and the particle-fluid flows under a wide range of feed solid concentrations are considered in this new model, in order to overcome the deficiency of the previously developed models. Reasonably good agreements between the predicted and experimental results indicate that this model is valid. The new model is also compared with the famous Plitt model and the recently proposed Narasimha model with regards to predicting the partition curves. The comparisons show that this new model is able to give more accurate predictions. Further, it has better applicability because it is developed based on the numerical results and considers comprehensive variables such as the material density.

8.2 Future works

The further studies are expected in the following aspects:

(1) The multiphase flow and separation performance of hydrocyclones are affected by a wide range of geometrical, operational and material conditions. The development of the predictive model in this thesis provides a strategy to predict the multiphase flow and separation performance in an easy, economical, and reliable way. The model applicability however needs to be further validated because not all of the variables are currently covered in this model. More variables and larger variation ranges should be considered to develop a more reliable model for practical applications.

(2) The new predictive model is based on the widely encountered geometrical, operational and material conditions. Note that some new geometrical designs and operations, such like the ‘spiral and slope’ inlet and the inserted rod, have been emerging in recent years. However, how to include these new variables in this model needs further research and some systematic studies are necessary.

(3) The effect of material density has been investigated in this thesis. However, the material properties not only include the density but also others like particle size distribution. In this work, the effect of feed size distributions is investigated with different values of σ_j (i.e., 0.5, 1, and 2) while the median size is at a fixed value. Apparently, such an effort does not fully cover the effect of size distribution, although some important issues related to the behaviours of particles with median size have been addressed. Therefore, a systemic study on the effect of size distribution is necessary in the future.

(4) There is a limited number (up to 20) of phases that can be calculated in the ANSYS Fluent for numerical stability, which leads to the difficulty in simulating a wide distribution of particle size/density by the TFM model. This deficiency can be overcome by combing the TFM model with DEM approach. However, the trial on adopting CG TFM-DEM approach indicates that it needs dedicated research to develop general methods/theories to determine the critical particle size below which particles can be considered as a continuum medium.

LIST OF REFERENCES

- ALOBALD, F. & EPPLER, B. 2013. Improvement, validation and application of CFD/DEM model to dense gas-solid flow in a fluidized bed. *Particuology*, 11, 514-526.
- ALOBALD, F., STROHLE, J. & EPPLER, B. 2013. Extended CFD/DEM model for the simulation of circulating fluidized bed. *Advanced Powder Technology*, 24, 403-415.
- ANSYS, I. 2012. ANSYS FLUENT theory guide.
- ARNOLD, B. J., KLIMA, M. S. & BETHELL, P. J. 2007. *Designing the coal preparation plant of the future*, United States, Society for Mining, Metallurgy, and Exploration (SME), Littleton, CO.
- ARTERBURN, R. A. 1982. The sizing and selection of hydrocyclones.
- ASOMAH, A. K. & NAPIER-MUNN, T. J. 1997. An empirical model of hydrocyclones, incorporating angle of cyclone inclination. *Minerals Engineering*, 10, 339-347.
- ATKINSON, B. & SWANSON, A. 2008. Improved efficiency of fine coal classification. *ACARP PROJECT 15059*.
- AZADI, M., AZADI, M. & MOHEBBI, A. 2010. A CFD study of the effect of cyclone size on its performance parameters. *J Hazard Mater*, 182, 835-41.
- BAI, Z. S., WANG, H. L. & TU, S. T. 2009. Study of air-liquid flow patterns in hydrocyclone enhanced by air bubbles. *Chem. Eng. Technol.*, 32, 55-63.
- BARBEE, C. J., LUTTRELL, G. H., WOOD, C. J. & BETHELL, P. J. 2005. Simulation of heavy medium cyclone performance. *Minerals & Metallurgical Processing*, 22, 38-42.
- BHARDWAJ, P., BAGDI, P. & SEN, A. K. 2011. Microfluidic device based on a micro-hydrocyclone for particle-liquid separation. *Lab Chip*, 11, 4012-21.
- BHASKAR, K. U., MURTHY, Y. R., RAJU, M. R., TIWARI, S., SRIVASTAVA, J. K. & RAMAKRISHNAN, N. 2007. CFD simulation and experimental validation studies on hydrocyclone. *Minerals Engineering*, 20, 60-71.
- BICALHO, I. C., MOGNON, J. L., SHIMOYAMA, J., ATAÍDE, C. H. & DUARTE, C. R. 2014. CFD applied to the analysis of hydrodynamics in a hydrocyclone. *Materials Science Forum*, 802, 226-231.
- BRADLEY, D. 1965. *The hydrocyclone*, London, Pergamon Press.
- BRAUN, T. & BOHNET, M. 1990. Influence of feed solids concentration on the performance of hydrocyclones. *Chem. Eng. Technol.*, 13 15-20.
- BRENNAN, M. 2006. CFD Simulations of Hydrocyclones with an Air Core. *Chemical Engineering Research and Design*, 84, 495-505.
- BRENNAN, M. S., NARASIMHA, M. & HOLTHAM, P. N. 2007. Multiphase modelling of hydrocyclones - prediction of cut-size. *Minerals Engineering*, 20, 395-406.
- CAI, P. & WANG, B. 2013. Numerical investigation on distribution characteristics of dense dispersed phase in hydrocyclones. *AIP Conference Proceedings* [Online], 1574.
- CELLO, F., DI RENZO, A. & DI MAIO, F. P. 2009. DEM-CFD simulations of layer inversion in two-component liquid fluidized beds. *Icheap-9: 9th International Conference on Chemical and Process Engineering, Pts 1-3*, 17, 627-632.
- CHEN, J., CHU, K. W., ZOU, R. P., YU, A. B. & VINCE, A. 2012. Prediction of the performance of dense medium cyclones in coal preparation. *Minerals Engineering*, 31, 59-70.
- CHEN, J., CHU, K. W., ZOU, R. P., YU, A. B., VINCE, A., BARNETT, G. D. & BARNETT, P. J. 2016. Systematic study of effect of particle size distribution in a dense medium cyclone by Johnson's S-B function. *Minerals Engineering*, 91, 16-33.
- CHEN, W., ZYDEK, N. & PARMA, F. 2000. Evaluation of hydrocyclone models for practical applications.
- CHINÉ, B. & CONCHA, F. 2000. Flow patterns in conical and cylindrical hydrocyclones. *Chemical Engineering Journal* 80 267-273.

- CHU, K., CHEN, J. & YU, A. 2016. Applicability of a coarse-grained CFD–DEM model on dense medium cyclone. *Minerals Engineering*, 90, 43-54.
- CHU, K. W., KUANG, S. B., YU, A. B. & VINCE, A. 2012a. Particle scale modelling of the multiphase flow in a dense medium cyclone: Effect of fluctuation of solids flowrate. *Minerals Engineering*, 33, 34-45.
- CHU, K. W., KUANG, S. B., YU, A. B., VINCE, A., BARNETT, G. D. & BARNETT, P. J. 2014. Prediction of wear and its effect on the multiphase flow and separation performance of dense medium cyclone. *Minerals Engineering*, 56, 91-101.
- CHU, K. W., WANG, B., VINCE, A. & YU, A. B. 2012b. Computational study of the multiphase flow in a dense medium cyclone: Effect of particle density. *Chemical Engineering Science*, 73, 123-139.
- CHU, K. W., WANG, B., XU, D. L., CHEN, Y. X. & YU, A. B. 2011. CFD–DEM simulation of the gas–solid flow in a cyclone separator. *Chemical Engineering Science*, 66, 834-847.
- CHU, K. W., WANG, B., YU, A. B., VINCE, A., BARNETT, G. D. & BARNETT, P. J. 2009. CFD-DEM study of the effect of particle density distribution on the multiphase flow and performance of dense medium cyclone. *Minerals Engineering*, 22, 893-909.
- CHU, K. W. & YU, A. B. 2008. Numerical simulation of complex particle–fluid flows. *Powder Technology*, 179, 104-114.
- CHU, L. Y., CHEN, W. M. & LEE, X. Z. 2000. Effect of structural modification on hydrocyclone performance. *Separation and Purification Technology*, 21, 71-86.
- CHU, L. Y., CHEN, W. M. & LEE, X. Z. 2002. Effects of geometric and operating parameters and feed characters on the motion of solid particles in hydrocyclones. *Separation and Purification Technology*, 26, 237-246.
- CILLIERS, J. J. 2000. Hydrocyclones for Particle Size Separation. *Particle size separation*
- CILLIERS, J. J. & HINDET, A. L. 1991. An improved hydrocyclone model for backfill preparation. *Minerals Engineering*, 4, 683-693.
- CULLIVAN, J. C., WILLIAMS, R. A., DYAKOWSKI, T. & CROSS, C. R. 2004. New understanding of a hydrocyclone flow field and separation mechanism from computational fluid dynamics. *Minerals Engineering*, 17, 651-660.
- CUNDALL, P. A. & STRACK, O. D. L. 1979. Discrete numerical-model for granular assemblies. *Geotechnique*, 29, 47-65.
- DABIR, D. 1983. *Mean velocity measurements in a 3 inches hydrocyclone using laser Doppler anemometry*. P.h.D, Michigan State University, USA.
- DAI, G. Q., CHEN, W. M., LI, J. M. & CHU, L. Y. 1999. Experimental study of solid-liquid two-phase flow in a hydrocyclone. *Chemical Engineering Journal* 74 211-216.
- DAVAILLES, A., CLIMENT, E., BOURGEOIS, F. & MAJUMDER, A. K. 2012. Analysis of swirling flow in hydrocyclones operating under dense regime. *Minerals Engineering*, 31, 32-41.
- DELGADILLO, J. A. & RAJAMANI, R. K. 2005. A comparative study of three turbulence-closure models for the hydrocyclone problem. *International Journal of Mineral Processing*, 77, 217-230.
- DELGADILLO, J. A. & RAJAMANI, R. K. 2007. Exploration of hydrocyclone designs using computational fluid dynamics. *International Journal of Mineral Processing*, 84, 252-261.
- DELGADILLO, J. A. & RAJAMANI, R. K. 2009. Computational fluid dynamics prediction of the air-core in hydrocyclones. *International Journal of Computational Fluid Dynamics*, 23, 189-197.

- DELGADILLO, J. A., ROSALES-MARIN, G., PEREZ-ALONSO, C. & OJEDA, C. 2012. CFD analysis to study the effect of design variables on the particle cut size in hydrocyclones. *Asia-Pacific Journal of Chemical Engineering*.
- DIETZ, P. W. 1981. Collection efficiency of cyclone separators.
- DLAMINI, M. F., POWELL, M. S. & MEYER, C. J. 2005. A CFD simulation of a single phase hydrocyclone flow field. *The Journal of The South African Institute of Mining and Metallurgy*, 105, 711-717.
- ERGUN, S. 1952. Fluid Flow through Packed Columns. *Chemical Engineering Progress*, 48, 89-94.
- EVANS, W. K., SUKSANGPANOMRUNG, A. & NOWAKOWSKI, A. F. 2008. The simulation of the flow within a hydrocyclone operating with an air core and with an inserted metal rod. *Chemical Engineering Journal*, 143, 51-61.
- FIRTH, B., O'BRIEN, M., EDWARD, D. & CLARKSON, C. 1999. Fine coal classification. *ACARP report*, C3084.
- FISHER, M. J. & FLACK, R. D. 2002. Velocity distributions in a hydrocyclone separator. *Exp. Fluids*, 32 302-312.
- FLINTOFF, D. O. & PLITT, L. R. 1987. Cyclone modelling: a review of present technology. *Cim Bulletin*, 39-49.
- FRACHON, M. & CILLIERS, J. J. 1999. A general model for hydrocyclone partition curves. *Chemical Engineering Journal* 73 53-59.
- FRIES, L., ANTONYUK, S., HEINRICH, S., DOPFER, D. & PALZER, S. 2013. Collision dynamics in fluidised bed granulators: A DEM-CFD study. *Chemical Engineering Science*, 86, 108-123.
- GAO, S. L., WEI, D. Z., LIU, W. G., MA, L. Q., LU, T. & ZHANG, R. Y. 2011. CFD numerical simulation of flow velocity characteristics of hydrocyclone. *Transactions of Nonferrous Metals Society of China*, 21, 2783-2789.
- GHADIRIAN, M., AFACAN, A., HAYES, R. E., MMBAGA, J. P., MAHMOOD, T., XU, Z. & MASLIYAH, J. 2015. A Study of the Hydrocyclone for the Separation of Light and Heavy Particles in Aqueous Slurry. *The Canadian Journal of Chemical Engineering*, 93, 1667-1677.
- GHODRAT, M. 2014. *Computational modeling and analysis of the flow and performance in hydrocyclones* P.h.D, The University of New South Wales
- GHODRAT, M., KUANG, S. B., YU, A. B., VINCE, A., BARNETT, G. D. & BARNETT, P. J. 2013. Computational study of the multiphase flow and performance of hydrocyclones: Effects of cyclone size and spigot diameter. *Industrial & Engineering Chemistry Research*, 52, 16019-16031.
- GHODRAT, M., KUANG, S. B., YU, A. B., VINCE, A., BARNETT, G. D. & BARNETT, P. J. 2014a. Numerical analysis of hydrocyclones with different conical section designs. *Minerals Engineering*, 62, 74-84.
- GHODRAT, M., KUANG, S. B., YU, A. B., VINCE, A., BARNETT, G. D. & BARNETT, P. J. 2014b. Numerical analysis of hydrocyclones with different vortex finder configurations. *Minerals Engineering*, 63, 125-138.
- GHODRAT, M., QI, Z., KUANG, S. B., JI, L. & YU, A. B. 2016. Computational investigation of the effect of particle density on the multiphase flows and performance of hydrocyclone. *Minerals Engineering*, 90, 55-69.
- GIDASPOW, D. 1994. *Multiphase flow and fluidization: Continuum and kinetic theory descriptions*, Boston, Academic Press.

- GIDASPOW, D., BEZBURUAH, R. & DING, J. 1991. Hydrodynamics of circulating fluidized beds: kinetic theory approach. Illinois Inst. of Tech., Chicago, IL (United States). Dept. of Chemical Engineering.
- HANG, Y. F., ILEA, C. G., AASEN, L. & HOFFMANN, A. C. 2011. Particle flow in a hydrocyclone investigated by positron emission particle tracking. *Chemical Engineering Science*, 66 4203-4211.
- HARARAH, M. A., ENDRES, E., DUECK, J., MINKOV, L. & NEESSE, T. 2010. Flow conditions in the air core of the hydrocyclone. *Minerals Engineering*, 23, 295-300.
- HEISKANEN, K. 1993. *Particle classification*, Netherlands, Springer.
- HERNÁNDEZ-JIMÉNEZ, F., GARCÍA-GUTIÉRREZ, L. M., SORIA-VERDUGO, A. & ACOSTA-IBORRA, A. 2015. Fully coupled TFM-DEM simulations to study the motion of fuel particles in a fluidized bed. *Chemical Engineering Science*, 134, 57-66.
- HIRT, C. W. & NICHOLS, B. D. 1981. Volume of fluid (VOF) method for the dynamics of free boundaries. *Journal of Computational Physics*, 39, 201-225.
- HONG, J.-I., KIM, Y. J., HAN, J.-G. & OH, J.-K. Performance characteristics of electrocyclone. ASME International Mechanical Engineering Congress and Exposition, 2005 Orlando, Florida USA.
- HSIEH, K.-T. 1988. *Phenomenological model of the hydrocyclone*. P.h.D, The University of Utah.
- HSIEH, K. T. & RAJAMANI, R. K. 1991. Mathematical model of the hydrocyclone based on physics of fluid-flow. *American Institute of Chemical Engineers Journal*, 37, 735-746.
- HSU, C.-W. 2014. An Experimental Study on Performance Improvement of the Stairmand Cyclone Design. *Aerosol and Air Quality Research*.
- HUANG, C., LV, W.-J., WANG, J.-G., WANG, J.-Y. & WANG, H.-L. 2014. Uniform distribution design and performance evaluation for UU-type parallel mini-hydrocyclones. *Separation and Purification Technology*, 125, 194-201.
- HWANG, K., HWANG, Y., YOSHIDA, H. & SHIGEMORI, K. 2012. Improvement of particle separation efficiency by installing conical top-plate in hydrocyclone. *Powder Technology*, 232, 41-48.
- INAKI SCHLABERG, H., PODD, F. J. W. & HOYLE, B. S. 2000. Ultrasound process tomography system for hydrocyclones. *Ultrasonics*, 38 813-816.
- IOZIA, D. L. & LEITH, D. 2007. The Logistic Function and Cyclone Fractional Efficiency. *Aerosol Science and Technology*, 12, 598-606.
- JI, H., NIE, S., SUN, H., CHENG, Y. & LI, Y. 2012. Effects of key structural parameters on solid-liquid separation behavior of hydrocyclone separator applied to hydraulic oil purification. *Proceedings of the Institution of Mechanical Engineers, Part E: Journal of Process Mechanical Engineering*, 227, 273-286.
- JI, L., KUANG, S., QI, Z., WANG, Y., CHEN, J. & YU, A. 2017. Computational analysis and optimization of hydrocyclone size to mitigate adverse effect of particle density. *Separation and Purification Technology*, 174, 251-263.
- JIANG, M. G., ZHAO, L. X., LI, F. & ZHANG, Y. 2007. Development of oil-water separation hydrocyclones for oilfield produced-fluid pre-treatment. *Proceedings of the 26th International Conference on Offshore Mechanics and Arctic Engineering, Vol 2*, 701-707.
- KAWATRA, S. K., BAKSHI, A. K. & RUSESKEY, M. T. 1996. The effect of slurry viscosity on hydrocyclone classification.
- KELSALL, D. 1952. A study of the motion of solid particles in a hydraulic cyclone. *Chem. Eng. Res. Des.*, 30, 87-108.

- KFUALL, D. F. 1953. A further study of the hydraulic cyclone. *Chemical Engineering Science*, 254-272.
- KLEIN, M. L. & SHINODA, W. 2008. Large-scale molecular dynamics simulations of self-assembling systems. *Science*, 321, 798-800.
- KNOWLES, S. R., WOODS, D. R. & FEUERSTEIN, I. A. 1973. The velocity distribution within a hydrocyclone operating without an air core. *Can. J. Chem. Eng.*, 51, 263-271.
- KRAIPECH, W., CHEN, W., DYAKOWSKI, T. & NOWAKOWSKI, A. 2006. The performance of the empirical models on industrial hydrocyclone design. *International Journal of Mineral Processing*, 80, 100-115.
- KUANG, S. B., CHU, K. W., YU, A. B. & VINCE, A. 2012. Numerical study of liquid–gas–solid flow in classifying hydrocyclones: Effect of feed solids concentration. *Minerals Engineering*, 31, 17-31.
- KUANG, S. B., QI, Z., YU, A. B., VINCE, A., BARNETT, G. D. & BARNETT, P. J. 2014. CFD modeling and analysis of the multiphase flow and performance of dense medium cyclones. *Minerals Engineering*, 62, 43-54.
- LAUNDER, B. E., REECE, G. J. & RODI, W. 1975. Progress in the development of a Reynolds-stress turbulence closure. *Journal of Fluid Mechanics*, 68, 537-566.
- LUN, C. K. K., SAVAGE, S. B., JEFFREY, D. J. & CHEPURNIY, N. 1984. Kinetic Theories for Granular Flow - Inelastic Particles in Couette-Flow and Slightly Inelastic Particles in a General Flowfield. *Journal of Fluid Mechanics*, 140, 223-256.
- LV, W. J., HUANG, C., CHEN, J. Q., LIU, H. L. & WANG, H. L. 2015. An experimental study of flow distribution and separation performance in a UU-type mini-hydrocyclone group. *Separation and Purification Technology*, 150, 37-43.
- LYNCH, A. J. 1977. *Mineral crushing and grinding circuits, their simulation, optimisation, design and control*, Elsevier, Amsterdam.
- LYNCH, A. J. & RAO, T. C. 1968. The operating characteristics of hydrocyclone classifiers. *Ind. J. of Tech.*, 6, 106.
- LYNCH, A. J., RAO, T. C. & BAILEY, C. W. 1975. The influence of design and operating variables on the capacities of hydrocyclone classifiers. *International Journal of Mineral Processing*.
- LYNCH, A. J., RAO, T. C. & RISBREY, K. A. 1974. The influence of hydrocyclone diameter on reduced-efficiency curves. *International Journal of Mineral Processing*, 1, 173-181.
- MARINS, L. P. M., DUARTE, D. G., LOUREIRO, J. B. R., MORAES, C. A. C. & FREIRE, A. P. S. 2010. LDA and PIV characterization of the flow in a hydrocyclone without an air-core. *Journal of Petroleum Science and Engineering*, 70, 168-176.
- MOGNON, J. L., DA SILVA, J. M., BICALHO, I. C., ATAÍDE, C. H. & DUARTE, C. R. 2015. Modular mini-hydrocyclone desilter type of 30mm: An experimental and optimization study. *Journal of Petroleum Science and Engineering*, 129, 145-152.
- MOKHTAR, M. A., KUWAGI, K., TAKAMI, T., HIRANO, H. & HORIO, M. 2012. Validation of the similar particle assembly (SPA) model for the fluidization of Geldart's group A and D particles. *AIChE Journal*, 58, 87-98.
- MOUSAVIAN, S. M. & NAJAFI, A. F. 2009. Influence of geometry on separation efficiency in a hydrocyclone. *Archive of Applied Mechanics*, 79, 1033-1050.
- MURTHY, Y. R. & BHASKAR, K. U. 2012. Parametric CFD studies on hydrocyclone. *Powder Technology*, 230, 36-47.
- MUZANENHAMO, P. 2014. *Assessing the effect of cone ratio, feed solids concentration and viscosity on hydrocyclone performance*. Master, University of Cape Town.

- NAGESWARARAO, K. 1978. *Futher developments in the modelling and scale up industrial hydrocyclones*. Doctor of Philosophy, University of Queensland.
- NAGESWARARAO, K., WISEMAN, D. M. & NAPIER-MUNN, T. J. 2004. Two empirical hydrocyclone models revisited. *Minerals Engineering*, 17, 671-687.
- NARASIMHA, M., BRENNAN, M. & HOLTHAM, P. N. 2006. Large eddy simulation of hydrocyclone-prediction of air-core diameter and shape. *International Journal of Mineral Processing*, 80, 1-14.
- NARASIMHA, M., BRENNAN, M. & HOLTHAM, P. N. 2007a. A review of CFD modelling for performance predicitions of hydrocyclone. *Engineering Applications of Computational Fluid Mechanics*, 1, 109-125.
- NARASIMHA, M., BRENNAN, M. S., HOLTHAM, P. N. & NAPIER-MUNN, T. J. 2007b. A comprehensive CFD model of dense medium cyclone performance. *Minerals Engineering*, 20, 414-426.
- NARASIMHA, M., MAINZA, A. N., HOLTHAM, P. N. & BRENNAN, M. S. 2012. Air-core modelling for hydrocyclones operating with solids. *International Journal of Mineral Processing*, 102, 19-24.
- NARASIMHA, M., MAINZA, A. N., HOLTHAM, P. N., POWELL, M. S. & BRENNAN, M. S. 2014. A semi-mechanistic model of hydrocyclones - Developed from industrial data and inputs from CFD. *International Journal of Mineral Processing*, 133, 1-12.
- NEESSE, T. & DUECK, J. 2007. Air core formation in the hydrocyclone. *Minerals Engineering*, 20, 349-354.
- NEESSE, T., DUECK, J., SCHWEMMER, H. & FARGHALY, M. 2015. Using a high pressure hydrocyclone for solids classification in the submicron range. *Minerals Engineering*, 71, 85-88.
- NOID, W. G. 2013. Perspective: Coarse-grained models for biomolecular systems. *The Journal of Chemical Physics*, 139, 090901: 1-25.
- NOROOZI, S. & HASHEMABADI, S. H. 2009. CFD simulation of inlet design effect on deoiling hydrocyclone separation efficiency. *Chemical Engineering & Technology*, 32, 1885-1893.
- NOWAKOWSKI, A. F., CULLIVAN, J. C., WILLIAMS, R. A. & DYAKOWSKI, T. 2004. Application of CFD to modelling of the flow in hydrocyclones. Is this a realizable option or still a research challenge? *Minerals Engineering*, 17, 661-669.
- NOWAKOWSKI, A. F. & DYAKOWSKI, T. 2003. Investigation of Swirling Flow Structure in Hydrocyclones. *Chemical Engineering Research and Design*, 81, 862-873.
- NOWAKOWSKI, A. F., KRAIPECH, W., WILLIAMS, R. A. & DYAKOWSKI, T. 2000. The hydrodynamics of a hydrocyclone based on a three-dimensional multi-continuum model. *Chemical Engineering Journal*, 80, 275-282.
- O'BRIEN, M., TAYLOR, A., NEMETH, D., FIRTH, B. & CLARKSON, C. 2001. Large diameter classifying cyclones *ACARP report*, C6047.
- PLITT 1979. Estimating the cut (d50) size of classifiers without product particle-size measurement. *International of Mineral Processing*, 5 369-378.
- PLITT, L. R. 1971. The analysis of solid-solid separations in classifiers. *Cim Bulletin*, 64, 42.
- PLITT, L. R. 1976. A mathematical model of the hydrocyclone classifier. *CIM Bulletin* 69, 114-123.
- QI, Z., KUANG, S. B. & YU, A. B. 2015. Numerical investigation of the separation behaviours of fine particles in large dense medium cyclones. *International Journal of Mineral Processing*, 142, 35-45.

- RAJAMANI, R. K. & MILAN, L. 1992. Fluid-flow model of the hydrocyclone for concentrated slurry classification. In: SVAROVSKY, L. & THEW, M. T. (eds.) *Hydrocyclone: Analysis and Application*. Dordrecht: Springer Netherlands.
- RAKESH, A., REDDY, V. T. S. R. K. & NARASIMHA, M. 2014. Air-Core Size Measurement of Operating Hydrocyclone by Electrical Resistance Tomography. *Chemical Engineering & Technology*, 37, 795-805.
- RAO, T. C., NAGESWARARAO, K. & LYNCH, A. J. 1976. Influence of feed inlet diameter on the hydrocyclone behaviour. *International Journal of Mineral Processing*, 3, 357-363.
- RENNER, V. G. & COHEN, H. E. 1978. Measurement and interpretation of size distribution of particles within a hydrocyclone. *Transactions of the Institution of Mining and Metallurgy*, 87, 139-145.
- RONG, L. W., DONG, K. J. & YU, A. B. 2013. Lattice-Boltzmann simulation of fluid flow through packed beds of uniform spheres: Effect of porosity. *Chemical Engineering Science*, 99, 44-58.
- RONG, R. 2007. Industrial trials of novel cyclones. *ACARP report*, C14067.
- SAENGCHAN, K., NOPHARATANA, A. & SONGKASIRI, W. 2009. Enhancement of tapioca starch separation with a hydrocyclone: effects of apex diameter, feed concentration, and pressure drop on tapioca starch separation with a hydrocyclone. *Chemical Engineering and Processing*, 48, 195-202.
- SAFA, R. & GOHARRIZI, A. S. 2014. CFD simulation of an industrial hydrocyclone with Eulerian–Eulerian approach: A case study. *International Journal of Mining Science and Technology*, 24, 643-648.
- SAKAI, M. & KOSHIZUKA, S. 2009. Large-scale discrete element modeling in pneumatic conveying. *Chemical Engineering Science*, 64, 533-539.
- SCHEID, C. M., CALÇADA, L. A., GONÇALVES, R. S. A. & MASSARANI, G. 2012. An investigation of the behavior of a classification hydrocyclone with pseudoplastic fluids
- SCHILLER, L. & NAUMANN, Z. 1933. A drag coefficient correlation. *Z. Ver. Deutsch. Ing.*, 77, 318-320.
- SCHUBERT, H. 2007. A Hydrocyclone Separation Model in Consideration of the Turbulent Multi-Phase Flow. *Particulate Science and Technology*, 3, 1-13.
- SILVA1, A. C., SILVA, E. M. S. & MATOS, J. D. V. 2012. A Modification in Plitt'S for Hydrocyclones Simulation. *IJRRAS* 13, 753-758.
- SLECHTA, J. & FIRTH, B. A. 1984. Classification of fine coal with a hydrocyclone. *International Journal of Mineral Processing* 4, 213-237.
- SVAROVSKY, L. 1984. *Hydrocyclones*, Technomic Publishing Inc: Lancaster, PA.
- SVAROVSKY, L. & THEW, M. T. 1992. *Hydrocyclones: analysis and applications*, Springer Science & Business Media.
- SWAIN, S. & MOHANTY, S. 2013. A 3-dimensional Eulerian-Eulerian CFD simulation of a hydrocyclone. *Applied Mathematical Modelling*, 37, 2921-2932.
- SYAMLAL, M., ROGERS, W. & O'BRIEN, T. J. 1993. *MFIX documentation: theory guide*, National Technical Information Service, Springfield, VA, DOE/METC-9411004, NTIS/DE9400087.
- T.C.RAO, NAGESWARARAO, K. & LYNCH, A. J. 1976. Influence of feed inlet diameter on the hydrocyclone behaviour. *International Journal of Mineral Processing*, 3 357--363.
- THAKUR, S. C., OOI, J. Y. & AHMADIAN, H. 2016. Scaling of discrete element model parameters for cohesionless and cohesive solid. *Powder Technology*, 293, 130-137.

- TOZZINI, V. 2005. Coarse-grained models for proteins. *Current Opinion in Structural Biology*, 15, 144-150.
- TUE NENU, R. K. & YOSHIDA, H. 2009. Comparison of separation performance between single and two inlets hydrocyclones. *Advanced Powder Technology*, 20, 195-202.
- WANG, B. 2009. *Modelling the multiphase flow in cyclones*. P.h.D, University of New South Wales.
- WANG, B., CHU, K. W. & YU, A. B. 2007. Numerical Study of Particle-Fluid Flow in a Hydrocyclone. *Industrial & Engineering Chemistry Research*, 46, 4695-4705.
- WANG, B., CHU, K. W., YU, A. B. & VINCE, A. 2014. Computational investigation of the mechanisms of the "breakaway" effect in a dense medium cyclone. *Minerals Engineering*, 62, 111-119.
- WANG, B., XU, D. L., CHU, K. W. & YU, A. B. 2006. Numerical study of gas-solid flow in a cyclone separator. *Applied Mathematical Modelling*, 30, 1326-1342.
- WANG, B. & YU, A. B. 2006. Numerical study of particle-fluid flow in hydrocyclones with different body dimensions. *Minerals Engineering*, 19, 1022-1033.
- WANG, B. & YU, A. B. 2009. Computational investigation of the mechanisms of particle separation and "fish-hook" phenomenon in hydrocyclones. *AIChE Journal*, 56, 1703-1715.
- WANG, J. G., BAI, Z. S., YANG, Q., FAN, Y. & WANG, H. L. 2016. Investigation of the simultaneous volumetric 3-component flow field inside a hydrocyclone. *Separation and Purification Technology*, 163, 120-127.
- WANG, Q., FENG, Y., LU, J., YIN, W., YANG, H., WITT, P. J. & ZHANG, M. 2015. Numerical study of particle segregation in a coal beneficiation fluidized bed by a TFM-DEM hybrid model: Influence of coal particle size and density. *Chemical Engineering Journal*, 260, 240-257.
- WEN, C. Y. & YU, Y. H. 1966. Mechanics of fluidisation. *Chem. Eng. Prog. Symp. Series*, 62, 100-111.
- WICK, G. L. 1977. Centrifugal buoyancy forces. *American Journal of Physics*, 45, 1074.
- WILCOX, D. C. 1994. *Turbulence modelling for CFD (second ed.)*, DCW Industries Inc: La Canada, CA, USA.
- WILLIAMS, R. A., ILYAS, O. M., DYAKOWSKI, T., DIEKIN, F. J., GUTTIERREZ, J. A., WANG, M., BECK, M. S., SHAH, C. & RUSHTON, A. 1995. Air core modelling in cyclonic separators: implications for separator design and modelling. *Chem. Eng. J.*, 56, 135-141.
- XU, B. H. & YU, A. B. 1997. Numerical simulation of the gas-solid flow in a fluidized bed by combining discrete particle method with computational fluid dynamics. *Chemical Engineering Science*, 52, 2785-2809.
- XU, P., WU, Z., MUJUMDAR, A. S. & YU, B. 2009. Innovative Hydrocyclone Inlet Designs to Reduce Erosion-Induced Wear in Mineral Dewatering Processes. *Drying Technology*, 27, 201-211.
- XU, Y. X., SONG, X. F., SUN, Z., LU, G. M., LI, P. & YU, J. G. 2012. Simulation Analysis of Multiphase Flow and Performance of Hydrocyclones at Different Atmospheric Pressures. *Industrial & Engineering Chemistry Research*, 51, 443-453.
- Y.H. ZHANG, P. Q., Y. LIU, H.L. WANG 2011. Experimental study of hydrocyclone flow field with different feed concentration. *Ind. Eng. Chem. Res.*, 50, 8176-8184.
- YANG, Q., WANG, H., WANG, J., LI, Z. & LIU, Y. 2011. The coordinated relationship between vortex finder parameters and performance of hydrocyclones for separating light dispersed phase. *Separation and Purification Technology*, 79, 310-320.

- YOSHIDA, H., TAKASHINA, T., FUKUI, K. & IWANAGA, T. 2004. Effect of inlet shape and slurry temperature on the classification performance of hydro-cyclones. *Powder Technology*, 140, 1-9.
- YOSHIDA, H., YOSHIKAWA, S., FUKUI, K. & YAMAMOTO, T. 2008. Effect of multi-inlet flow on particle classification performance of hydro-cyclones. *Powder Technology*, 184, 352-360.
- YOUNG, G. A. B., WAKLEY, W. D., TAGGART, D. L., ANDREWS, S. L. & WORRELL, J. R. 1994. Oil-water separation using hydrocyclones - an experimental search for optimum dimensions. *Journal of Petroleum Science and Engineering*, 11, 37-50.
- YU, A. B. 1994. Johnson's SB distribution function as applied in the mathematical representation of particle size distributions. *Part. Part. Syst. Charact.*, 11 291-298.
- YU, A. B. & STANDISH, N. 1990. A Study of Particle Size Distributions. *Powder Technology*, 62 101-118.
- ZHANG, C., WEI, D., CUI, B., LI, T. & LUO, N. 2017. Effects of curvature radius on separation behaviors of the hydrocyclone with a tangent-circle inlet. *Powder Technology*, 305, 156-165.
- ZHANG, L., WEI, L., CHANG, B. H., XING, J. L. & JIA, K. 2013. CFD numerical simulation of Archimedes spiral inlet hydrocyclone. *6th International Conference on Pumps and Fans with Compressors and Wind Turbines (Icpf2013)*, 52.
- ZHAO, B. & SU, Y. 2016. Cyclone performances depend on multiple factors: comments on "A CFD study of the effect of cyclone size on its performance parameters" by Mehdi Azadi et al. (2010). *J Hazard Mater*, 303, 174-6.
- ZHAO, B., SU, Y. & ZHANG, J. 2006. Simulation of Gas Flow Pattern and Separation Efficiency in Cyclone with Conventional Single and Spiral Double Inlet Configuration. *Chemical Engineering Research and Design*, 84, 1158-1165.
- ZHOU, Q., WANG, C., WANG, H. & WANG, J. 2016. Eulerian-Lagrangian study of dense liquid-solid flow in an industrial-scale cylindrical hydrocyclone. *International Journal of Mineral Processing*, 151, 40-50.
- ZHOU, Y. C., WRIGHT, B. D., YANG, R. Y., XU, B. H. & YU, A. B. 1999. Rolling friction in the dynamic simulation of sandpile formation. *Physica a-Statistical Mechanics and Its Applications*, 269, 536-553.
- ZHOU, Z. Y., KUANG, S. B., CHU, K. W. & YU, A. B. 2010. Discrete particle simulation of particle-fluid flow: model formulations and their applicability. *Journal of Fluid Mechanics*, 661, 482-510.
- ZHU, G., LIOW, J. & NEELY, A. 2011. Computational study of centrifugal instabilities in a micro-sized hydrocyclone. *Chemeca: Engineering a Better World* Sydney Hilton Hotel, NSW, Australia: Barton, A.C.T.: Engineers Australia.
- ZHU, H. P., ZHOU, Z. Y., YANG, R. Y. & YU, A. B. 2008. Discrete particle simulation of particulate systems: A review of major applications and findings. *Chemical Engineering Science*, 63, 5728-5770.